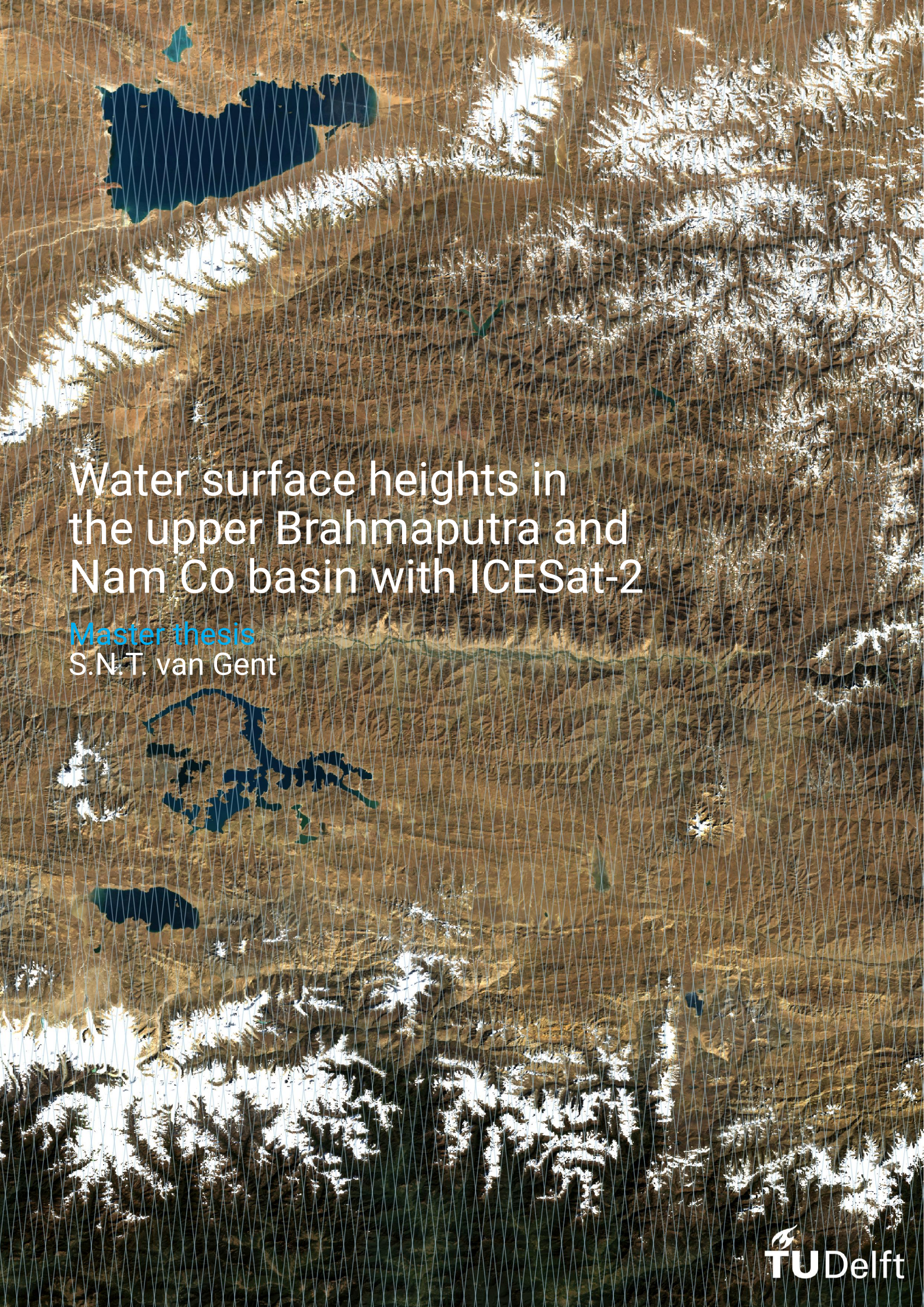

Water surface heights in the upper Brahmaputra and Nam Co basin with ICESat-2

Master thesis

S.N.T. van Gent

TU Delft

Water surface heights in the upper Brahmaputra and Nam Co basin with ICESat-2

Master thesis

by

S.N.T. van Gent

to obtain the degree of Master of Science
at the Delft University of Technology,
to be defended publicly on Tuesday July 13, 2021 at 09:15 AM.

Student number:	4467981	
Project duration:	November 3, 2020 – July 13, 2021	
Thesis committee:	Dr. R. C. Lindenbergh,	TU Delft
	Dr. J. E. A. Storms,	TU Delft
	Dr. Ir. B. Wouters	TU Delft

An electronic version of this thesis is available at `http://repository.tudelft.nl/`.

Front page: Landsat image of a part of the study area (upper Brahmaputra and Nam Co basin) visualized with Google Earth Engine (Vermote et al., 2016) and covered with ICESat-2 tracks.

TU Delft

Preface

This thesis in front of you is written for the fulfilment of the Master of Science degree at the Delft University of Technology. This master thesis is mainly focussed on remote sensing, but has a link with climate change as well. Climate change is a challenging problem and it is important that people are or become aware of this problem. I therefore would like to contribute to the awareness amongst people.

I have learnt a lot during this research and this would not have been possible without my committee. First, I would like to thank Dr. Roderik Lindenbergh, who was my daily supervisor. I am very grateful for our meetings where you always were such enthusiastic and gave valuable feedback. I also would like to thank Dr. Joep Storms and Dr. Ir. Bert Wouters for being involved in this master thesis. I really appreciated the regular meetings with the committee members and the feedback.

Next, I would like to thank my family and friends for motivating and supporting me. In special I would like to thank Jorrit and Fransje who always had motivational words and helped me relaxing during the stressful moments.

I started my thesis during the pandemic, which resulted in that all the meetings were online and from out of my room. It was nice to hear what everyone in the OLRS group was working on during the regular online meetings. If anyone faced a problem, everyone was very helpful during these meetings. Even though, I finally got a bit used to the online meetings, I am happy to present my master thesis at the faculty.

S.N.T. van Gent
Delft, July 2021

Summary

Due to climate change, glaciers are melting on the Tibetan Plateau. These glaciers are the water source for big rivers as the Brahmaputra which stream towards the most densely populated area on Earth. Previous studies indicated that water surface heights of lakes connected to the glaciers are increasing in the north of the Tibetan Plateau, while they are decreasing in the south. Current literature does not provide a clear answer on the reason why the north and the south are behaving differently. For determining why the south is behaving different than the north, the processes in the basin should be identified and distinguished. For addressing what all the processes in the basin are, the waterbodies in the upper Brahmaputra should be monitored and their relation to the processes and the other waterbodies should be determined. For determining this relation it is of importance to first determine the lake surface heights and river surface heights in this area. This research focusses on determining water surface heights in the upper Brahmaputra and Nam Co basin (located in south of the Tibetan Plateau) using remote sensing, which is the preferred method since waterbodies in this area are difficult to reach for in-situ measurements.

In this study, data of ICESat-2 is used for water surface height measurements. The laser satellite mission ICESat-2 has been launched in 2018 and makes use of three pairs of beams. Lake surface heights are determined by first computing the water surface heights per beam and finally per ICESat-2 passing. Several additional steps to determine the river surface heights are required due to the slope of rivers. Therefore, the passing beams are clustered, resulting in several locations in the river which can be further analysed. It is found that river surface heights are harder to determine due to the presence of bars and shorelines. Therefore, the method for determining the river surface heights should only be used for non-braiding rivers.

A precision for both lake surface heights and river surface heights of 0.1 meters is found. This research found that ICESat-2 can have a contribution for determining lake and river surface heights due to its relatively good precision, but also due to its high spatial resolution. The ground-track spacing of ICESat-2 is lower than other satellite missions, resulting that ICESat-2 passes the most amount of lakes and river locations. In total the water surface heights of 299 lakes and 127 river locations are determined. This small ground-track spacing is at the cost of the temporal resolution resulting in large time gaps in the timeseries of the lakes and river locations. Therefore, a seasonal variation and generic water surface height curve will be difficult to assess. It is possible that ICESat-2 will miss the moments with the extreme water surface heights resulting in a misconception of the water surface heights. But, over a longer time period it may be possible to fit a generic water surface height curve through the water surface heights of lakes larger than 10 km^2 due to its higher amount of ICESat-2 passings.

Contents

1

Introduction

The Tibetan Plateau is a region in Central Asia covering a great part of China. The average elevation of the Tibetan Plateau is 4500 meters. It covers an area of approximately 2.5 million square kilometres, which makes it the highest and biggest plateau on Earth. After the Arctic and Antarctic, the Tibetan Plateau consists of the largest amount of snow and ice, which is the reason it is also called the 'Third Pole'. The glaciers of the Tibetan Plateau are the water source for thousands of lakes and big rivers as the Brahmaputra, Indus, Mekong, Salween, Yellow River and Yangtze (see Figure 1.1). These rivers stream towards the most densely populated region on earth (south-east Asia). Therefore, the Tibetan Plateau is also called the water tower of Asia.

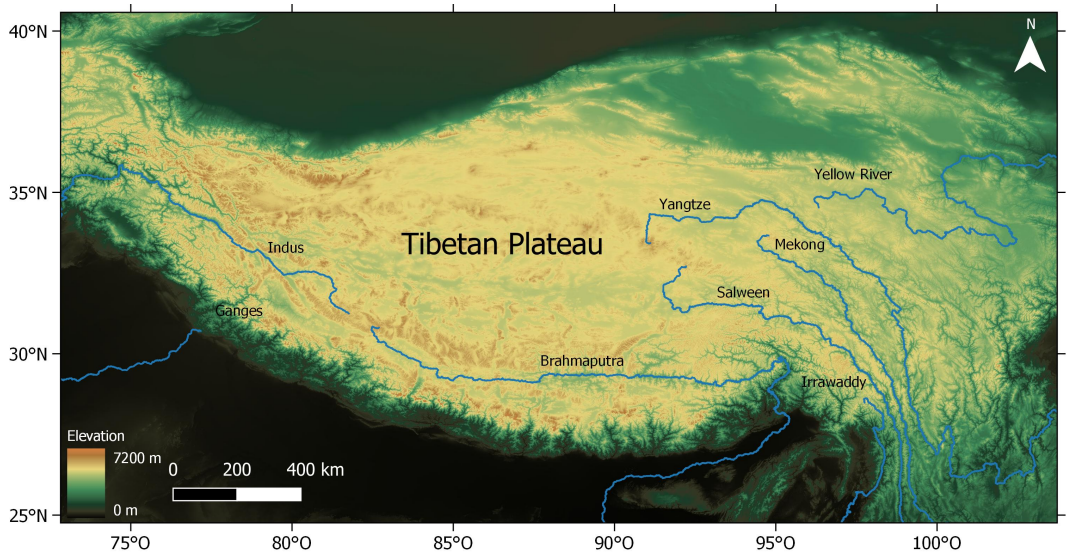

Figure 1.1: The Tibetan Plateau has a much higher elevation than the surrounding areas. It is the origin of big rivers as the Brahmaputra, Indus, Mekong, Salween, Yellow River and Yangtze. The Digital Elevation Model and the big rivers are downloaded via HydroSHEDS (Lehner et al., 2008).

Since the glaciers on the Tibetan Plateau are rapidly melting due to climate change (Maurer et al., 2019), the water surface heights of the waterbodies will increase in short term. However, the water storage of the most densely populated area decreases and therefore the water surface heights will decrease in long term. Both the local and downstream population will be affected. The melting glaciers will affect the nearby lakes. Research found that due to climate change and glacial retreat the glacial lakes in Tibet are expanding fast since 1990 (Shugar et al., 2020). Besides the amount and size of lakes, also the water surface heights of lakes change due to climate change and glacial melt (Tan and Liu, 2020).
The Brahmaputra river is located on the south of the Tibetan Plateau. It is one of the largest rivers in the world and the longest river in Tibet. The river originates from Mount Kailash and Lake Manasarovar located on the Tibetan Plateau and streams towards the Bay of Bengal. It is found that the south of the Tibetan Plateau, so the upper Brahmaputra basin, is behaving different than the north. Instead of an increase in lake surface heights,

most of the lake surface heights in the upper Brahmaputra basin are slightly decreasing (Zhang et al., 2020; Kleinherenbrink et al., 2015; Phan et al., 2012), while the Brahmaputra basin consist of 30% of the glaciers on the Tibetan Plateau and is a sensitive area to climate change. So, especially in this area the relation between the waterbodies is interesting. Why the upper Brahmaputra basin is behaving differently than the north of the Tibetan Plateau is still quite unclear.

1.1. Research scope

For determining why the south is behaving different than the north, the processes in the basin should be identified and distinguished. For addressing what all the processes in the basin are, the waterbodies in the upper Brahmaputra basin should be monitored and their relation to the processes and the other waterbodies should be determined. The relation between the heights of the glaciers and lakes has been studied in literature, but the relation between the river surface heights, glaciers and lakes have not been studied extensively. For determining this relation it is of importance to first determine the lake surface heights and river surface heights in this area.

This research focusses on the upper Brahmaputra basin located on the south of the Tibetan Plateau. The salt basin Nam Co has been added to the study area for comparison. Since a salt basin is disconnected from rivers and oceans, the water balances of the lakes in the salt basin are simplified. So, their lake surface height changes are an important indicator for climate change and give a good impression of the glacier state. Other than the lakes in upper Brahmaputra basin, the lakes in the Nam Co basin are increasing in height, area and volume, Nam Co is therefore considered as a part of the north of the Tibetan Plateau. Figure 1.2 shows the complete study area of this research, with in the right bottom corner the location of the basin as a red dot on the world map.

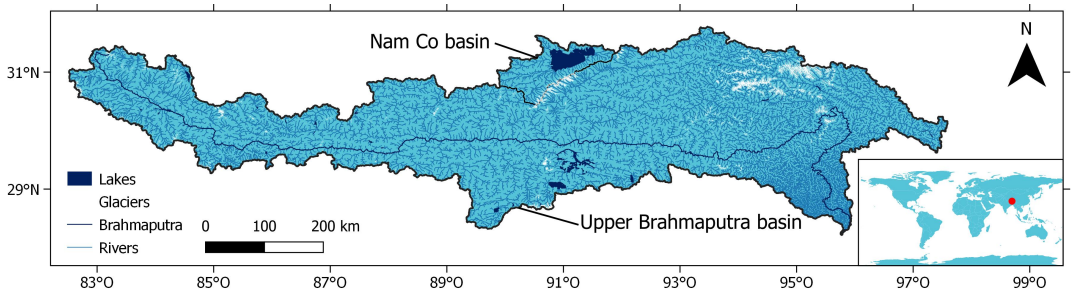

Figure 1.2: The upper Brahmaputra river basin and the Nam Co basin with glaciers (white), river and lakes (blue). Data available via HydroSHEDS (Lehner et al., 2008; Lehner and Grill, 2013; Lehner and Döll, 2004). The right bottom corner shows the location of the basin as a red dot on the world map.

Due to the mountainous area, waterbodies are difficult to reach for in-situ measurements. In-situ measurements of the Nam Co lake are available but in the upper Brahmaputra basin no in-situ measurements of lakes are available. Furthermore, only three hydraulic gauging stations for the river are present in the basin, of which the data is not easily accessible. Remote sensing is thus a preferred method for measuring waterbody surface heights in the upper Brahmaputra and the Nam Co basin.

Since 2018, the satellite mission ICESat-2 has been launched with the laser instrument ATLAS. ATLAS is capable of measuring water surface heights of many waterbodies on Earth. ATLAS has a relatively high resolution, small footprint and a high sampling interval compared to other sensors of satellite missions, leading to the possibility of measuring smaller objects. Besides this, ICESat-2 has a relatively small ground-track spacing, which would result in measuring heights on more locations compared to other satellite missions. Research has found that it is possible to measure lakes with a relatively high accuracy (Yuan et al., 2020; Ryan et al., 2020; Zhang et al., 2019). Rivers have not yet been studied using ICESat-2, while the specifications indicate that river surface heights should be possible to determine. This leads to another motivation of this research: what could be the contribution of ICESat-2 to river surface height measurements? It is important to determine the water surface heights of these waterbodies before the relation between the waterbodies in the upper Brahmaputra and Nam Co basin could be determined. Due to the promising specification of ICESat-2, the contribution of ICESat-2 for measuring water surface height in the upper Brahmaputra and Nam Co basin should be studied.

1.2. Research questions

The main research question of this master thesis is as follows:

What is the contribution of ICESat-2 for measuring waterbodies in the upper Brahmaputra and Nam Co basin located on the Tibetan Plateau?

This main research question is split up in three parts and six sub-questions:

A. **Motivation**

- A.1 Why is it important to monitor waterbodies in the upper Brahmaputra and Nam Co basin?

B. **ICESat-2**

- B.1 What data products of ICESat-2 can be used for monitoring changes in waterbodies and what are their properties?
- B.2 What processing steps should be applied to ICESat-2 data to be able to estimate water surface heights?

C. **Waterbody surface heights**

- C.1 What is the precision of the measured water surface heights by ICESat-2?
- C.2 What are the seasonal variations in water surface heights of the waterbodies in the upper Brahmaputra and Nam Co basin?
- C.3 What can be concluded from the water surface height measurements of ICESat-2?

1.3. Thesis organisation

This report consist of seven chapters in total. The study area is evaluated in Chapter 2 regarding elevation, landcover and weather. Chapter 3 discusses the literature about monitoring water surface heights, followed by a more detailed description of the ICESat-2 mission. Next, Chapter 4 presents the methodology of this research. Chapter 5 contains the results of the water surface height measurements based on ICESat-2. Chapter 6 discusses the results. Chapter 7 presents the conclusions of this research and gives recommendations for further research.

2

Study area

This chapter describes the study area in more detail. Section 2.1 discusses the waterbodies in the upper Brahmaputra and Nam Co drainage basins. Section 2.2 describes the elevation of the study area. Section 2.3 shows the landcover of the study area. In Section 2.4 the weather in the study area is discussed, focussed on precipitation and temperatures.

2.1. Waterbodies in the basins

The complete study area consists of the upper Brahmaputra basin and the Nam Co basin (see Figure 1.2). The upper Brahmaputra and Nam Co basin are two drainage basins located on the Tibetan Plateau. A drainage basin is a land area that drains water (from example precipitation) to rivers. The rivers transport the water to outflow points as for instance the oceans. This section discusses the waterbodies of both the upper Brahmaputra and Nam Co basin.

Upper Brahmaputra basin

The upper Brahmaputra basin is the upper drainage basin of Brahmaputra with an area of 260.000 km^2 and is located north to the Himalayan mountains. The upper Brahmaputra basin contains of 30% of the total amount of glaciers on the Tibetan plateau (Consortium, 2017) which are the source of the Brahmaputra river and many lakes. The upper Brahmaputra basin consists of approximately 600 lakes with a total area of 1700 km^2. 85% of the lakes is smaller than 1 km^2 and 99% of the lakes is smaller than 50 km^2. Most of the lakes in the upper Brahmaputra basin are therefore relatively small. The two largest lakes in the upper Brahmaputra basin are Yamdrok lake (567 km^2) and Puma Yumco lake (283 km^2). All these lakes are connected to the Brahmaputra river which has a length of 2200 km in the upper Brahmaputra basin.

Nam Co basin

The Nam Co basin is named after the largest lake of the basin: Nam Co. Nam Co lake is the largest lake in the whole study area with an area of 1964 km^2. Besides this lake, the basin consist of approximately 24 lakes, which are all smaller than 2.5 km^2. As mentioned earlier, the salt basin Nam Co is added to the study area for comparison. Salt lakes are a good indicator for climate change and glacial melt. Salt lakes are endorheic (disconnected from rivers or oceans) and have a high concentration of salts due to evaporation (Zhang et al., 2011). Since the salt lakes are disconnected, the water balances of these lakes are simplified. So, the water surface height change in salt lakes are an important indicator for climate change and give a good impression of the glacier state. But, since salt lakes are by definition not in a water basin (disconnected from rivers) and thus also not present in the upper Brahmaputra basin, a salt basin (Nam Co basin) is included in this research. This makes it possible to study the influence of glacial melt on the water storage in this area.

2.2. Elevation

The upper Brahmaputra basin is part of the Tibetan Plateau. Figure 2.1 shows the elevation of the basin. The elevation in this figure is based on Shuttle Radar Topography Mission (SRTM) with a resolution of 90 meters and is downloaded via HydroSHEDS (Lehner et al., 2008).

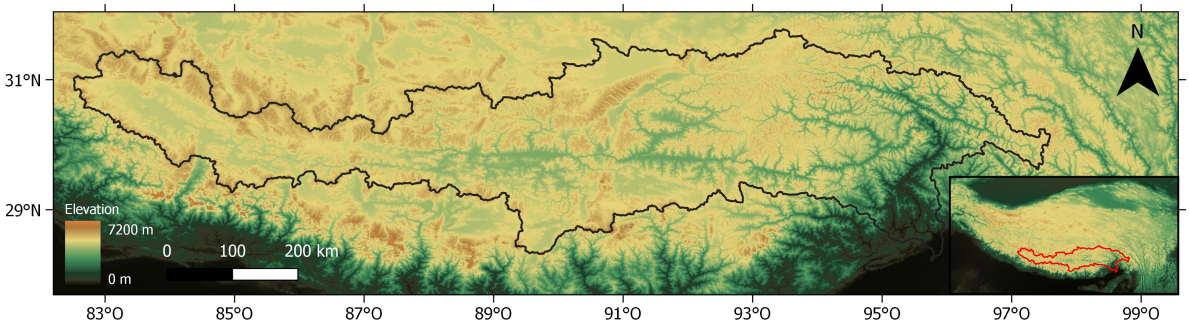

Figure 2.1: Elevation of the upper Brahmaptura an Nam Co basin (Lehner et al., 2008). The basin mostly includes parts of the Tibetan Plateau, but also a small part off the plateau. The right bottom corner shows the location of the study area on the Tibetan Plateau.

Figure 2.1 also shows multiple lower elevated parts in the basin. Most of these lower elevated parts are part of a river valley. The river valley has a lower elevation than its surroundings, this is clarified in Figure 2.2. Figure 2.2.1 is from a more upstream part and Figure 2.2.3 from a more downstream part of the river. The height difference between the river and the surroundings is clearly visible. Water streams from a high elevation to a lower elevation, the western part of the basin has a higher elevation resulting that the river flows from west to east. Another lower elevated region is in the south-east of the basin. These areas indicate the end of the Tibetan Plateau. So the upper Brahmaputra basin also includes a part just outside of the Tibetan Plateau.

Figure 2.2: Pictures from the upper Brahmaputra river valley on three different locations. The river has a lower elevation than its surroundings. The location of each picture is indicated by a red dot in the study area located on the right bottom corner. 1. Upstream in the river, bare soil, not much vegetation (picture made by Krystian Kwiecień, from google maps). 2. Middle of the upper Brahmaputra basin. Vegetation started growing (picture made by unknown, from google maps). 3. More downstream in the upper Brahmaputra basin. Vegetation is present (picture made by Junyin Chen, from google maps).

2.3. Landcover

The largest part of the basin has an elevation of higher than 4000 meters. No vegetation will grow in these higher elevated areas. However, as seen in Section 2.2, the basin also covers a part just outside of the plateau where vegetation can grow. Therefore, different landcover types are expected. This section discusses the landcover types in the study area.

Figure 2.3 shows the landcover types in the upper Brahmaputra basin. There is a clear difference between the western and eastern part of the basin. This contrast is also visible in Figure 2.2. Figure 2.2.1 shows a bare area while Figure 2.2.3 consists of more vegetation. Besides brown and green areas in Figure 2.3, multiple blue areas can be seen as well, which indicates the water or glaciers. Especially in the north-east corner of the basin, a large blue area is clearly visible.

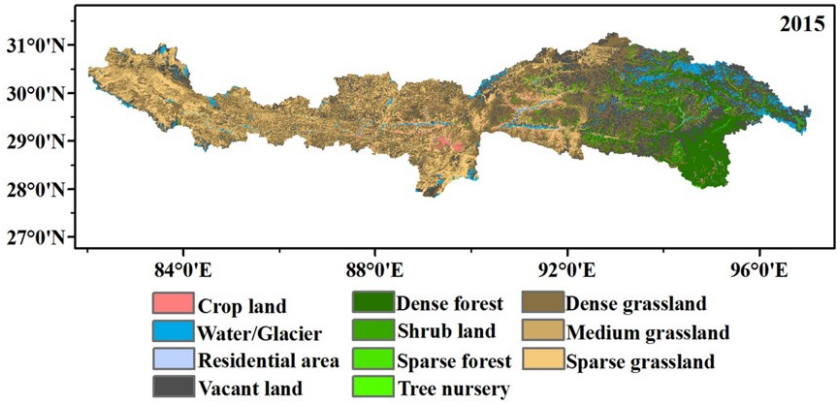

Figure 2.3: Landcover in the upper Brahmaputra basin, edited from Cuo et al. (2019). The upstream part has a brown colour, which mainly consist of dense/medium and sparse grasslands. In the east of the basin, where the elevation is lower (see Figure 2.1), vegetation starts to grow.

Cuo et al. (2019) studied the landcover of the upper Brahmaputra basin over a period from 1990 until 2015 and found an increase in tree nursery, residential area and vacant land while the grasslands reduced. The snow and glacier cover decreased as well in this period. Every year a large area of the basin is covered in snow from October until March. However, the annual mean and maximum snow cover in the basin slightly decreases from 2003 until 2014 (Cuo et al., 2019). Besides this, the annual snow depth in the basin decreases with 0.02 centimeters per year during a period from 1979 until 2016 (Cuo et al., 2019). This would mean that a larger snow melt component of the discharge in the upper Brahmaputra river is expected. In addition to that, the glacier cover has also decreased over time. A comparison between two glacier inventories of China showed that the glacial area reduced from 11.719 km^2 in 1986 to 9725 km^2 in 2014. Especially in the western part of the basin the glaciers retreated or disappeared in the second glacier inventory (Cuo et al., 2019).

2.4. Weather

The basin is characterized by two different seasons, the dry winter season from November - March and the wet summer season from May - September (Phan et al., 2015). In the summer, the basin is exposed to the Indian monsoon. This monsoon causes winds (Westerlies) from the north-east during the winter and from the south-west during the summer, resulting in heavy precipitation in the summer months (Krishnamurti, 2015). The weather in the basin catchment influences the water surface heights of the lakes and rivers. Precipitation in the basin will result in higher water surface heights of lakes and rivers. Not only the precipitation which immediately reaches the lakes or rivers, but also a part of the precipitation that has fallen on the soil will finally stream towards the lakes and rivers resulting in an increase of water surface height. Besides precipitation, the temperatures in the basin also influence the water surface heights. An increase in temperature could lead to glacial retreat resulting in an increase of water surface heights. This section discusses the precipitation and temperature in the basin during the year.

2.4.1. Precipitation

The precipitation in the basins is analysed using satellite imagery from NASA's Global Precipitation Measurement (GPM) Mission. NASA is working on global satellite based estimates of surface precipitation with the algorithm of IMERG (Integrated Multi-satEllite Retrieval for Global Precipitation Measurement). The IMERG products are generated from polar-orbiting satellites, geosynchronous satellites and from the calibration data that is derived from satellite observation or rain gauges (Kelly, 2020). The product has a resolution of approximately 11 kilometers and a precision of 0.1 mm. Monthly precipitation data from 2016 until 2020 is downloaded (Huffman et al., 2014). Figure 2.4 shows the average monthly precipitation between 2016 until 2020 in the Brahmaputra and Nam Co basin based on GPM data. An important remark is that the colour-bar from

0 to 400 millimeters is linear, followed by 400 till 800 millimeters, which are coloured black. This measure is taken because only a small part of the basin contains such high precipitation in particular months which will cause that other variations would fade.

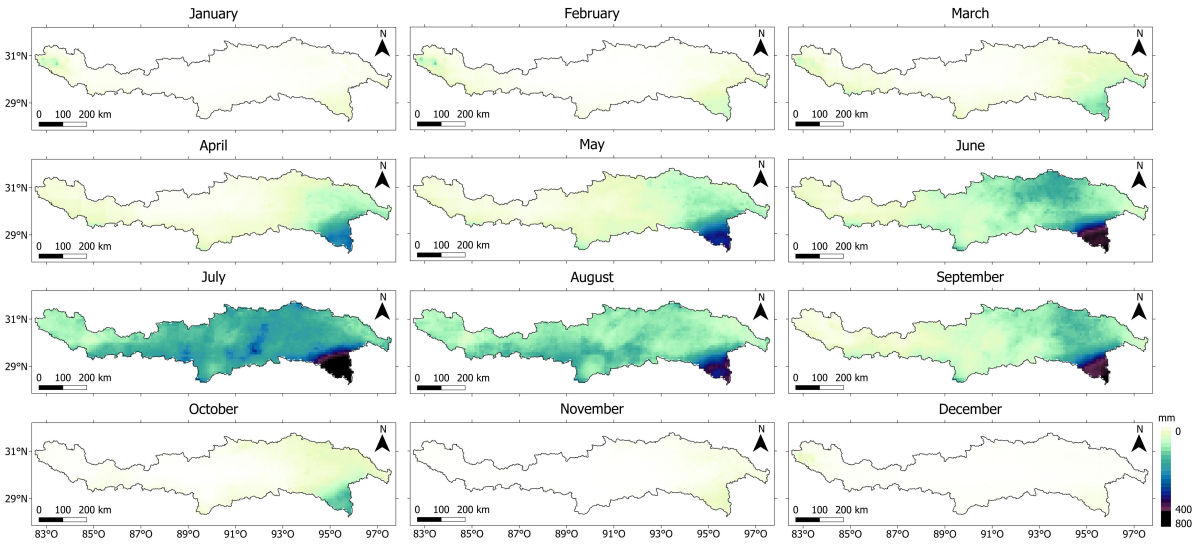

Figure 2.4: Average monthly precipitation between 2016 until 2020 in the Brahmaputra and Nam Co basin based on GPM data (Huffman et al., 2014).

The basin is exposed to precipitation from approximately April until September. Especially a small area in the south-east is highly exposed, which is likely caused by the Indian Monsoon. This area is also the lower elevated area. A possible explanation for the transition from high to low precipitation in that area, could have to do with the plateau forming a barrier for the clouds. Furthermore, the figure shows that from approximately November till March the precipitation is low.

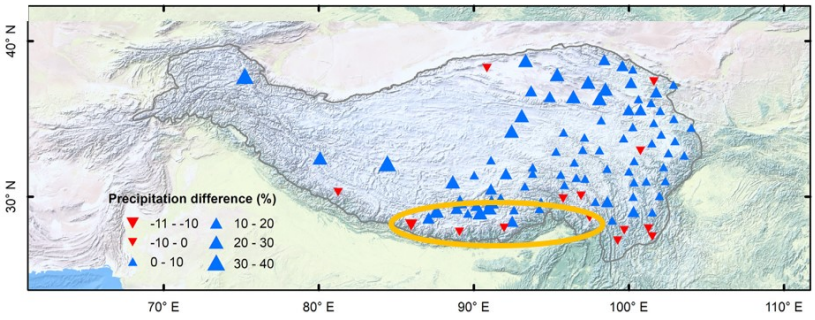

Figure 2.5: The precipitation differences between 1998-2018 and 1980-1997. Figure edited from Zhang et al. (2020). The study area is marked with an orange circle.

The precipitation varies over the seasons due to the Indian monsoon and the Westerlies. The Indian monsoon is dominant in the east of the basin (Cuo et al., 2019) and causes high precipitation in the warm season (June - September). The precipitation is low in cold seasons (November - February) due to Westerlies. Earlier studies have found that the precipitation is greater in the upstream part than in the downstream part in the upper Brahmaputra leading to a variability in seasonal distribution of the precipitation (Sang et al., 2016). A downward trend is visible in the last four decades as well. The weakening of the Indian Summer Monsoon has caused a decrease in precipitation in the basin. This decrease in precipitation will probably result in a water shortage in the basin (Sang et al., 2016). The precipitation differences between 1998-2018 and 1980-1997 are shown in Figure 2.5. The figure shows that the precipitation is decreasing in a part of the upper Brahmaputra basin, while the precipitation in the other basins of the Tibetan Plateau is increasing. Thus, the decreasing precipitation in the upper Brahmaputra basin could be a possible contributor for the decrease of water surface heights of the lakes.

2.4.2. Temperature

The temperature is derived from MODIS Land Surface Temperature (LST) Products (Wan et al., 2015). MOD11A1 Daily LST is downloaded from Google Earth Engine and has a one kilometer spatial resolution. The product is validated with in-situ measurements during clear skies and in a temperature range from -10 till 58 degrees Celsius. The latest version, version 6, is released in 2016 and is validated by Duan et al. (2019). It was found that the land surface temperature matched better during nighttime. The RMSE values during nighttime were found to be smaller than 2 Kelvin, compared to values larger than 2 Kelvin (between 2 and 6 Kelvin) during daytime. Since the temperature could deviate a lot between day and nighttime, both times are observed. Figure 2.6 and Figure 2.7 show the average temperatures, for each month over a period of 2016 until 2020.

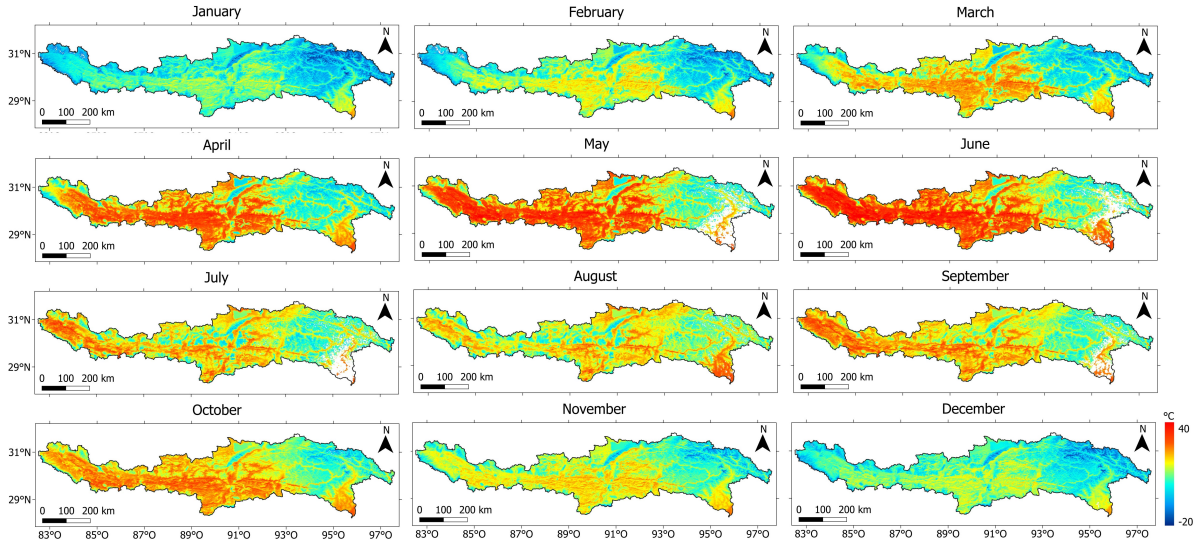

Figure 2.6: Average monthly temperature during daytime between 2016 until 2020 in the Brahmaputra and Nam Co basin based on MODIS Land Surface Temperature. No data is marked in white. Data accessed by Google Earth Engine from Wan et al. (2015)

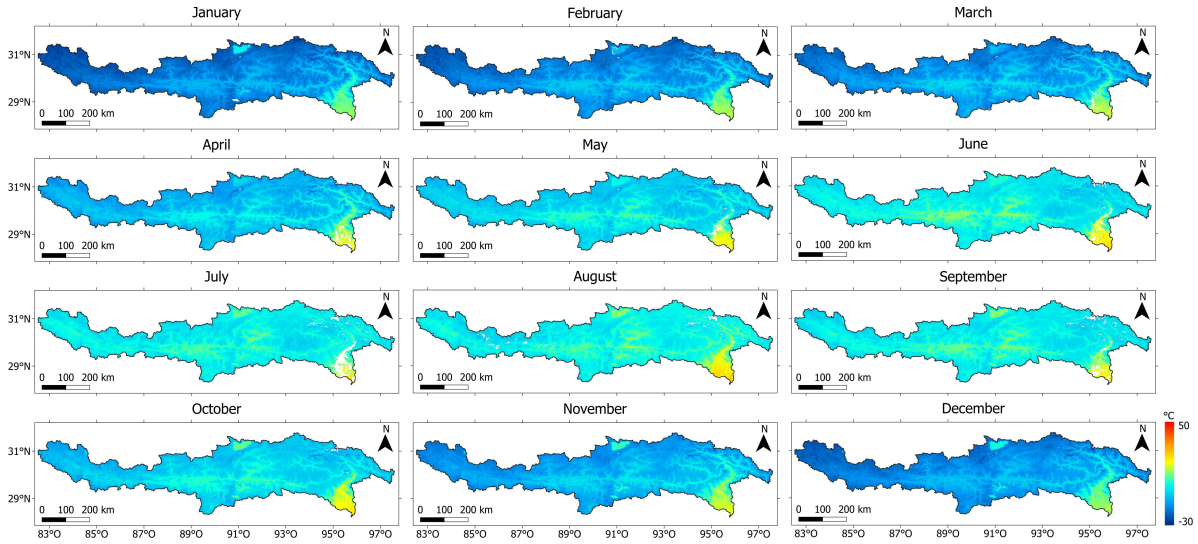

Figure 2.7: Average monthly temperature during nighttime between 2016 until 2020 in the Brahmaputra and Nam Co basin based on MODIS Land Surface Temperature. No data is marked in white. Data accessed by Google Earth Engine from Wan et al. (2015)

The daytime temperatures show that April, May and June are the warmest months. However, according to Figure 2.7, June, July and August are the warmest. The area which is most affected by precipitation, is one of the warmest areas in the basin. The north-east area, on the other hand, is an area which is always the coolest in the basin. A large part of the glaciers is situated here.

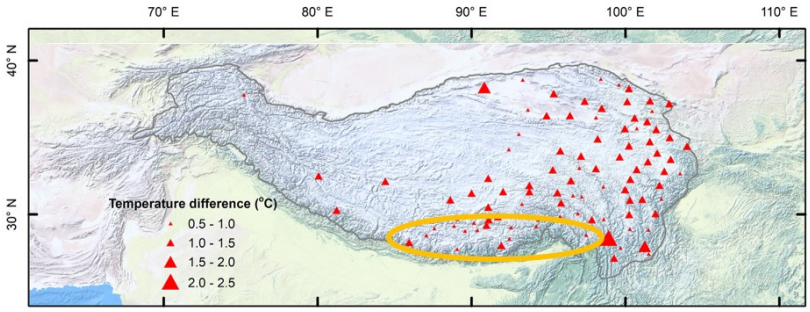

Figure 2.8: The temperature differences between 1998-2018 and 1980-1997. Figure edited from Zhang et al. (2020). The study area is marked with an orange circle.

Earlier studies found that the temperatures on the Tibetan Plateau (Zhang et al., 2020) and also in the upper Brahmaputra basin are increasing (Cuo et al., 2019). The temperature differences between 1998-2018 and 1980-1997 of the Tibetan Plateau are shown in Figure 2.8. The study area is marked with an orange circle. The figure shows that the temperatures over the whole Tibetan Plateau are increasing. In the upper Brahmaputra basin the mean annual temperatures are determined based on ten hydrological stations (Cuo et al., 2019). The temperatures varied from -0.3 to 8.9 degrees during 1979 - 2017. The warming rates during the cold seasons are higher than in the warm seasons (Cuo et al., 2019). The increased temperatures on the Tibetan Plateau resulted in rapid glacial retreat and snow melt leading to a reduction of water storage of the most densely populated area on Earth (Zhang et al., 2020). The rapid glacial retreat and snow melt will, in short term, result in an increase of the water surface heights in the area.

Conclusion about the study area

Thus, the study area of this research is the upper Brahmaputra and Nam Co basin. It is located on a higher elevated plateau where the landcover types grasslands, glaciers and snow cover reduced over the last decade. Besides the landcover types, the weather in this area is significantly changing. The precipitation in a part of the upper Brahmaputra basin reduced which could contribute to a decrease water surface heights. The temperatures have increased resulting in rapid glacial retreat and snow melt which could contribute to an increase of water surface heights.

3

Monitoring water surface heights

Before the water surface heights can be determined, the locations of the waterbodies need to be determined. This is discussed in Section 3.1. Section 3.2 discusses some processes that influence the water surface heights in the upper Brahmaputra and Nam Co basin. Followed by Section 3.3 where multiple satellite missions for determining water surface heights are presented. Section 3.4 introduces the ICESat-2 mission. Finally, Section 3.5 discusses previous studies on determining water surface heights based on ICESat-2.

3.1. Location of the waterbodies

Before the water surface height can be determined the locations of the waterbodies need to be determined. This is often done by using a water mask. A water mask is a vector layer of polygons on the locations of the waterbodies. A lake mask can be created based on Landsat images or Sentinel-2 images using the Normalized Difference Water Index (NDWI). This index marks the pixels of the waterbodies such that they can be distinguished. From the waterbody pixels a vector layer can be created. Another method to create a waterbody mask is based on Shuttle Radar Topography Mission data. An already existing lake mask is created by Hydrological data and maps based on SHuttle Elevation Derivatives at multiple Scales (HydroSHEDS) (Messager et al., 2016) and Global Lakes and Wetlands Database (GLWD) (Lehner and Döll, 2004). This lake mask can be acquired from the HydroLAKES database of WWF (Messager et al., 2016) in a line vector layer that also includes the smaller rivers.

3.2. Processes in the upper Brahmaputra and Nam Co basin

Literature is available about the lake surface heights and river surface heights in the upper Brahmaputra and Nam Co basin. Especially the lake surface heights on the Tibetan Plateau is studied extensively. In this section the available literature about the lake surface heights and river surface heights is presented.

Lake surface heights

Most of the found literature discusses the lake surface height changes on the Tibetan Plateau. Several studies found that on the Tibetan Plateau the lake area, surface height and volume are increasing since the mid-1990s (Zhang et al., 2020; Kleinherenbrink et al., 2015; Phan et al., 2012). However, the south of the Tibetan Plateau, thus the upper Brahmaputra, is behaving differently. Instead of an increase in area, surface height and volume of the lakes, they are all decreasing in the upper Brahmaputra (Zhang et al., 2020; Kleinherenbrink et al., 2015; Phan et al., 2012). Although it should be noted that these decreasing changes are small compared to the increasing changes. Figure 3.1 shows the changes of the area, surface heights and volumes of the lakes of the whole Tibetan Plateau. The study area is marked with an orange circle. Nam Co (located in the north within the orange circle) is considered as the north of the Tibetan Plateau, since the lake area, lake surface height and lake volume are increasing.

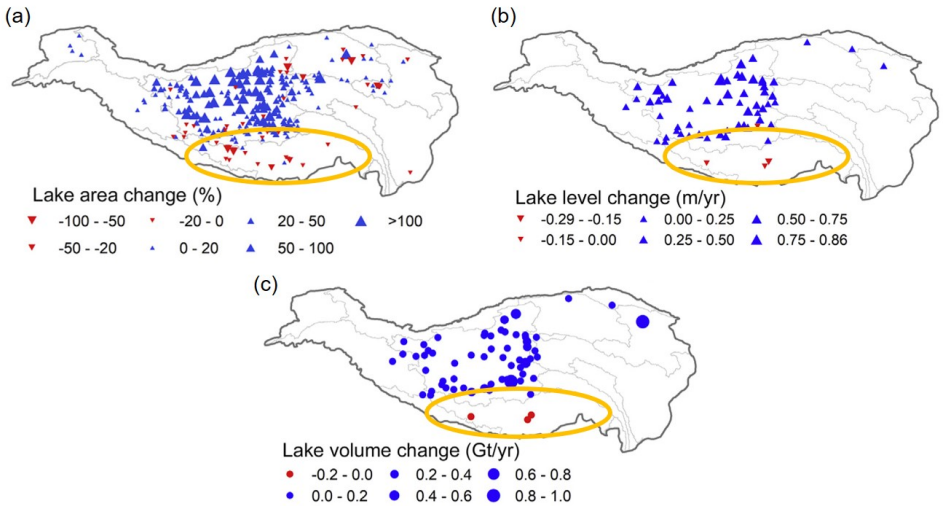

Figure 3.1: Lake area, surface height and volume changes for the Tibetan Plateau, figure edited from Zhang et al. (2020). The study area is marked with an orange circle. The figure shows that the south of the Tibetan Plateau is behaving differently than the north of the Tibetan Plateau. The lakes in the south are decreasing in lake area, lake surface height and lake volume. (a) Lake area changes. (b) Water surface height changes on the Tibetan Plateau. (c) Lake volume changes on the Tibetan Plateau.

Possible processes that influence the water surface height are acceleration of glacial melt, changes of lake temperatures and changes in precipitation. Lake water temperature changes are negatively correlated with water surface height changes (Zhang et al., 2020). This means that an increase in lake water temperature goes together with a decrease of water surface height. The temperature of the lakes is again correlated with the ice cover duration. A lower ice cover duration could result in an increased rate in lake temperature, so a positive feedback. It is found that the lakes in the north of the Tibetan Plateau are cooling while the lakes in the south are warming up (Zhang et al., 2020).
Another contributor of the lake surface height changes is the acceleration of glacial melt. An increase of glacial melt could result in an increase in water surface height. Beside that, the melting glaciers could again result in lower lake temperatures (Zhang et al., 2020) which goes together with an increase of water surface height. Non glacier-fed lakes have a higher warming rate than glacier-fed lakes as a result of the inflow of glacier melt (Zhang et al., 2020).
Additionally, changes in precipitation could lead to change in water surface heights. An increase in precipitation results in an increase in water surface height, while a decrease in precipitation will results in a decrease in water surface height. As discussed in Section 2.4.1, a decreased precipitation is found in a part of the upper Brahmaputra basin. Besides, it was found that the Terrestrial Water Storage (TWS) has decreased in the upper Brahmaputra, which is possibly caused by decreased precipitation (Zhang et al., 2020; Brun et al., 2020) and groundwater pumping (Zhang et al., 2020).

The increased precipitation is found to be playing a big role in the increase of the lake surface height of the lakes on the north of the Tibetan Plateau followed by melting glaciers and thawing permafrost, while the decrease of lake surface heights is found to be highly influenced by a decrease in precipitation (Zhang et al., 2020; Brun et al., 2020) in the upper Brahmaputra basin, but also groundwater pumping could play a role (Zhang et al., 2020).

River surface heights
The found literature about river surface heights from the upper Brahmaputra is scarce. Two studies will be discussed, first a study about the average annual hydrograph of the upper Brahmaputra followed by a study which estimates the changes of the runoff at three hydraulic stations and its contributing components.
The first study used a 'large-scale, high-resolution cryospheric-hydrological model' for evaluating the water system (Lutz et al., 2014). This resulted in average annual hydrographs for multiple rivers on the Tibetan Plateau, so also for the upper Brahmaputra river. The average annual hydrograph from 1998 till 2007 for the sink location of the upper Brahmaputra is shown in Figure 3.2. The blue line represent the total discharge of the upper Brahmaputra and consist of several contributors. The red area corresponds to the base flow, the orange area to the snow melt, the blue area to the glacier melt and finally the green corresponds to the

precipitation. The figure shows that the discharge is the largest in August and the lowest around February. A large contribution of the highest discharge in August is the precipitation followed by glacier melt. The glacier melt component is the largest in August while the snow melt component is the largest in June.

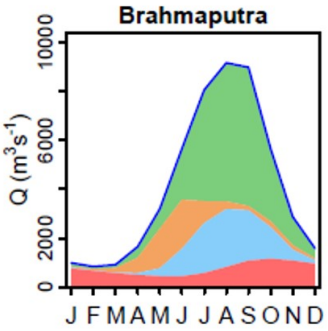

Figure 3.2: The average annual hydrograph from 1998 till 2007 for the sink location of the upper Brahmaputra. The blue line represent the total discharge of the upper Brahmaputra and consist of several contributor. The red area corresponds to the base flow, the orange area to the snow melt, the blue area to the glacier melt and finally the green corresponds to the precipitation. This figure is edited from Lutz et al. (2014).

The second study investigated the runoff in the upper Brahmaputra river by analysing three hydraulic gauging stations: Nugesha, Yangcun and Nuxia (Xuan et al., 2020) (the locations of these stations are shown in Figure 3.3). The runoff of the basin is the excess water (from precipitation, snow and glacial melt or other sources) which does not infiltrate in the soil and therefore flows to a lower elevated area. This water will finally end up in the river resulting in a higher river surface height. The analysis resulted in that the total runoff at the Nugesha and Nuxia stations will decrease with a probability of 60% in the period 2069 - 2099. This decrease in Nugesha will probably be caused by a higher decrease in groundwater runoff than the increase from precipitation and snowmelt, while the decrease in Nuxia will probably be caused by a reduction in groundwater and snowmelt runoff. At the Yangcun station the runoff is likely to increase with a probability of 80%, probably caused by an increase of precipitation and snowmelt runoff (Xuan et al., 2020). An important note is that the data of these three hydraulic gauging stations is not available (anymore).

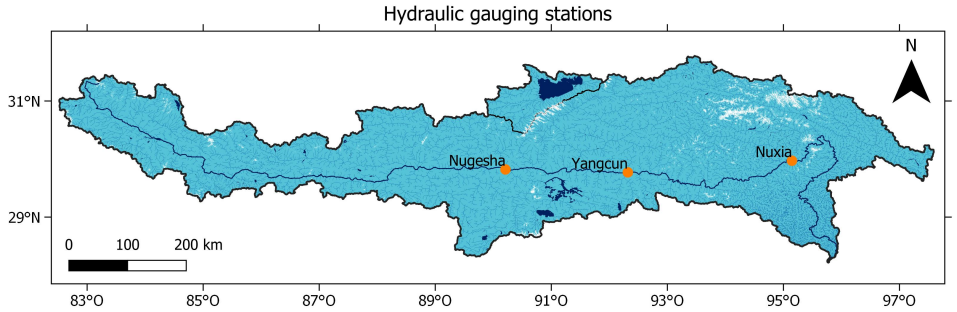

Figure 3.3: Hydraulic gauging stations in the upper Brahmaputra.

Thus, it is expected that the snow melt runoff at two out of three hydraulic gauging stations (Nugesha and Yangcun) will increase, while for one out of three (Nuxia) the snowmelt will decrease. For all three locations it is expected that the precipitation component will increase and the groundwater runoff will decrease. The increasing precipitation component corresponds to the findings in Section 2.4.1.

The found literature about the processes that affect river surface heights from the upper Brahmaputra is scarce. But the found literature shows that it is expected that for three hydraulic gauging stations in the upper Brahmaputra river the precipitation component will increase and for two out of the three hydraulic gauging station the snow melt components will increase. Thereafter, it is found in the literature that the discharge and therefore also the water surface heights of the river is the highest in August and the lowest in February. In August the contribution of the glacial melt component is at its largest, but the main contributor of the high discharge in August is the precipitation component.

3.3. Satellite missions for determining water surface heights

The water surface heights of rivers and lakes are measured by many different satellites. A lot of literature is available on various applied techniques. There are two types of satellite altimeters: radar altimeters and laser altimeters. The sensors of the satellite altimeters can be distinguished into two types: passive and active sensors. Figure 3.4 shows the two sensor types. Passive sensors do not emit a signal itself, but only receive a signal from Earth. Passive sensor can be divided into a passive sensor which is receiving a signal from the reflection of the sun (as for example visible imagery, see Figure 3.4a) and a passive sensor receiving a signal also without the reflection of the sun (such as thermal infrared, see Figure 3.4b). An active sensor emits a signal and receives its signal after reflecting from Earth. Both radar and laser altimeters use an active sensor. This section discusses satellite radar altimeters with active sensors (Jason-2/3, Envisat, SARAL, CryoSat-2 and Sentinel-3 missions) and laser altimeters with active sensors (ICESat-1 and ICESat-2 missions).

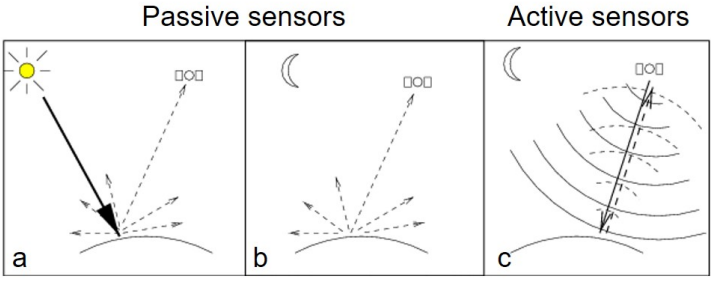

Figure 3.4: The sensors of the satellite altimeters can be distinguished into two types: passive and active sensors. Both (a) and (b) shows the working of passive sensors. (a) shows the working of a passive sensor which receives a signal due to the reflection of the sun (such as visible imagery). (b) shows the working of a passive sensor which receives a signal also without the reflection of the sun (such as thermal infrared). (c) shows the working of an active sensor which is emitting a signal and receiving the signal after reflecting from Earth.

Radar altimetry

The water surface heights can be measured by radar altimetry. Radar altimetry can determine the heights (almost) right below the satellite. Radar stands for RAdio Detection And Ranging. The radar altimeters carries an active sensor. This sensor transmits radio signals in a particular direction which is reflected back by an object on the earth surface and subsequently captured by the satellite. The travel time of this radio signal determines the position of an object. Besides the position of the object, the amplitude of the signal contains information about the object type and reflection properties. Radar altimetry does not have problems with the weather or cloud cover, they still have valuable measurements regardless of the weather. Fives types of radar altimetry missions will be discussed: Jason-2/3, Envisat, SARAL, CryoSat-2 and Sentinel-3. Table 3.1 shows the operation time, repeat cycle, ground-track spacing, footprint and accuracy of the discussed radar altimeters.

Table 3.1: Operation time, repeat cycle, ground-track spacing, footprint and accuracy of the discussed radar altimeters.

	Operation time	**Repeat cycle**	**Ground-track spacing**	**Footprint**	**Accuracy**
Envisat	2002 - 2012	35 days	70 km	1 - 3 km	0.4 m (Huang et al., 2018)
Jason-2	2008 - 2019	10 days	315 km	2 - 4 km	0.034 m (Huang et al., 2018)
Jason-3	2016 - present	10 days	315 km	2 - 4 km	0.034 m (Huang et al., 2018)
CryoSat-2	2010 - present	369 days	7.5 km	0.3 - 0.4 km	Decimeters (Kleinherenbrink et al., 2015)
SARAL	2013 - present	35 days	80 km	1.4 km	0.25 m (Yuan et al., 2020)
Sentinel-3	2016 - present	27 days	52 km	~ 0.7 km	-

Huang et al. (2018) used a combination of the radar satellite altimeters Jason-2/3 and Envisat to measure the water surface height of the upper Brahmaputra river (river width > 200 meters). The satellite mission Jason-2 has been operating from 2008 till 2019 and Jason-3 is launched in 2016 and is still operating. The repeat cycle of Jason-2/3 is 10 days and the ground track spacing of both satellites is 315 kilometers at the Equator (Biancamaria et al., 2018). Even though an accuracy of 3.4 centimeters was found with Jason-2 and 3, the performance in mountainous area was found to be limited. The Envisat mission has been launched in 2002

and ended in 2012. It had a repeat cycle of 35 days and a ground-track spacing of 85 kilometers. Different algorithms were performed on the altimeter data of Jason-2/3 and Envisat, which resulted in lower standard deviations of the estimated river surface height and a better footprint selection. The performed algorithms resulted in standard deviations from 0.3 till 0.9 meters compared to gauging stations. The radar altimeter Envisat is also capable of measuring river surface heights with a small width (river width > 100 meters) (Liu et al., 2018). This was validated with US Geological Survey gauging stations. However, this method performs better on rivers with a rather flat topography (Liu et al., 2018; Huang et al., 2018).

The radar altimeter SARAL has been operating from 2013 and is still operating. The footprint of SARAL is 1.4 kilometers and has a ground-track spacing of 80 kilometers. Lake surface heights on the Tibetan Plateau were measured by SARAL and showed a relative altimetric error of 0.25 meters (Yuan et al., 2020). Another radar satellite is CryoSat-2. This radar satellite mission of ESA is launched in 2010 and is still operating. CryoSat-2 has a repeat orbit of 369 days with a sub-cycle of 30 days resulting in a relatively dense ground-track spacing of 7.5 km at the Equator (Kleinherenbrink et al., 2015). CryoSat-2 passed approximately 3 lakes from the upper Brahmaputra basin with an area of larger than 50km^2 in the time window from 2012 till 2014 with an accuracy of 0.01 till 0.26 meter (Kleinherenbrink et al., 2015). In addition, CryoSat-2 was capable of measuring more than 10 lakes in the upper Brahmaputra basin with an area larger than 10 km^2 and a minimum of 10 passings from 2010 till 2019 (Jiang et al., 2020). CryoSat-2 is also capable of measuring river surface heights, even with a wide of 20 meters (Boergens et al., 2017), however their results were not validated with hydraulic gauge stations. An advantage of CryoSat-2, next to the relatively small footprint and ground-track spacing, is the long operating time which results in long timeseries. However, a drawback of CryoSat-2 is the possible difficulties in positioning the range window (Jiang et al., 2020).
Sentinel-3 is another potential mission for measuring lake and river surface heights. Sentinel-3 is a radar altimeter with a high resolution in the along track direction, while in the cross track direction the resolution is lower. Hydroweb provides lake and river surface height timeseries world wide based on several missions, also based on Sentinel-3 (Crétaux et al., 2011; Normandin et al., 2018). The product used on Hydroweb is a level two product of inland water surface heights. Sentinel-3 has a repeat-orbit of 27 days. This high repeat of the Sentinel-3 mission will be at the expense of the density of the ground-tracks. The tracks of Sentinel-3 have a ground-track spacing of 52 kilometers at the equator (ESA, NDa) resulting in a relatively low density of ground-tracks. Thus, Sentinel-3 will pass less lakes due to its low density of ground-tracks, but will have more measurements in time due to its high repeat-orbit.

An important note, is that the radar signal could be distorted by a nearby water body within the cross-track measurement footprint (Kleinherenbrink et al., 2020). If a lake has a rough surface, the radar signal will result in diffuse scattering and thus a relatively weak signal. However, if the water surface has a flat surface a strong signal will be reflected to the radar satellite due to the specular reflection. A larger sized lake could have a high roughness due to generated waves resulting in a relatively weak signal. If a small sized lake where no waves were generated is located nearby a larger sized lake, the signal of this smaller sized lake could be taken into account instead of the larger sized lake, resulting in a distortion of the water surface height measurements.

Laser altimetry
Laser altimeters also carry an active sensor. Laser stands for Light Amplification by Simulated Emission of Radiation. A laser sends light of a single frequency (single colour of light) to the Earth surface. The Earth surface reflects this signal back to the altimeter resulting in a travel time of the signal. The travel time of the signal is a measure for distance and therefore also a measure of the height of the Earth surface. Next to radar altimetry, laser altimeters also have a good performance in measuring water surface heights. A laser altimeter is ICESat-2 which is the successor of ICESat-1. Both ICESat-1 and ICESat-2 will be discussed. Table 3.2 shows the operation time, repeat cycle, ground-track spacing, footprint and accuracy of the discussed laser altimeters.

ICESat-1 had a footprint of 72 meters which made it possible to measure 5 lakes in the upper Brahmaputra basin with a size of greater than 7 km^2 (Phan et al., 2012). Also river surface heights are measured by ICESat-1 (Koudijs et al., 2008; Baghdadi et al., 2011). Koudijs et al. (2008) estimated water surface heights of the Mekong River. It was concluded that ICESat-1 had potential to observe river surface heights, but the measurements tend to be less precise in mountainous areas. Also Baghdadi et al. (2011) studied the determination surface heights of small rivers. However, with a RMSE of 1.14 meters they indicated that small rivers

could not be monitored accurately using ICESat-1. Another drawback of this laser altimeter is that it did not operate continuously but only several months per year from 2003-2009.

Table 3.2: Operation time, repeat cycle, ground-track spacing, footprint and accuracy of the discussed laser altimeters.

	Operation time	**Repeat cycle**	**Ground-track spacing**	**Footprint**	**Accuracy**
ICESat-1	2003 - 2009	91 days	30 km	72 m	≤ 0.10 m (Phan et al., 2012) (Zhang et al., 2011)
ICESat-2	2018 - present	91 days	3.6 km	17 m	0.02 - 0.34 m (see Section 3.5)

Since 2018, measurements of laser satellite ICESat-2 are available. ICESat-2 is continuously operating with six beams instead of one, has a footprint of 17 meters and a small ground-track spacing, which results in a larger spatial resolution compared to other missions. ICESat-2 also has a higher temporal resolution compared to ICESat-1. As a result of the higher spatial of ICESat-2 compared to other missions, it is supposed to identify more lakes and rivers in the upper Brahmaputra and Nam Co basin.

Comparison satellite missions
A comparison between the discussed satellite missions is shown in Table 3.3. CryoSat-2 performs good in this comparison with good results for the repeat (sub-)cycle, operation time, weather, footprint and accuracy. But they score less for ground-track separation and nearby waterbodies. ICESat-2 also performs good in this comparison. Especially the ground-track separation and its footprint is an advantage of ICESat-2 compared to the other missions.

Table 3.3: The advantages and limitations of satellite missions for measuring water surface heights.

		Temporal resolution	**Ground-track separation**	**Operation time**	**Weather**	**Footprint**	**Accuracy**	**Nearby waterbodies**
Radar altimetry	**Jason-2* and 3**	++	- -	+	+	-	+	-
	Envisat*	+	-	+	+	-	-	-
	SARAL	+	-	+	+	-	-	-
	CryoSat-2	+**	+	++	+	+/-	+	-
	Sentinel-3	+	-	-	+	+/-	/	-
Laser altimetry	**ICESat-1**	-	+	+/-	-	+	+	+
	ICESat-2	-	++	-	-	++	+	+

* not operating anymore
** based on sub-cycle

ICESat-2 has thus a small ground-track spacing and small footprint compared to the other satellite missions, indicating that ICESat-2 will find more lakes. Therefore, it is of interest to analyse the contribution of ICESat-2 for measuring waterbodies.

3.4. ICESat-2 mission

This section introduces the ICESat-2 mission in more detail. Ice, Cloud and land Elevation Satellite 2 (ICESat-2) is launched in September 2018 with a nominal duration of three years. Figure 3.5 shows the ICESat-2 satellite. The main goal of this mission of NASA is to measure the elevation of ice sheets. ICESat-2 contains the height measuring instrument ATLAS which is short for Advanced Topographic Laser Altimeter System. Although the main goal of ICESat-2 is to measure elevations of ice sheets, ICESat-2 also surveys cloud cover, elevations of water surfaces and land surfaces which add a third dimension to the data from space. This section discusses the ATLAS instrument, spatial and temporal resolution and the data products of ICESat-2.

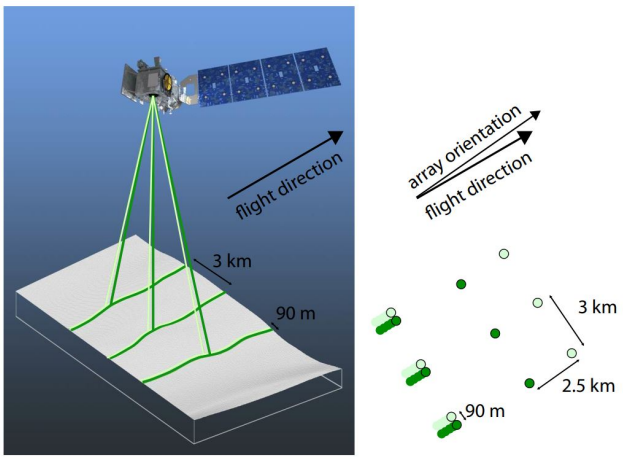

Figure 3.5: Three pairs of two beams with each a strong and a weak beam, the pairs are separated by a distance of 3 kilometers. The distance between the pairs is 90 meters (Neumann et al., 2020a).

3.4.1. ATLAS instrument

ATLAS is the laser instrument carried by ICESat-2. ATLAS uses a low energy laser of 532 nm (green) and a repetition rate of 10 kHz, which creates a sampling interval of 0.7 meters. The laser sends photons to the earth and receives the photons that bounce back from earth (Markus et al., 2017). Each of those returned photons will get a travel time and location allocated, based on the position, altitude, velocity of the spacecraft and the time of flight of the photons (Neumann et al., 2019). With the time of flight principle, the actual distance above the WGS-84 reference ellipsoid can be determined. These photons are called geolocated photons. Each of those sent pulses by ICESat-2 contains about a 10^{14} photons and only a few of them return back to the satellite due to surface reflection and cloud cover (Neumann et al., 2020a).

3.4.2. Spatial resolution

ATLAS makes use of three pairs of beams (GT1L/GT1R, GT2L/GT2R and GT3L/GT3R) each with a diameter footprint of 17 meters with a sampling interval of 0.7 meters (Markus et al., 2017). Each of those pairs consist of a strong and a weak beam separated by 90 meters. The exact width depends on the inclination of the satellite (Markus et al., 2017). The aim of using pairs of beams is to achieve high spatial resolution and to have the possibility to determine the slope between those beams. The energy ratio between the strong and weak beam is 4:1. This means that the strong beam will send approximately four times more photons than the weak beam (Markus et al., 2017). The different beams are shown in Figure 3.5. Dark green corresponds to the strong beam and light green corresponds to the weak beam. The distance between each pair of beams is 3 kilometers. The weak beam is approximately 2.5 kilometers ahead of the strong beam, but this has no consequence on the collected data (Markus et al., 2017).

The small footprint and the high sampling interval leads to a large overlap of the footprints. Due to the large overlap, the spatial resolution is high, even high enough to detect tree tops, vegetation, ground and ocean waves. This is shown in Figure 3.6 which is a Landsat image from Mexico with below the processed photon data of ICESat-2.

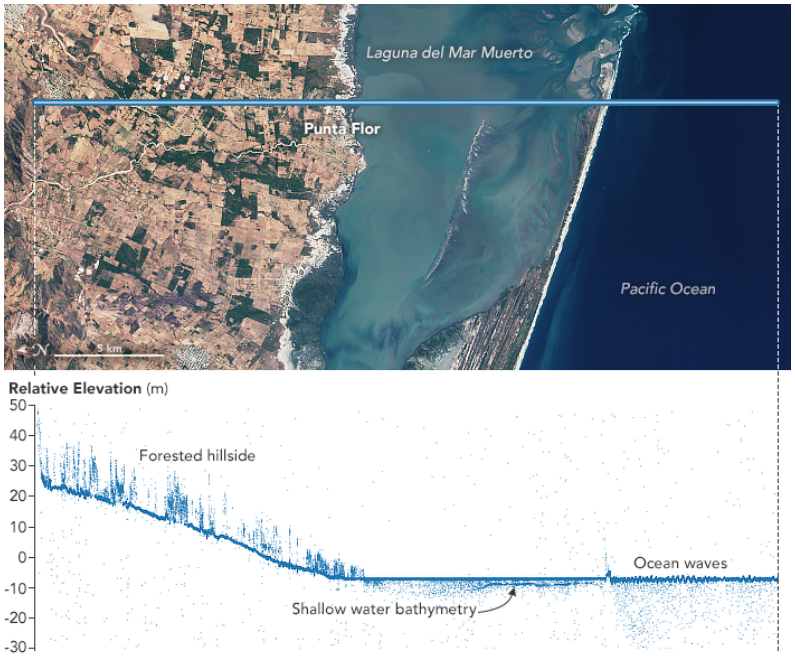

Figure 3.6: ICESat-2 is capable of measuring tree tops, vegetation, ground and ocean waves. Landsat data from the U.S. Geological Survey (top). ICESat-2 processed photon data (below) (Stevens et al., 2018).

3.4.3. Temporal resolution

ICESat-2 consists of eight cycles of 91 days. After these eight cycles the satellite passes the same location as where it started. In Figure 3.7, cycle 1 in ascending and descending track is shown with all the six beams for Puma Yumco lake located in the study area. The strong beams are visualized in dark green and weak beams in light green. The red tracks in this figure are the corresponding reference ground tracks (RGTs). Note that the strong and weak beam might overlap each other a bit in this figure due to the close distance of 90 meters to each other, also the RGTs overlap the middle strong and weak beam. After one orbit around the earth, the satellite flies 28.8 kilometers further than the previous track, this is still cycle 1. A part of this next track could be seen in the right of Figure 3.7. This pattern will shift eight times, leading to the complete ground track pattern of ICESat-2.

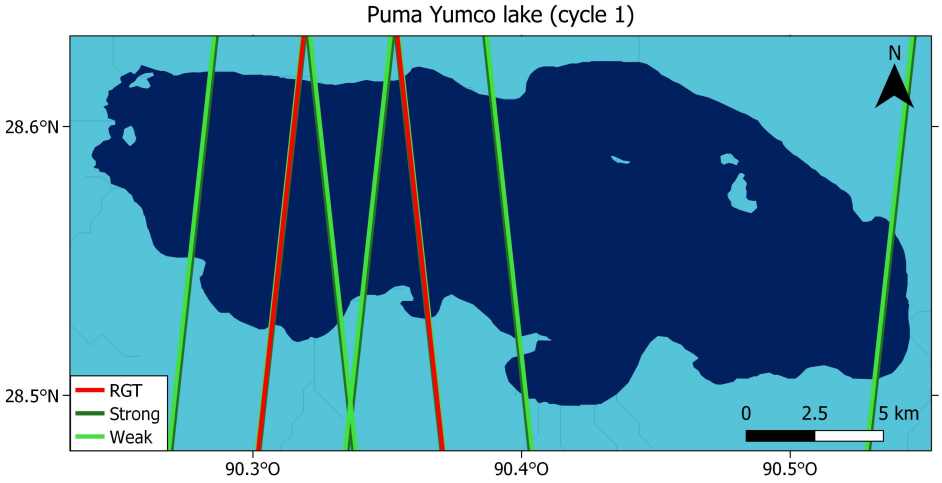

Figure 3.7: Cycle 1 over Puma Yumco lake located in the study area. The red tracks in this figure are the corresponding reference ground tracks (RGTs). Note that the strong and weak beam might overlap each other a bit in this figure due to the close distance to each other, also the RGTs overlap the middle strong and weak beam. The data of the ground track patterns is downloaded from the NASA website (NASA, NDa).

The reference ground track (RGT) pattern is shown in Figure 3.8, note that these are only the reference ground tracks and not the complete ground-track pattern, meaning that there are more tracks than visible in the figure. The reference ground track of cycle 1 is shown in black. 91 days after the start of cycle 1, the track is shifted with 14.4 kilometers (cycle 2, yellow line) which reduces the gap between the tracks of cycle 1 by half (Markus et al., 2017). The 9th cycle will then coincide with cycle 1.

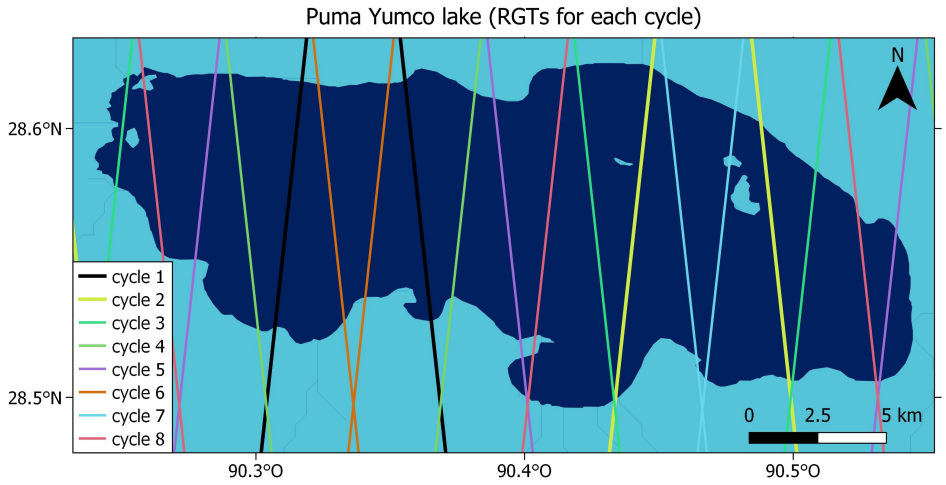

Figure 3.8: Reference ground track pattern over Puma Yumco lake located in the study area. Each cycle is marked with another colour. The data of the ground track patterns is downloaded from the NASA website (NASA, NDa).

3.4.4. Data products

ICESat-2 provides several products of different levels. All the data products are shown in Figure 3.9. The data product of level 0 consist of the raw data. In the level 1 data product, the time of flight of each of the photon is determined and the data is corrected for temperature and voltage effects. Level 2 determines the location and elevation of each photon. And finally level 3 consists of multiple surface-specific datasets (NSIDC, ND).

The data product ATL03 provides all geolocated photons, which forms the basis of the higher level data products. Figure 3.6 shows an example of the ATL03 product. ICESat-2 will geolocate all the photons that come into the satellite regardless of their source, so also photons from sunlight. The photons from the sun or other sources than the location where the laser was pointed at, causes errors in the photon cloud. This is called background noise. An algorithm of ICESat-2 identifies these background noises from the signal. The algorithm indicates for every photon whether this is part of the signal or background noise. The clouds are also flagged as noise, only photons within a range of 30 meters from the reference DEM height are considered as a signal (Neumann et al., 2020a). For each higher level data product, only the signal is used and the background noise is removed. Thereafter ATL03 photons are classified based on their quality. Each photon receives a quality flag. Only the photons with the highest quality are used for the higher order product. The higher level data products are constructed by using surface masks. The aim of these higher level data products is to reduce the amount of data for examining a particular surface (Neumann et al., 2020a).

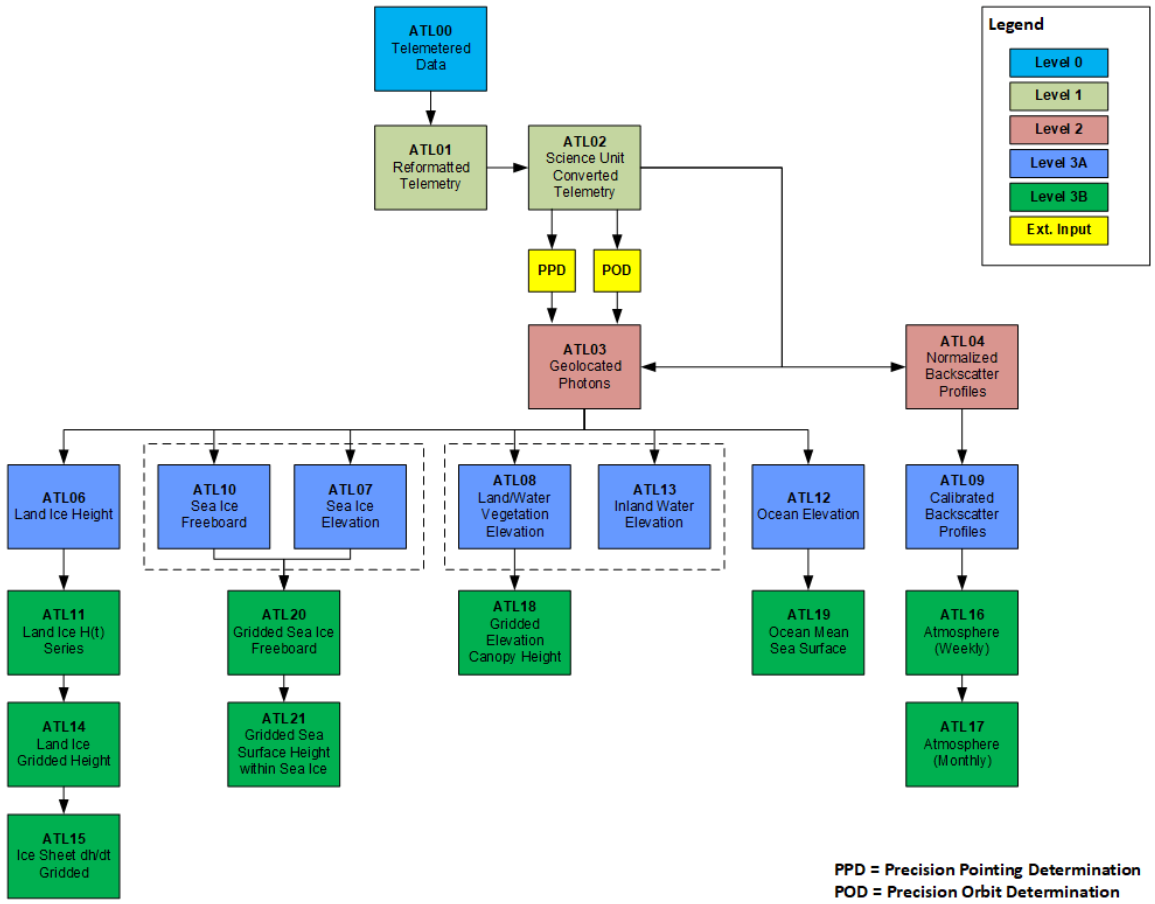

Figure 3.9: Data products levels of ICESat-2 (NSIDC, ND). The data product of level 0 consist of the raw data. In the level 1 data product, the time of flight of each of the photon is determined and the data is corrected for temperature and voltage effects. Level 2 determines the location and elevation of each photon. Finally level 3 consists of multiple surface-specific datasets. The ATL13 data product provides the estimated elevation of inland water bodies, meaning that this product only provides the data at locations of waterbodies.

The data products that are of interest for determining water surface heights of waterbodies are ATL08 (Land/ Water Vegetation Elevation) and ATL13 (Inland Water Elevation), which are a products of ATL03. The data product ATL08 provides estimates of terrain, height and canopy height at small scales. The water mask of this data product is used from the Global Raster Water Mask and has a spatial resolution of 250 meters (Neuenschwander et al., 2020).

The ATL13 data product provides the estimated elevation of inland water bodies, meaning that this product only provides the data at locations of waterbodies. Version 3 of ATL13, released in March 2020, provides lakes and reservoirs larger than 0.01 km^2, rivers greater than 100 meters, transitional water and a near-shore buffer of 7 kilometres. For presenting only the data of waterbodies five different water masks are used in ATL13. The sources of the masks are HydroLAKES (Messager et al., 2016), Global Lakes and Wetland Database (Lehner and Döll, 2004), Named Marine Water Bodies(ESRI), GSHHG Shoreline (Wessel and Smith, 1996) and Global River Widths from Landsat (Allen and Pavelsky, 2018).

Data product ATL08 has its main focus on canopy while ATL13 has its main focus on waterbodies. Besides this, ATL08 uses a water mask with 250 meters spatial resolution which is a much coarser resolution than ATL13 provides. For these reasons ATL13 is preferred above ATL08 for determining water surface heights.

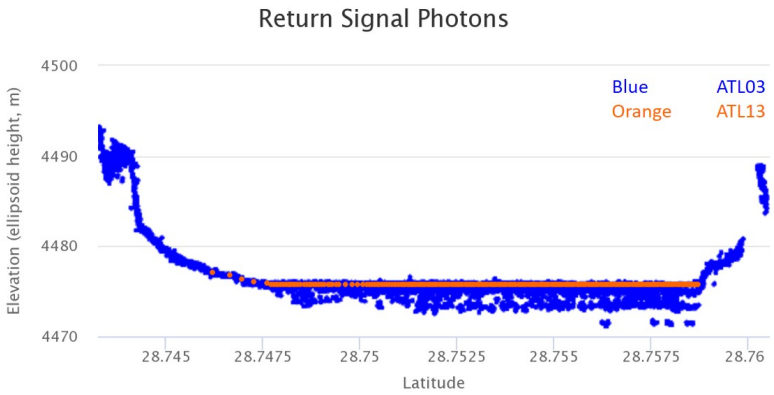

Figure 3.10: An example of data product ATL03 and ATL13 over a lake. Data product ATL03 consists of all the photons (blue), ATL13 is the subsampled data product of ATL03 (orange). ATL13 stops at approximately the shore of the lake. The data is extracted from the open altimetry data of NASA (NDc).

ATL13 is constructed by estimating the mean height for short segments of each beam of signal photons from ATL03. These segments vary from 30 till 100 meters depending on the water and meteorology conditions (Jasinski et al., 2020). For computing the mean height of the segments, only the water surface photons are of interest. Most of the returned photons are from the water surface, but also a part of these photons are background noise, including solar radiation, backscatter from foam on the water surface and subsurface backscatter. Some of the background photons generally appear uniformly distributed above and below the water surface, which makes it possible to subtract the uniform amount of the surface height, which only leaves the backscatter from the water surface, from foam on the water surface and subsurface backscatter. The backscatter of the water surface height and subsurface are extracted by a deconvolution method of ICESat-2 (Jasinski et al., 2020). This technique is not discussed in more detail in this thesis (a more detailed explanation can be found in the paper of Jasinski et al. (2020)). The subsurface backscatter is used for estimations of bathymetry and other subsurface anomalies and the water surface height is used for the extraction of the orthometric height, which is of interest for determining water surface heights.

Table 3.4: Literature about lake surface heights based on ICESat-2. The table shows, the writers, data products of ICESat-2, start and end data, size of the lakes, location of the lakes and the found accuracy.

Paper	**Product**	**Start**	**End**	**Size**	**Location**	**Accuracy**
Yuan et al. (2020)	ATL13 v1	Oct-18	May-19	Lakes > 10 km^2	Reservoir in China, also some on the Tibetan Plateau.	Relative altimetric error of 0.06 m.
Ryan et al. (2020)	ATL08 v2	Oct-18	Nov-19	Lakes from < 1 till >10.000 km^2	3712 reservoirs globally.	Accuracy of approximately 0.141 m.
Rao (2020).	ATL13 v1	Dec-18	May-19	Lakes of unknown size.	15 reservoirs in India.	RMSE of 0.29 m for strong beams and 0.34 m for weak beams.
Zhang et al. (2019)	ATL13 v1	Sep-18	Dec-18	Lakes of unknown size.	Lakes on the Tibetan Plateau.	A moment (one day) comparison of ICESat-2 leads to a difference with gauge data of only 0.02 m.
Cooley et al. (2021).	ATL08 v3	Oct-18	Jul-20	Lakes from 0.02 km^2 till 190.000 km^2.	460.000 lakes globally.	Mean absolute error of 0.14 m.

3.5. Previous studies on determining water surface heights with ICESat-2

Several papers are available about water surface height measurements of lakes based on ICESat-2. Papers about determining river surface heights based on ICESat-2 were not found. Five of the papers about lake surface heights are shown in Table 3.4. The used data products by these five papers are ATL08 or ATL13. Lakes ranging from an area of 0.02 km^2 till 190.000 km^2 are considered (Cooley et al., 2021). Since the spatial resolution of ICESat-2 is high enough to even detect waves in the ocean, it is expected that the sizes of the lakes for which the water surface height could be determined, is mainly depended on the areas of the lakes in the used lake mask. Since the data product ATL13 consists of observations every 30 till 100 meters, water surface heights of lakes with a width of 100 meter and therefore an area of approximately 0.01 km^2 (= 0.1 km x 0.1 km) can be determined theoretically with the data product ATL13. Also for smaller lakes the water surface height can theoretically be determined with the data product ATL03.

The found accuracy by the papers of Table 3.4 varies between 0.02 till 0.34 meters. Yuan et al. (2020) examined the performance of ATL13 of ICESat-2 of thirty lakes on the Tibetan Plateau using gauge data and found a relative altimetric error of 0.06 meters. Additionally, Cooley et al. (2021) found a mean absolute error of 0.14 meters for the computed water surface heights, but also notes that the error is probably overestimated due to the wind set-up which results in lake surface height differences. Zhang et al. (2019) even found a difference of only 0.02 meters between in-situ measurements for a lake and the determined water surface heights based on ATL13 of ICESat-2. The largest error of 0.34 meters is found by Rao (2020). Explanations for this error were related to the conversion of ellipsoidal to orthometric height, shallow depths or waves.
Since the strong and the weak beam perform with a different energy ratio, the performance between the two types of beams can differ. Two papers examined the performance of the strong beam compared to the weak beam. Rao (2020) found a difference of 0.05 meters, whereas Cooley et al. (2021) stated that the difference in performance between the strong and weak beam is in the order of millimeters.

Methods for determining water surface heights

Different methods for determining water surface heights are discussed in the papers. The ATL13 data of ICESat-2 consists of multiple observations over a cross-section for each lake. This can be seen in Figure 3.10. Each study determined one water surface height for each cross-section, but the method for this varies per research.
Yuan et al. (2020) first detected outliers of each cross-section by applying an inter-quartile range (IQR) method and finally computed the mean or median over the remaining measurements. Another approach to extract water surface heights from the ATL13 observations without the anomalies, is to use a simple normalized median absolute deviation method, which removes the outliers and finally computes the median or mean over the observations laying within a range between $[\text{Median} - 2\sigma, \text{Median} + 2\sigma]$ (Zhang et al., 2019; Jiang et al., 2019).
A partly similar approach, is the approach of Cooley et al. (2021), who first removed height observation outside 10th/90th percentile of all water surface height observations. Thereafter, all observations with a standard deviation larger than 0.25 meters were removed. This threshold was derived by analysing thresholds varying from 0.05 till 1.0 meters. For each threshold, statistics were computed, like the amount of measured lakes and the differences with the median. From the remaining observations the median is computed as water surface height measurement for that cross-section.
Also Ryan et al. (2020), computed the water surface elevations based on the median, because it is a more robust method against outliers. Besides this, they also excluded measurements within 100 meters from the shoreline. For removing the last outliers, the observations which have a Z-score larger than 2 have been removed. The Z-score is based on the mean and standard deviation ($Z = \frac{\mu - X}{\sigma}$).
Thus, all discussed methods for determining the water surface height are based on computing the median of the observations from the cross-section of the lakes.

4

Methodology for determining water surface heights

This chapter present the methodology for determining water surface heights for lakes and rivers based on ICESat-2. Figure 4.1 shows the workflow of this chapter. First the data should be acquired and be preprocessed. Section 4.1 discusses the preprocessing of the water mask, both the lake and river mask will be discussed. Section 4.2 discusses the preprocessing steps of the ICESat-2 data, this consists of four main steps. After the preprocessing, the lake surface heights and the river surface heights can be determined. The determination of the lake surface heights consist of two main steps and is explained in Section 4.3 and the determination of the river surface heights consist of five main steps and is explained in Section 4.4. Based on these results, a conscientious attempt is done to determine the seasonal differences. The approach used for determining the seasonal difference is discussed in Section 4.5.

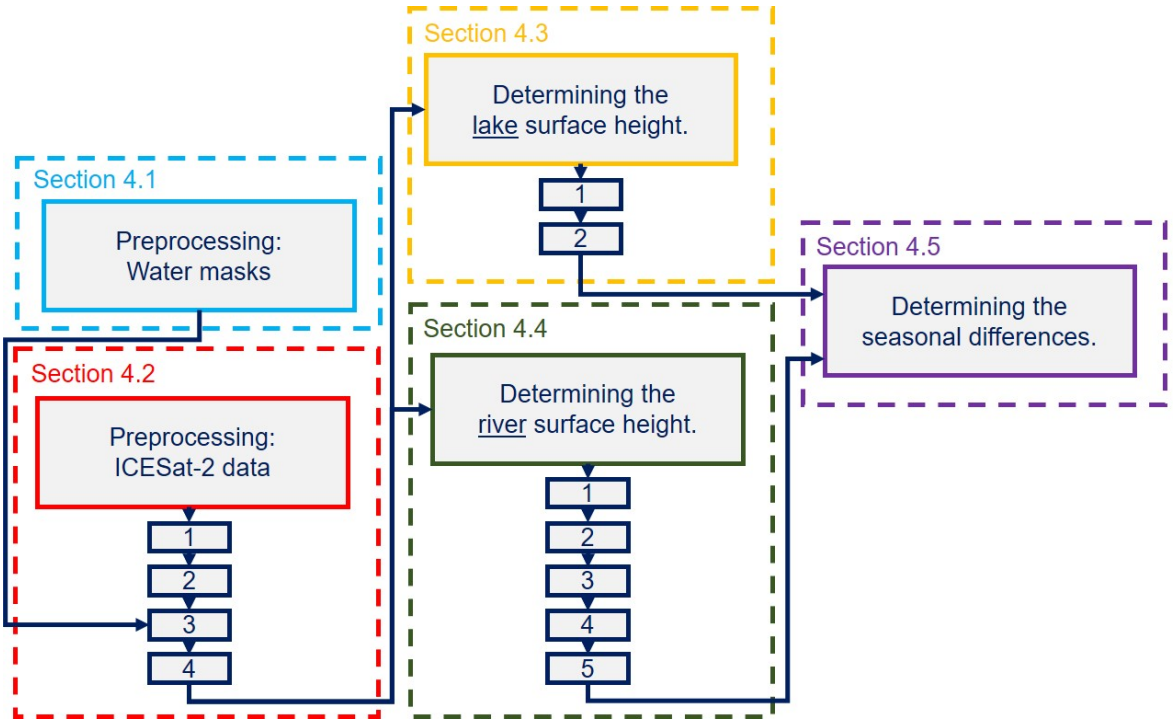

Figure 4.1: Workflow of the methodology for determining water surface heights. First the preprocessing steps of the water masks are discussed, followed by the preprocessing steps of the ICESat-2. Then the methods for determining the lake and river surface heights is presented. Finally a conscientious attempt is done to determine the seasonal difference based on the water surface height results.

4.1. Preprocessing: Water masks

Before the water surface heights can be determined, the locations of the waterbodies need to be determined. This is the first blue box in Figure 4.1.

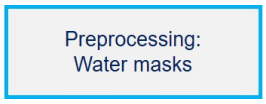

Figure 4.2: This section discusses the preprocessing of the water masks, which is the first part of the workflow in Figure 4.1.

Determining the location of the waterbodies is often done by using a water mask (see Section 3.1). This research uses an existing lake mask and an edited river mask. It is possible to create the water mask based on Landsat images using the Normalized Difference Water Index (NDWI). Since this will be time consuming and it is not the focus of this research, it is chosen not to create a mask but extract the water masks from external sources. The existing lake mask is created by Hydrological data and maps based on SHuttle Elevation Derivatives at multiple Scales (HydroSHEDS) (Messager et al., 2016) and Global Lakes and Wetlands Database (GLWD) (Lehner and Döll, 2004). Rivers are also included in these databases, however only as a line vector layer, so without the width of the rivers. For extracting the correct data, polygons of rivers are required so the width of the rivers are required, which is available in the Global River Widths from Landsat (GRWL) Database (Allen and Pavelsky, 2018). This section contains a more detailed explanation of these water masks. The locations of the waterbodies can be found in Figure 1.2.

4.1.1. Lake mask

The lake mask shown in Figure 1.2 is acquired from the HydroLAKES database of WWF (Messager et al., 2016). The upper Brahmaputra river basin is downloaded from the HydroBASINS of WWF (Lehner and Grill, 2013). The HydroLAKES database is a combined database created by the following eight datasets: Canadian hydrographic dataset (CanVec), Shuttle Radar Topographic Mission (SRTM) Water Body Data (SWBD), MODerate resolution Imaging Spectro-radiometer (MODIS) MOD44W water mask, US National Hydrography Dataset (NHD), European Catchments and Rivers Network System (ECRINS), Global Lakes and Wetlands Database (GLWD) and finally the Global Reservoir and Dam database (GRanD) (Messager et al., 2016), which leads to a total of 1.427.688 lakes around the world. The dataset includes lakes with a surface area of 0.10 km^2 or greater. One of the variables is 'Lake_type'. This variable indicates whether a lake is a natural lake, reservoir or a natural lake with a regulation structure. A note is made within the data that the default type is a natural lake, indicating that it is possible that more lakes should have been marked as reservoir or natural lake with a regulation structure. So the lake type 'natural lake' will include all unidentified smaller human-made reservoirs and regulated lakes (Messager et al., 2016).

4.1.2. River mask

The river vector layer is also acquired via the HydroSHEDS database of WWF (Lehner et al., 2008). These contains all rivers including the small ones. Each river segment is provided with some attributes. One of these attributes is 'ENDORHEIC', which indicates whether a river is part of an endorheic basin, meaning that it has no outflow into other waters, such as another river or ocean. The Brahmaputra river flows into the Bay of Bengal and is thus not an endorheic basin, so the endorheic river parts are removed. Another attribute is the 'ORD_CLAS', which shows the river order by the classical ordering system. The order '1' is the main stream river. The Brahmaputra river is acquired by removing all the lower orders.

However, this river vector layer consist of lines without a width. For the river width, the Global River Widths from Landsat Database (GRWL) derived by Allen and Pavelsky (2018) is used. The GRWLD database is created of rivers with a width greater than 30 meters. The width of the river is determined by using Landsat images from a particular month of which is known that it covers the mean annual discharge of that river. The derived river widths were validated by 1250 river width measurements of U.S. Geological Survey and the Water Survey of Canada. With this approach, the Global River Widths from Landsat (GRWL) Database is created. An important note is that by validating the river width, it has been found that river widths wider than 90 meters are the most accurate Allen and Pavelsky (2018).
The GRWL database contains tiles of 4 degrees latitude by 6 degrees longitude, which each contain line (river) segments with the width parameters as attribute. The tiles also contain side branches of the main river, which

should first be removed from the data, since only the main stream river is of interest. This is done based on the processed river vector layer acquired earlier from HydroSHEDS containing only the main stream river. Since the basin involves a large distance from west to east, the basin consist of several Universal Transverse Mercator (UTM) coordinate systems, concerning UTM 44, UTM 45 and UTM 46. So before adding a width to the line segments, each tile should be converted into its own UTM coordinate system. Thereafter, it is possible to add a width to the line segments. This is done using a buffer function in QGIS, leading to a vector layer with a river polygon. The river mask contains one polygon (the whole main river), while the lake mask consists of multiple polygons of lakes. It should be noted that is method (with the buffer function) does not lead to an accurate vector layer of the river, but is accurate enough to extract only the main stream river without the side river branches from the data product ATL13 of ICESat-2.

So two external sources are used to create this river mask with each different needed variables: HydroSHEDS and Global River Width from Landsat. However, beside the fact that GRWL contains the width of the rivers, the accuracy of the location of river of GRWL is also better. The river of GRWL consists of smaller line segments, which lead to a more accurate representation of the river (see Figure 4.3). For these reasons, the river lines are extracted from GRWL. In the end, the river vector layer of HydroSHEDS was only useful for extracting the main river stream from the GRWL database because the GRWL database does not distinguish between a main river and smaller rivers.

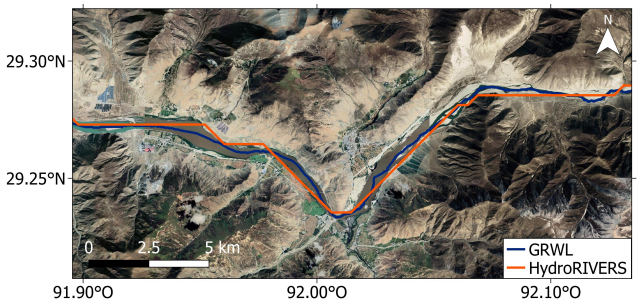

Figure 4.3: Part of the Brahmaputra river. The river is extracted from two sources: HydroRIVERS (Lehner et al., 2008) and Global River Width from Landsat (GRWL) (Allen and Pavelsky, 2018). The figure shows the difference using a Google Satellite images as background.

4.2. Preprocessing: ICESat-2 data

This section describes the preprocessing steps of the ATL13 data for determining the water surface height for lakes and rivers.

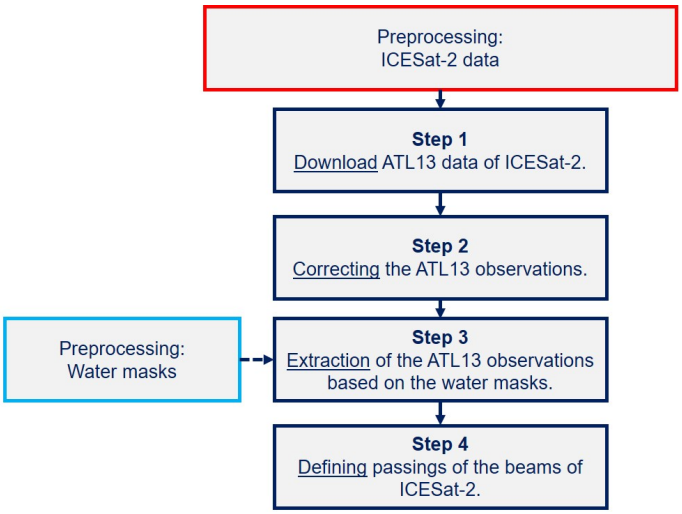

Figure 4.4: The preprocessing steps of the red box of Figure 4.1. First the ATL13 data of ICESat-2 should be downloaded. Then the data should be corrected. Thereafter the ATL13 observation within the water mask should be extracted and finally the passings of the beams of ICESat-2 over the waterbodies should be defined.

Data product ATL13 is chosen since it has its main focus on waterbodies. Before the data of data product ATL13 of ICESat-2 could be analysed, it should be extracted and preprocessed. The preprocessing steps of the red box of Figure 4.1 are shown in Figure 4.4. First the ATL13 data of ICESat-2 should be downloaded. Then the data should be filtered. Thereafter the ATL13 observation within the water mask should be extracted and finally the passings of the beams of ICESat-2 over the waterbodies should be defined.

Step 1: Download ATL13 data of ICESat-2.
ICESat-2 data can be freely downloaded from the National Snow and Ice Data Center (NSIDC). Before downloading the data, the data is filtered by date and area on the website itself. This research focusses on the time period of September 2018 till November 2020 (approximately 2 years). Next, the data is filtered spatially by a bounding box, where the area of interest could be selected. Based on these filters, granules are selected, which have a format of *.h*5 and can be downloaded. The files/granules consist of multiple variables, which could be easily explored by using a HDFviewer. For each beam (GT1L, GT1R, GT2L, GT2R, GT3L and GT3R) a list of multiple variables is available. Besides this, the data consist also of metadata, ancillary data, orbit info and quality assessment parameters. Fortunately not all variables are needed, only the required variables are extracted from the granules files. The variables in Table 4.1 are used in this research.

Table 4.1: ICESat-2 data used in this research, ATL13 Data Dictionary (Neumann et al., 2020b). The used data is divided into five different sections (Location, Time, Tracks, Height and Quality).

	Variables	Units	Description
Location	segment_lat	[degrees]	Latitude of reporting location for all short segment statistics.
	segment_lon	[degrees]	Longitude of reporting location for all short segment statistics.
Time	delta_time	[seconds]	Time of reporting for all short segment statistics.
Tracks	rgt	[-]	The reference ground track (RGT) is the track on the Earth at which a specified unit vector within the observatory is pointed.
	cycle_number	[-]	Number of exact repeats of this reference orbit.
	sc_orient	[-]	This parameter tracks the spacecraft orientation between backward(0), forward(1) and transitional(2) flight modes.
Height	stdev_water_surf	[meters]	Standard deviation of water surface.
	ht_ortho	[meters]	Orthometric height converted from ellipsoidal height.
	segment_fpb_correction	[meters]	First photon bias correction. May be applied at user disrection by subtracting from mean height produts ht_ortho and ht_water_surf.
Quality	qf_subsurf_anomaly	[-]	Likelihood that the bottom or other subsurface anomaly is bottom based on the threshold value at which an anomaly was found. 1 = Subsurface anomaly due to bottom likely; 2 = Subsurface signal may indicate bottom or other anomaly; 3 = Possible subsurface anomaly; invalid = No subsurface anomaly detected.

Step 2: Correcting the ATL13 observations.
The raw data should be preprocessed, before the ATL13 observations can be used for the determination of the water surface heights. By using ATL13 which is a level 2 product of ICESat-2, a large part of the corrections is already done. So does ATL03 include geophysical corrections such as Earth tides and atmospheric delay (Jasinski et al., 2020). Furthermore, ATL03 classifies photons as background if the photons are without a range of -30 meters till +30 meters from the digital elevation model (DEM), which results in an exclusion of most of the clouds. Since only signal photons of ATL03 are used (photons with the highest quality flag) for ATL13, performing corrections for removing clouds is not necessary.

The remaining corrections on the ATL13 data product of ICESat-2 data are divided into five topics: *Location*, *Time*, *Height*, *Tracks* and *Quality*. For each of those topics the necessary corrections are described below.

Location
After the required variables are extracted, the granule is clipped by a bounding box which covers the study area. This is done by indicating a minimum and maximum longitude and latitude. Only the ATL13 observations of the granule inside this region are kept, the other observations are removed.

Time
Each ATL13 observation is provided with a time label. The time is in seconds with a start on 01-01-2018, so this should first be converted to the actual time by adding the seconds to the start.

Height
The ATL13 data product is derived from the photons of ATL03. Data product ATL13 consist of segments from approximately 30 to 100 meters depending on the water and meteorological conditions. For each segment the mean elevation ('ht_ortho') and standard deviation ('stdev_water_surf') is determined. In this research the orthometric height of ICESat-2 with a reference to the geoid model EGM2008 is used. Before an analysis could be performed, the water surface height are corrected for the first photon bias. The first photon bias is a bias due to a short time span where the detector is unable to detect photons after the previous photon is detected. Therefore early photos are more likely to be detected. This bias (available in the data as 'segment_fpb_correction') is subtracted from the water surface height (Jasinski et al., 2020).

Tracks
As discussed, each granule consist of six beams (GT1L, GT1R, GT2L, GT2R, GT3L and GT3R), to distinguish them all, a specific column with the name of the particular beam is added to the other variables of the ATL13 observations. Next to the possibility to distinguish the six beams, this will also lead to the possibility to identify the strong and weak beams. The strong and weak beams depends on the orientation of the satellite. In the forward orientation of the satellite the most left beam (GT1L) is a weak beam, but in the backward orientation the most left beam (GT1L) is a strong beam. For distinguishing the weak and strong beams the orientation of the satellite (given by the variable 'sc_orient') and the name of the beam should be known.

Quality
The water measurements in ATL13 are derived from all the photons in ATL03. The photons sometimes bounce back from the subsurface instead of the top of the water. By deriving ATL13 from ATL03 a likelihood was computed whether ATL13 was computed from subsurface photons. Since in this research the focus is on determining water surface heights, the subsurface measurements should be removed. So all the measurements with flag 1 ('bottom_likely') and 2 ('bottom_or_other_anomaly') are removed, leaving all the ATL13 observations with possible subsurface anomaly 'is likely' or 'no subsurface anomaly is detected'.

Step 3: Extraction of the ATL13 observations based on the water masks.
After the data is preprocessed, the ATL13 observations inside the lake and river masks (from Section 4.1) are extracted. The other ATL13 observations are removed.

Step 4: Defining passings of the beams of ICESat-2.
A lake or river could be passed by six beams several times, depending on the location of the satellite and the area of the lake or river. Those six beams are individually distinguished with the variables: 'rgt', 'cycle_number' and the ground tracks. So for each satellite passing, each beam will get an unique ID. Figure 4.5 shows this for one satellite passing. The IDs for next satellite passing will be 7, 8, 9, 10, 11 and 12 leading to a unique ID for each passing beam.

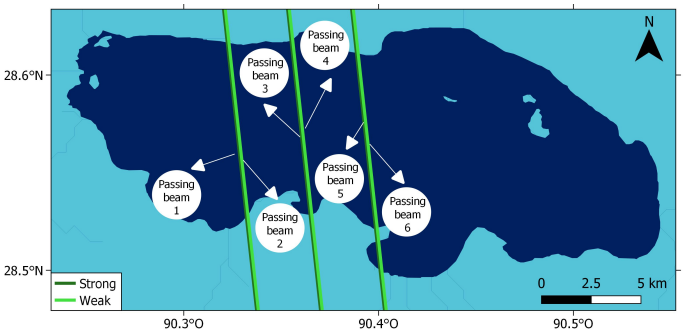

Figure 4.5: For each satellite passing, each beam of ICESat-2 will get an unique ID. The IDs for next satellite passing will be 7, 8, 9, 10, 11 and 12 leading to a unique ID for each passing beam.

The shape of a lake or river could cause that the ICESat-2 beam passes a part of land; rivers could meander and lakes could have a 'u'-shape. This won't be a problem for lakes. Only the ATL13 observations which are within a lake of the lake mask were extracted and all the ATL13 observations outside the lake mask are removed, resulting that for some lakes, some ATL13 observations will be missing within one beam track due to land. But since the ATL13 observations of one beam track belong to the same lake and the water surface of the lake is assumed to be flat, it will not be a problem to compute the water surface height over one beam track. For a river this is slightly different due to their slope and due to that the river mask consists of one polygon for the whole river. A single beam could pass the river twice or even more, but on a different location, this is illustrated in Figure 4.6. Since rivers have a slope, the location of the beam is even more important. The beams in Figure 4.6 measure the river on two locations, these locations could have a different surface height due to the slope in the river, it is thus of importance to distinguish these passing beams of ICESat-2 and not to compute one elevation over the whole beam.

To distinguish those different passings over the river within one beam track, the latitudes of the ATL13 observations are analysed. First, the observations of each beam are sorted by latitude, thereafter the step size between each ATL13 observation is determined. In case the step size between the latitudes is larger than a particular threshold value, a new ID is assigned, resulting that one passing beam could have more than one unique ID. This threshold value should not be too small, since it is possible that some observations of ICESat-2 are missing within one beam track. The observations are for instance marked as the subsurface leading to gaps between the ATL13 observations, resulting in more division within one beam track than needed. However, the threshold value should also not be too large. This would lead to less division of the beam track than needed. By evaluating various threshold values, a step size of 0.004 degrees Latitude (≈ 440 meters) is chosen. This threshold leads to the detection of most of the meander locations within the river and has the least amount of unnecessary divisions of the beam track.

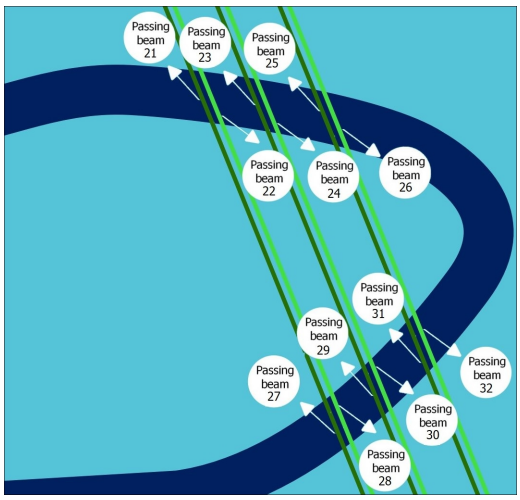

Figure 4.6: The river could have been passed by the satellite more than once due to the shape of the river. For each location ICESat-2 passes the river, a unique ID should be assigned.

4.3. Lake surface heights

The goal is to determine timeseries over two years by extracting lake surface heights from the ATL13 observations of ICESat-2. Figure 4.1 shows that determining the lake surface heights consist of two steps. Figure 4.7 shows these two steps and how this goal is reached. These steps are demonstrated in this section for lake Baiju Co (see Figure 4.8), the same steps will be applied for all other lakes in the study area. In step 1, the median of the ATL13 observation of one passing beam is computed and in step 2, per satellite passing, one water surface height is computed leading to timeseries for each lake. Each step is further explained in this section.

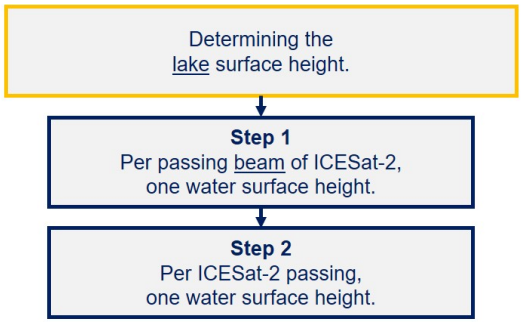

Figure 4.7: Steps for determining water surface heights of the ATL13 observations of ICESat-2. Step 1: Per passing beam, one water surface height is computed. Step 2: Per satellite passing, one water surface height is computed.

Step 1: Per passing beam of ICESat-2, one surface height

In a time window of two years, lakes are passed by several beams several times. Every time ICESat-2 passes a lake, the lake could be passed by six beams or less. In this step it is of interest to gain one water surface height estimation per passing beam of ICESat-2. Each passing beam consist of several ATL13 observations (Equation 4.1). The lower the amount of ATL13 observations in one passing beam, the stronger the impact of the errors will be on the final water surface height. Thus, with regard to the quality of the data, only the passing beams over lakes which consist of more than five ATL13 observations are taken into account. From the beams which have more than five ATL13 observation, only one water surface height is of interest. An example of one passing beam over a lake is shown in Figure 4.8b.

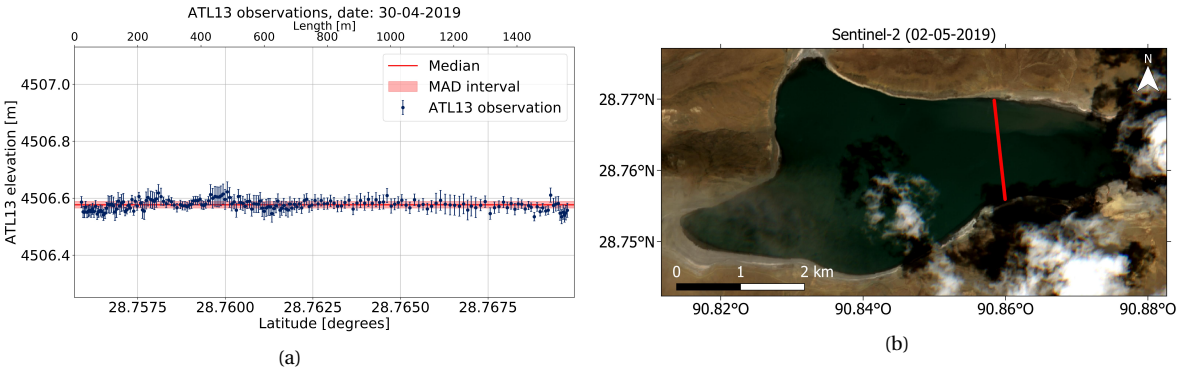

Figure 4.8: (a) ATL13 observations of one passing beam over lake Baiju Co on 30 April 2019. (b) The track of the beam shown in Figure (a) overlaying a Sentinel-2 image of lake Baiju co of 2 May 2019.

At first, the ATL13 observations with a standard deviation larger than 0.25 meters are removed from the data, this number is used based on the paper of Cooley et al. (2021). From the remaining ATL13 observations, the median is computed with Equation 4.2. It is seen in Section 3.5 that all discussed methods used the median of all the observations per beam, since this method is less prone to outliers. Therefore, this is also used in this research. For a robust measure of the spread of the ATL13 observations, the Median Absolute Deviation (MAD) is computed using Equation 4.3.

$$h_{ATL13} = [h_1, h_2, ..., h_{n-1}, h_n] \tag{4.1}$$

$$h_{GTxx} = \text{median(h)} = \begin{cases} \frac{h_{n/2}+h_{n/2+1}}{2} & \text{even} \\ h_{(n+1)/2} & \text{odd} \end{cases} \tag{4.2}$$

$$\text{MAD(h)} = \text{median}(|h_{ATL13} - \text{h}_{GTxx}|) \tag{4.3}$$

where:

h_{ATL13}	Set of the elevations of the ATL13 observations [m].
h_n	The elevations of the ATL13 observations [m].
h_{GTxx}	Estimated height of a passing beam (GT1L, GT1R, GT2L, GT2R, GT3L and GT3R) in meters [m].

The ATL13 observations of one passing beam over lake Baiju Co are shown in Figure 4.8a, the median (red) and the MAD (red band) are marked in this figure. Figure 4.8b shows the location of this passing beam of ICESat-2. Figure 4.8a shows the elevations of the ATL13 observations against the latitude, which is the y-axis. Since meters is a more convenient measuring unit than latitude, the x-axis on the top of the figure shows the distance in meters starting from zero at the lowest latitude. The conversion from latitude degrees to meters is latitude depended. But an approximation of 1 degrees latitude is 111 kilometers based on the circumference of Earth which is 40.075 kilometers.

Step 2: Per ICESat-2 passing, one water surface height
For each passing beam over the lake, the median over the ATL13 observations is computed, leading to the dark and light green dots in Figure 4.9. For some ICESat-2 passings, more than one green dot is present. This is due to the fact that the ICESat-2 has three strong beams and three weak beams and thus could be passed by multiple beams. If more than one water surface height per ICESat-2 passing is present, the mean from these water surface heights is computed based on least squares estimates resulting in one water surface height per ICESat-2 passing. The method is discussed in this step.

The computation of the mean water surface height based on the water surface heights per beam computed in *step 1* is shown in Equation 4.4. This is the formula for least squares estimations. The least square estimate is based on minimizing the sum of the squared errors. $\widehat{x}$ represents the estimated mean over the water surface heights of the beams. The sizes of the matrices is based on the amount of beams that passes the lake for that ICESat-2 passings, this could vary per ICESat-2 passing. Each passing beam has its own error (σ_{GTxx}) which is the MAD computed in *step 1*. This method also takes the variances of each beam into account. If the mean water surface height over two beams should be computed and one beam has a smaller variance than the other beam, the mean water surface height will be more attracted to the beam with the smaller variance.

$$\widehat{x} = (A^T Q_{yy} A)^{-1} A^T Q_{yy} y \tag{4.4}$$

where:

$$A = \begin{bmatrix} 1 \\ 1 \\ \vdots \\ 1 \end{bmatrix}, \quad Q_{yy} = \begin{bmatrix} \sigma^2_{GTxx,1} & 0 & \cdots & 0 \\ 0 & \sigma^2_{GTxx,2} & \ddots & 0 \\ \vdots & \vdots & \ddots & \vdots \\ 0 & 0 & \cdots & \sigma^2_{GTxx,n} \end{bmatrix}, \quad y = \begin{bmatrix} h_{GTxx,1} \\ h_{GTxx,2} \\ \vdots \\ h_{GTxx,n} \end{bmatrix}$$

$\widehat{x}$	Estimated mean over the water surface heights of the beams [m].
A	Design matrix. *Matrix size:* [n × 1].
Q_{yy}	Variance matrix of the water surface heights of the beams. *Matrix size:* [n × n].
σ_{GTxx}	MAD of the passing beam (GT1L, GT1R, GT2L, GT2R, GT3L and GT3R) in meters [m].
y	Water surface heights of the beams. *Matrix size:* [n × 1].
n	Amount of beams that passed the lake (with a maximum of 6 beams) [-].
h_{GTxx}	Estimated height of a passing beam (GT1L, GT1R, GT2L, GT2R, GT3L and GT3R) in meters [m].

This method also determines the variance (Q_{xx}) of the mean water surface height per ICESat-2 passing ($\hat{x}$). Equation 4.5 shows the computation of the variance. The standard deviation of the mean water surface height could be determined by taking the square root of the variance, see Equation 4.6.

$$Q_{xx} = (A^T Q_{yy} A)^{-1} \tag{4.5}$$

$$\sigma_{\hat{x}} = \sqrt{Q_{xx}} \tag{4.6}$$

where:

Q_{xx} Variance matrix of the estimated mean water surface heights of the beams *Matrix size:* [1 × 1].
$\sigma_{\hat{x}}$ Standard deviation of the estimated mean surface heights of the beams [m].

However, it is possible that the spread of the beams is larger than the computed standard deviation ($\sigma_{\hat{x}}$) of the mean water surface height ($\hat{x}$). As a result the computed standard deviations are too optimistic, therefore the spread of the beams is also taken into account. The spread of the beams is computed in Equation 4.7.

$$\sigma_{beams} = \sqrt{\frac{1}{n}\sum_{i=1}^{n}(h_{GTxx,i} - \mu)^2} \tag{4.7}$$

where:

σ_{beams} Spread of the beams [m].
μ Mean of the height of the beams [m].

So since it is possible that the spread of the beams is larger than the standard deviation of the estimated mean surface heights of the beams, both are compared. The largest of the both computed values will be used as the error of the mean water surface height per ICESat-2 passing. This is shown in Equation 4.8.

$$\begin{cases} \text{if: } \sigma_{\hat{x}} > \sigma_{beams} & \text{then: Error} = \sigma_{\hat{x}} \\ \text{if: } \sigma_{\hat{x}} < \sigma_{beams} & \text{then: Error} = \sigma_{beams} \end{cases} \tag{4.8}$$

The final result is shown in Figure 4.9b. Figure 4.9a shows the result after *step 1* and Figure 4.9b shows the results after *step 2*. The measurements in May 2019 are a good example for the used method, these measurements are marked with an orange circle. The measurements of the beams are relatively far away from each other. The lowest beam of the two beams has a smaller error than the highest beam on May 2019, resulting in that the mean water surface height should be closer to the lowest beam, which is indeed the case in Figure 4.9b. Besides this, the error of both beams are smaller than the distance between the beams, resulting that the spread of the beams should be used as error, therefore the error in Figure 4.9b is larger than the error of both individual beams.

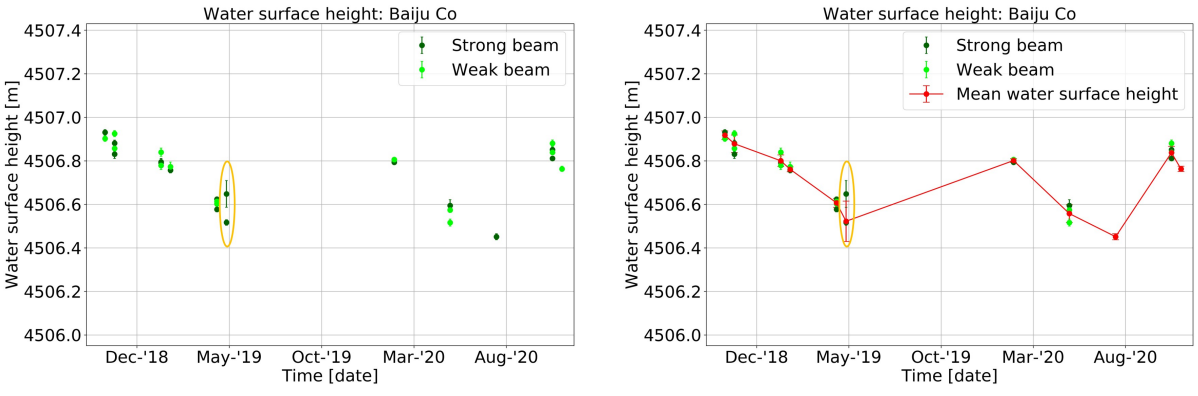

(a) (b)

Figure 4.9: (a) Result after *step 1*: Each beam has its own water surface height and its own error (MAD). (b) Result after *step 2*: Water surface height over time of Baiju Co lake. For each ICESat-2 passing the mean (red) over the passing beams (green) is computed.

4.4. River surface heights

This section shows the steps for the determination of the river surface heights. The determination of the river surface heights has a slightly different method due to the fact that rivers have a slope. As discussed in Section 3.4, ICESat-2 returns to the same location in theory after two years, for this research only two year of data is available. For lakes, this does not lead to a problem, due to that the surface of a lake is assumed to be flat, leading to a larger reach for ICESat-2 which could provide more passings of ICESat-2 over the lake within the two years. This is different for rivers, since rivers have a slope, particularly in the mountainous area. This is illustrated in Figure 4.10 in extreme conditions. The height measurements of ICESat-2 have the geoid as reference. Assuming a constant geoid, the height measurements of the river on location 1 and 2 are different and therefore not possible to compare.

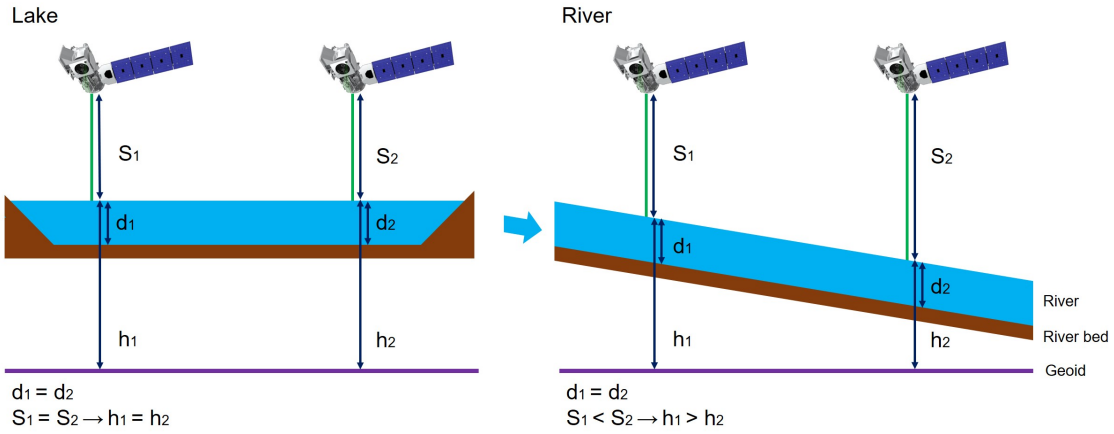

Figure 4.10: The height measurements of ICESat-2 have the geoid as reference. Lakes are assumed to be flat and therefore measurements on several locations in the lake could be compared. However, rivers have a slope. Assuming a constant geoid, the height measurements on location 1 and 2 are different and therefore not possible to compare. ICESat-2 figure from NASA (NDb).

This results in some additional and slightly different steps than already explained for lakes. By evaluating the locations of the ICESat-2 passings in the upper Brahmaputra river, it is found that some locations in the river are more densely packed by ICESat-2 passings. Figure 4.11 shows an example of one of these locations. In this figure nine passing beams could be distinguished, for each passing beam a different colour is given. ICESat-2 passes this location six times and includes nine beams. The distance between these passing beams is in this case approximately 100 meters and therefore the slope in the river could be neglected. For this reason it is chosen to find more locations like shown in Figure 4.11 and compare the ICESat-2 passings on these locations.

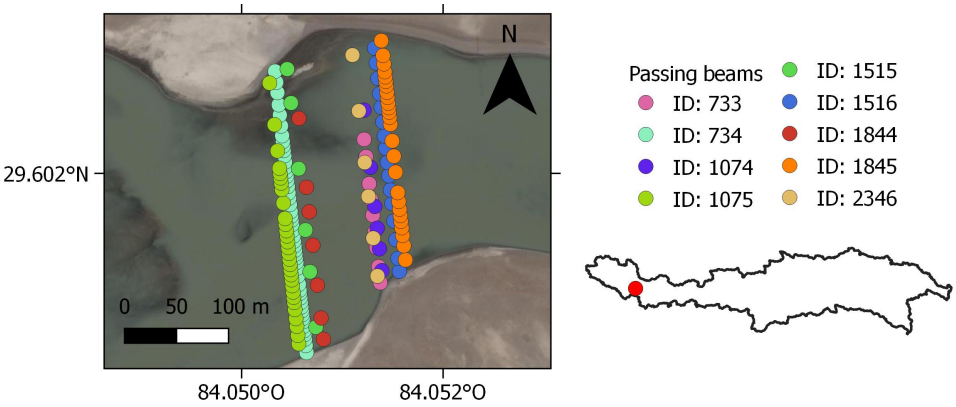

Figure 4.11: Nine passing beams over the river could be distinguished, each beam is given a different colour. Note that this figure includes weak and strong beams.

Figure 4.1 showed that determining the river surface heights consists of five steps. The steps for determining the river surface heights are shown in Figure 4.12. First in step 1, the location of the passing beams of ICESat-2 in the river profile is determined. In step 2 clusters of passing beams are determined. Whereafter, in the step 3, the slope of the cluster locations will be checked. In step 4, the median of the ATL13 observations of one passing beam of ICESat-2 is estimated. Finally, the weak and strong beam pairs are averaged to one water surface height since they have passed the same river location at the same time. This will result in one water surface height per ICESat-2 passing and eventually timeseries can be created.

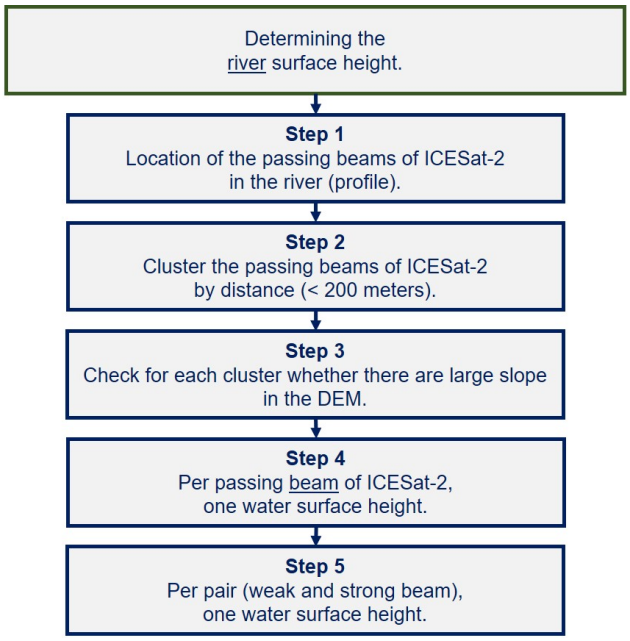

Figure 4.12: The steps for a timeseries of the river surface heights. First in step 1, the location of the passing beams of ICESat-2 in the river profile is determined. In step 2 clusters of passing beams are determined. Whereafter, in the step 3, the slope of the cluster locations will be checked. In step 4, the median of the ATL13 observations of one passing beam of ICESat-2 is estimated. Finally, the weak and strong beam pairs are averaged to one water surface height since they have passed the same river location at the same time.

Step 1: Location of the passing beams of ICESat-2 in the river (profile).
Before the location of the passing beams of ICESat-2 in the river profile could be determined, the river profile itself should be created. For the determination of the elevation of the river, SRTM data with a resolution of 30 meter is downloaded with an absolute vertical accuracy of 16 meters (USGS and EROS, 2015) from the year 2015. This is the same data as in Figure 2.1, but with a better resolution. It is possible that some of these satellite images misses some data, it should be checked whether this is a problem for the extraction of the river profile. The elevation data consist of 1 degree tiles, which means that several tiles need to be downloaded.
This data consist of the elevation of the whole upper Brahmaputra basin, but only the elevation of the river is of interest here. To reach this, the river vector line of GRWL (see Section 4.1) is first converted to points with a maximum distance of 30 meters, this is illustrated in Figure 4.13. The distance between the points is computed and eventually accumulated. Thereafter, for each of those points the elevation of the DEM is extracted. The result is shown in Figure 4.14, the start of the river (0 km) is the approximate origin of the upper Brahmaputra river.

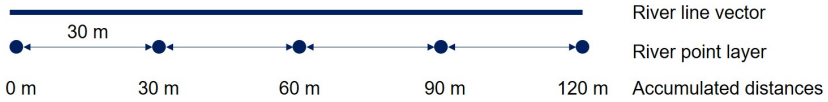

Figure 4.13: The river line vector is converted to a point layer and the distances between the points are accumulated.

From the result could be obtained that at the location of 1800 kilometers distance, the elevation start to decrease fast. A possible explanation for this, is the ending of the Tibetan Plateau. Also some gaps are visible at this location, this has to do with missing data in the SRTM data.

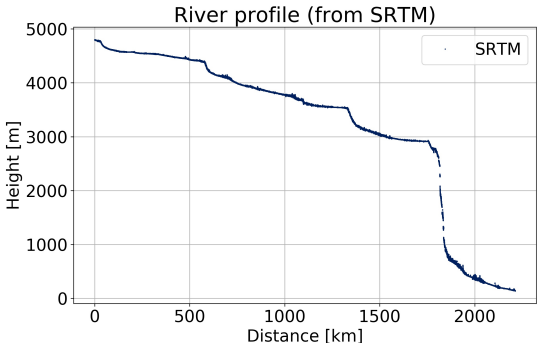

Figure 4.14: The river profile based on SRTM data (USGS and EROS, 2015) and the river vector line of GRWL (Allen and Pavelsky, 2018)

Each passing beam of ICESat-2 has a location in the river with as reference the approximate origin of the Brahmaputra river (0 km). For each passing beam the distance to this most upstream point in the river is determined. This is illustrated in Figure 4.15. The location of the origin of the Brahmaputra river and the location where one of the beams of ICESat-2 passes the river are marked with a red dot. The distance which is computed for each beam is shown by an orange line.

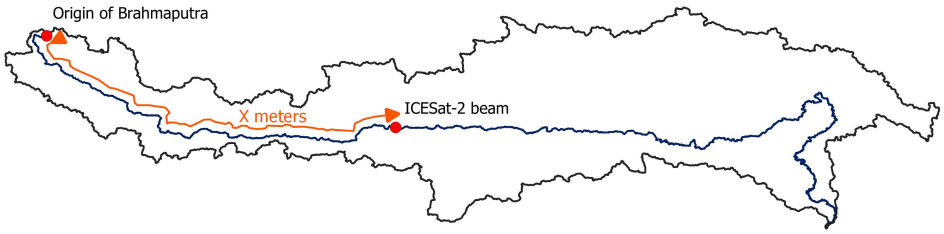

Figure 4.15: For each passing beam the distance to the origin of the Brahmaputra river is determined. The distance is shown in orange.

This is done by computing the nearest neighbour of the location of the passing beam by using the smallest distance to the DEM points of the river profile shown in Figure 4.14. This river profile consists of many DEM points which all have a latitude and longitude. The distance between two points (location of the passing beam and each DEM point in the river profile) is computed using the Haversine formula (Chopde and Nichat, 2013), shown in Equation 4.9.

$$\Delta\text{lat} = \text{lat}_1 - \text{lat}_2$$

$$\Delta\text{long} = \text{long}_1 - \text{long}_2$$

$$a = \sin^2\left(\frac{\Delta\text{lat}}{2}\right) + \cos(\text{lat}_1)\cdot\cos(\text{lat}_2)\cdot\sin^2\left(\frac{\Delta\text{long}}{2}\right) \tag{4.9}$$

$$c = 2\cdot\text{atan2}(\sqrt{a}/\sqrt{1-a})$$

$$\text{d} = \text{R}\cdot\text{c}$$

where:

lat_1	Latitude of a point location in the river [deg].
long_1	Longitude of a point location in the river [deg].
lat_2	Latitude of one passing beam of ICESat-2 over the river [deg].
long_2	Longitude of one passing beam of ICESat-2 over the river [deg].
R	Radius of the Earth [m].
d	Distance between point 1 and point 2 [m].

This leads to a location for each passing beam of ICESat-2 in the river profile. This is illustrated in Figure 4.16. The red dots are the passing beams of ICESat-2. By comparing the river profile with the location of the passing beams, it can be concluded that the measurements of ICESat-2 follow the river profile, only some outliers are visible.

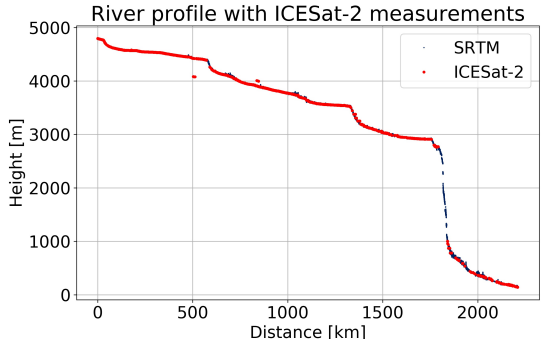

Figure 4.16: The locations of the ICESat-2 beams in the river (profile).

Step 2: Cluster the passing beams of ICESat-2 by distance (<200 meters).
By analysing all the ICESat-2 beams passing the upper Brahmaputra, it became clear that some locations in the river have more densely packed beams, an example was already shown in Figure 4.11. For extracting the locations (also called *clusters*), the distance between each passing beam must be computed. For example, the distance between for ID: 733 and beam ID: 743 in Figure 4.11, is approximately 90 meters. The distance between the most outer beams (beam ID: 1075 and beam ID: 1845) is less than 100 meters, which means that the distances between all the passing beams is less than 100 meters. The total amount of locations is depended on the maximum allowed distance between the passing beams. Another important factor whether a location will be further analysed is the amount of ICESat-2 passings. If ICESat-2 passed a location only once, no comparison in time could be done on that location. The total amount of locations is analysed by comparing the amount of ICESat-2 passings over each location and the maximum distance between the passing beams for each location, see Table 4.2.
From the table one sees that less locations are available if the cluster should require more ICESat-2 passings over the location. Also the smaller the maximum distance between the passing beams, the less locations are available to use further in this research. The maximum distance is of importance because a too high maximum distance between the passing beams will lead to a larger difference in slope in the river. However, a too low maximum distance between passings beams will lead to exclusion of beams leading to a lower amount of ICESat-2 passings. This leads to a trade-off between the maximum distance and the amount of ICESat-2 passings.

Table 4.2: Amount of locations with the thresholds distance and amount of ICESat-2 passings.

Maximum distance between passing beams	**At least 3 satellite passings**	**At least 4 satellite passings**	**At least 5 satellite passings**
100 m	70	12	3
200 m	104	32	6
500 m	162	54	15
1000 m	201	99	46

It is chosen to use in this research a maximum distance of 200 meters between passings beams. The maximum distance of 100 meters will lead to significantly less amount of locations and for the maximum distance of 500 meters, the slope of the river will play a much larger role and therefore larger errors are expected. Although, it would be interesting to determine the errors with another maximum distance between the passing beams.

Step 3: Check for each cluster whether there are large slopes in the DEM.
It is possible that within a cluster, the slope is not negligible. Since it is chosen to use a maximum distance of 200 meters between the passing beams, a slope of 0.0001 meter/meter would result into a maximum height difference of $200 \cdot 0.0001 = 0.02m$, which is a negligible amount. However, if the slope will be an order larger, the maximum height difference will be 0.2 meters, which is not negligible anymore and would affect the water surface heights too much. For this reason, the slope from 5 kilometers upstream of the cluster location till 5 kilometers downstream of the cluster location is estimated as shown in Figure 4.17. This is done by using the river profile derived in *step 1*. The DEM from which the river profiles is derived, has an absolute vertical accuracy of 16 meters, only consist of integer numbers and has a resolution of 30 meters. This leads to a general understanding of the river profile, but is not accurate enough to determine the exact elevation of the river. By determining the slope of the river on the cluster locations, some locations with too large slopes will be filtered out. It is chosen to still compute the slope based on the DEM with a relatively low quality, such that locations as for example on the steep slope around 1800 kilometers in Figure 4.14 will be filtered out and not considered further. But it is very important to know that this would give only an indication of the real river slope.

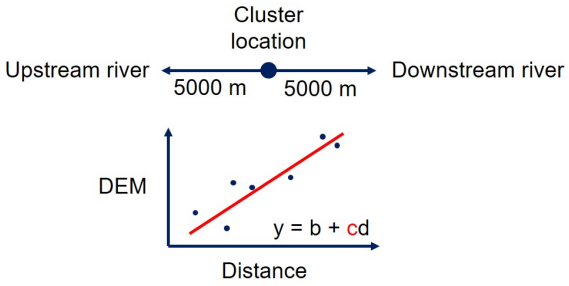

Figure 4.17: From 5 kilometers upstream of the cluster location in the river till 5 kilometers downstream of the cluster location in the river the slope through the DEM elevations in the river will be estimated.

Through the DEM elevations a line is fitted. An approach to do this is least square estimates, which means that the coefficients are estimated with Equation 4.11. The least square estimate is based on minimizing the sum of the squared errors. The red line in Figure 4.17 consist of an offset (b) and a slope (c), which are both unknown and estimated by least square estimates.

$$y = b + cd \quad \rightarrow \quad y = \underbrace{\begin{bmatrix} 1 & d_1 \\ \vdots & \vdots \\ 1 & d_n \end{bmatrix}}_{A} \underbrace{\begin{bmatrix} b & c \end{bmatrix}}_{\hat{x}} \tag{4.10}$$

$$\hat{x} = (A^T A)^{-1} A^T y \tag{4.11}$$

where:

y	DEM elevations (observations) [m]
b	Unknown offset [m]
c	Unknown slope [m/m].
d	Distance, in this case 0 till 10.000 meters [m].
A	Design matrix [-]. *Matrix size:* [n × 2].
$\hat{x}$	Matrix of estimated slope [m/m] and offset [m] *Matrix size:* [1 × 2].

If the computed slope is equal or smaller than 0.0001 meter/meter, the cluster is further used, otherwise the cluster will be removed and not further analysed. From the 32 locations left in the previous step, only 11 locations are left after checking the slope. The water surface heights will be estimated with ICESat-2 for the 11 locations shown in Figure 4.18.

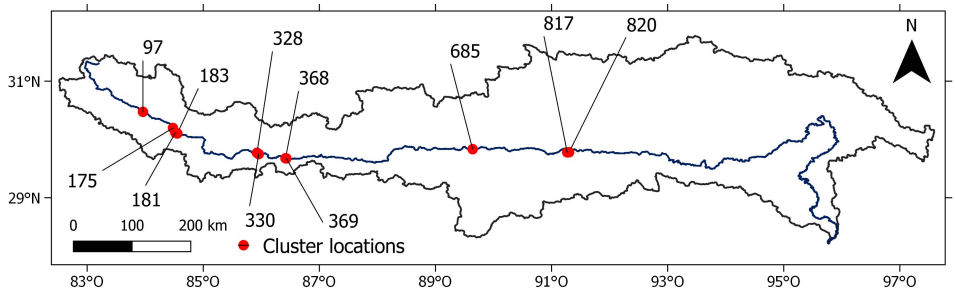

Figure 4.18: The locations of the clusters which are at least four times passed by ICESat-2 and have a slope smaller than 0.0001 meter/meter in the study area.

Step 4: Per passing beam of ICESat-2, one water surface height

Step 4 for river surface heights is almost the same as *step 1* for lake surface heights. In this step, the median and MAD are estimated for each passing beam leading to one surface height per passing beam, however the measurements of the river are sometimes dominated by the variation in the river cross-section. Figure 4.19 shows an example of the variation in river cross-section. This river cross-section profile could be divided into five parts. The five parts are indicated in the figure in red. The most left part (1) of the river cross-section is a higher elevated area, which is probably the shore of the river. The second part (2) has a lower elevation, third (3) again a higher elevation, fourth (4) lower and the fifth (5) higher again. The figure shows the ATL13 observations and the photons of the strong beam. The MAD interval is shown as a transparent band.

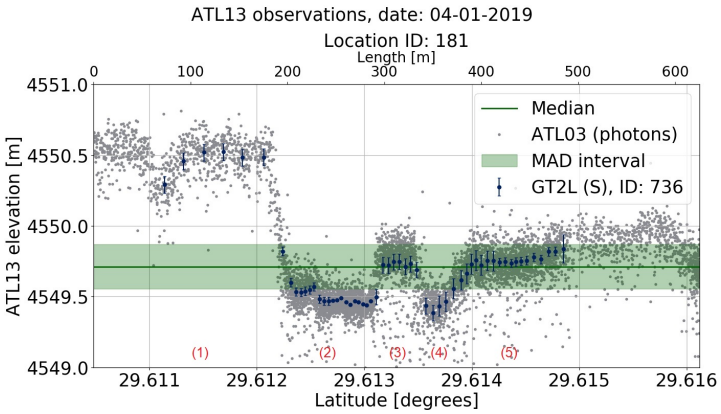

Figure 4.19: ATL13 observations of one strong beam passing the river. The observations are dominated by variation and higher and lower plateaus are visible. The photons are also indicated to get a better understanding of the river cross-section profile, but note that these are not used for the estimation of the water surface height. The MAD interval is shown as a transparent band.

A possible explanation for the variation in the elevation is the exposure of bars. Some months of the years the water surface height of the river is higher than other months. This could lead to the exposure of bars on some locations of the river, affecting the ATL13 observations. The exposing bars are illustrated in Figure 4.20.

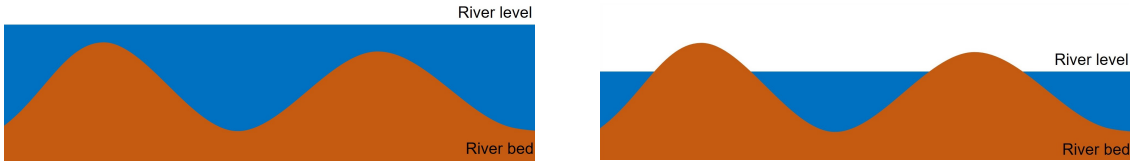

(a) (b)

Figure 4.20: The exposure of bars. (a) If the water surface height in the river is high, the bars are submerged and won't be visible in the observations of ATL13, the water surface will be flat. (b) If the water surface height in the river is low, the bars will be exposed and will be visible in the ATL13 observations.

This problem is tackled by assuming that the lower parts (part (2) and (4) in Figure 4.19) in the river cross-section represent the water surface and the higher parts (part (1), (3) and (5) in Figure 4.19) the bars or shorelines. Since only the ATL13 observations of the water surface are of interest, only the lowest parts should be extracted and used for the determination of the water surface height. For extracting only the observations of the water surface, for each passing beam a histogram of the ATL13 observations is computed. Of all the ATL13 observations of one beam a histogram is computed of the ATL13 elevation with a bin size of 0.1 meters. An example of a histogram is shown in Figure 4.21, which is the histogram of the observations of Figure 4.19.

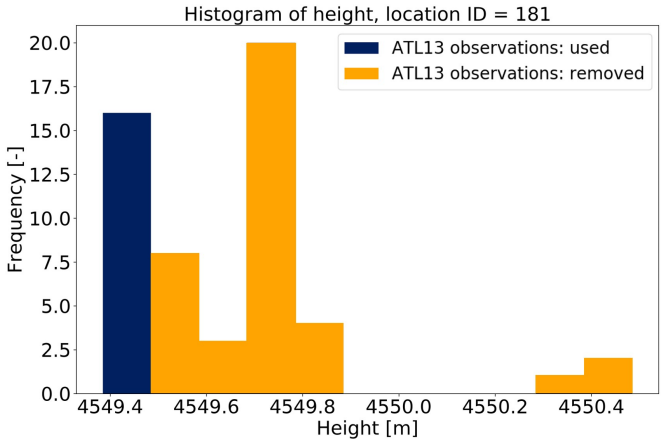

Figure 4.21: Histogram of the height observation of Figure 4.19. The observations within the lowest bin have been assumed to be water observations.

Since it is assumed the lowest parts are often the water surface, all the ATL13 observations from the lowest bin are used for the computation of the water surface height. This would mean that all the ATL13 observations between 4549.4 and 4549.5 meters (marked in blue in Figure 4.21) will be used for the computation of the median. It is possible that outliers are present which are likely the subsurface or the bottom that were not removed by their Subsurface Anomaly Quality Flag (as described in Section 4.2). If the lowest bin consist of only one ATL13 observation or the two following bins do not contain any ATL13 observation, the next not empty bin is used for estimating the median over the ATL13 observations. This is repeated till a bin is found which follow these two condition.

In Figure 4.22 the used ATL13 observations are marked in blue and the other ATL13 observation which are not used are marked in orange. The median of the ATL13 observations is computed again, but now only over the blue ATL13 observation. The median is shown as a green line. The estimated median in this figure is closer to the lower plateau than the estimated median of all observations as in Figure 4.19. The difference in median between without removing ATL13 observations and with removing ATL13 observations is approximately 0.25 meters.

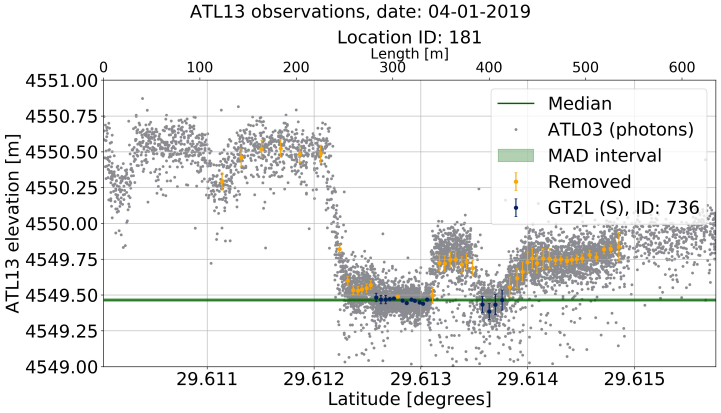

Figure 4.22: The ATL13 observations of the lowest bin are used, (blue) for the computation of the median. The ATL13 observations which are removed are shown in orange.

Step 5: Per pair (weak and strong beam), one water surface height
Step 5 is slightly different from *step 2* for lakes. Instead of computing the mean over the possible six beams, the mean water surface height is computed over the pairs within a cluster. So the mean of the weak and strong beam (if both the weak and strong beam are present) is determined. This will lead to one water surface height for each ICESat-2 passing of the cluster location. The method to determine the mean water surface height is almost the same as for lakes, therefore a more detailed explanation of determining the mean water surface height can be found in Section 4.3 in *step 2*. The only difference for this computation of the mean water surface height is that the mean is not depended on the matrix Q_{yy}, since the MAD value is not representative, which changes Equation 4.4 into Equation 4.12. The weak (light green) and strong (dark green) beams are shown in figure 4.23b. The computed means of the beams are shown in red.

$$\hat{x} = (A^T A)^{-1} A^T y \tag{4.12}$$

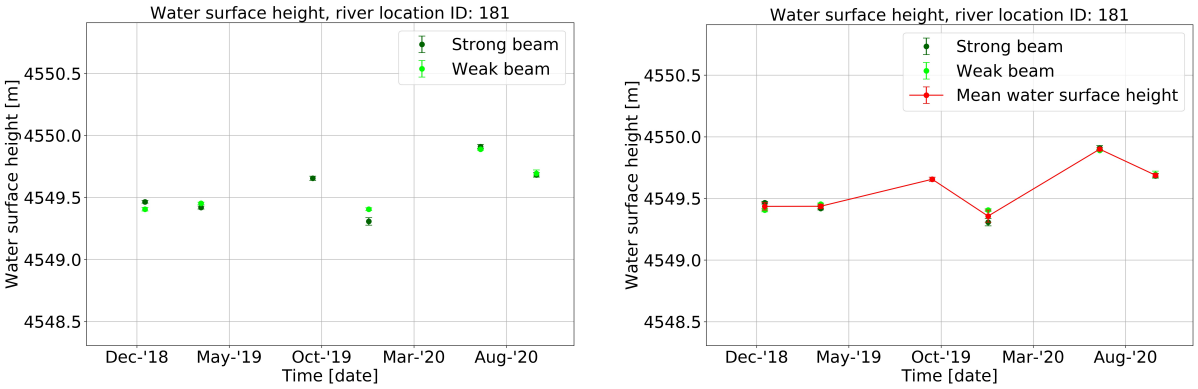

(a) (b)

Figure 4.23: (a) Result after *step 4*: Each beam has its own water surface height and its own error (MAD). (b) Result after *step 5*: Water surface height of river location ID:181. For each ICESat-2 passing the mean (red) over the passing beams (green) is computed.

4.5. Approach for seasonal differences

This section discusses the last box in the workflow of Figure 4.1, also seen in Figure 4.24. Based on the results from the lake surface heights (Section 4.3) and the river surface heights (Section 4.4), a conscientious attempt is done to determine the seasonal differences in water surface heights.

Figure 4.24: This section presents an approach for determining the seasonal differences, which is the last part of the workflow in Figure 4.1.

It is seen in Section 3.2 that the river discharges, and therefore also the water surface heights, are the lowest in February and the highest in August. Therefore, for determining the seasonal differences, the water surface height differences (ΔWSH) between February and August of each year for each lake or each river location are computed. Since ICESat-2 data from September 2018 till November 2020 is used, the seasonal difference of two years can be computed, these are shown in Equation 4.13.

$$\begin{aligned} \Delta WSH_{2019} &= h_{\text{August,2019}} - h_{\text{February,2019}} \\ \Delta WSH_{2020} &= h_{\text{August,2020}} - h_{\text{February,2020}} \end{aligned} \tag{4.13}$$

Not all lakes or river locations will have an ICESat-2 measurement in both February and August, in that case no ΔWSH_{2019} and/or ΔWSH_{2020} can be computed. Another possibility is that a lake or river location will have more than one measurement in February or August. In case more measurements are present in February, the lowest water surface height in that month is used and in case more measurements are present in August, the highest water surface height in that month is used.

5

Results and interpretation of the water surface heights based on ICESat-2

This chapter presents and discusses the results for the water surface height for lakes in the study area and for the upper Brahmaputra river by using ATL13 of ICESat-2. The aim of this research is to determine the water surface heights and their errors for lakes and rivers based on ICESat-2 data. With these water surface heights, it is examined whether it is possible to generate a generic water surface height curve, which shows the (seasonal) variation of water surface over a year. In the months November until March low water surface heights are expected due to the dry and winter season. Conversely, in the months May until September the water surface heights are expected to be high due to the wet and summer season. The results and interpretation of the water surface heights of lakes in the upper Brahmaputra and Nam Co basin and the upper Brahmaputra river are separately discussed in Section 5.1 and 5.2 respectively. Based on these results, three case studies are applied in Section 5.3: a comparison of the water surface height timeseries between two lakes in the two different basins, a comparison of the water surface height timeseries of a lake nearby the upper Brahmaputra river and lastly a case of a lake neighbouring a glacier.

5.1. Results of lake surface heights based on ATL13

This section discusses the results of the lake surface heights. First the total amount of lakes measured by ICESat-2 is discussed. This is followed by the error of lake surface heights by ATL13, then a comparison of the lake surface heights is made with Hydroweb data, thereafter a seasonal variation in water surface heights is analysed and finally three more detailed examples of timeseries of lake surface heights is discussed.

5.1.1. Total amount of lakes measured by ICESat-2

The study area consists of 621 lakes according to the HydroLAKES database of WWF (Messager et al., 2016). In total 299 lakes are passed by ICESat-2 in two years time, which are shown in Figure 5.1.

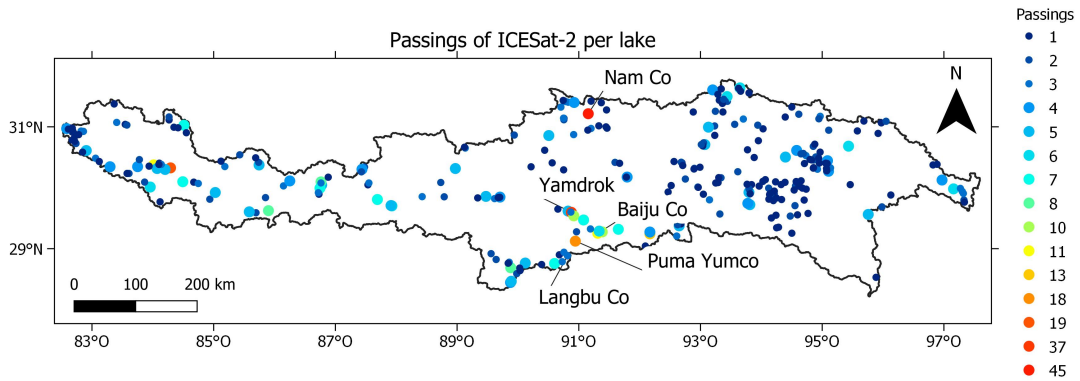

Figure 5.1: The amount of passings of ICESat-2 per lake in a period of two years.

As discussed in Chapter 3, ICESat-2 has a ground-track spacing of 3.6 kilometers. This ground-track spacing is the smallest of all discussed satellite altimeters in Section 3.3. A small ground-track spacing will result that the satellite will pass more lakes than in case of a larger ground-track spacing. ICESat-2 will therefore pass the most amount of lakes of all discussed satellite altimeters. ICESat-1 was for example only capable of measuring six lakes in the area, indicating the better spatial resolution of ICESat-2 compared to ICESat-1.

Amount of passings

Table 5.1 shows the total amount of lakes in the study area subdivided by area. 72% of the lakes in the study area have an area of 0.5 km^2 or smaller. The second column shows the amount of lakes which are passed and measured by ICESat-2. It should be noted that only the ICESat-2 passings resulting in a water surface height measurement are taken into account. The third and fourth column shows the amount of lakes which are passed at least four or eight times by ICESat-2 respectively. 64 lakes are passed at least four times by ICESat-2 and 13 lakes are passed at least eight times by ICESat-2. The table shows that the largest lakes have a higher chance to be passed by ICESat-2 more often than the smaller lakes. This is logical, because of the lower chance of ICESat-2 passing lakes with a small area compared to large area lakes.

Table 5.1: Lakes subdivided by area. Note that only the amount of ICESat-2 passings resulting in a water surface height measurement are taken into account.

	Total amount of lakes in the lake mask	**Amount of lakes passed by ICESat-2**	**Amount of lakes passed at least 4 times by ICESat-2**	**Amount of lakes passed at least 8 times by ICESat-2**
< 0.5 km^2	448	168	11	0
0.5 - 1.0 km^2	77	47	3	0
1.0 - 10 km^2	78	66	32	2
10 - 50 km^2	12	12	12	6
> 50 km^2	6	6	6	5
Total	621	299	64	13

Interpretation

From the previous alinea can be concluded that ICESat-2 is a suitable mission in sense of determining water surface heights for a high amount of lakes including lakes with an area of smaller than 0.5 km^2. Due to the high spatial resolution of ICESat-2, 48% (=299/621) of the lakes in the study area could be measured. Multiple lakes with an area of smaller than 0.5 km^2 are measured by ICESat-2 and even a few of them are passed at least four times by ICESat-2 in two years.

Height of the lakes

ICESat-2 is thus capable of measuring the water surface heights of 48% of the lakes in the upper Brahmaputra and Nam Co basin. Figure 5.1 shows that most of the lakes are passed only once by ICESat-2 in a period of two years. For these lakes never a generic water surface height curve could be determined, but these measurements do give information about the mean height of these lakes. For each lake the mean water surface height in two years time is determined. Figure 5.2 shows the results.

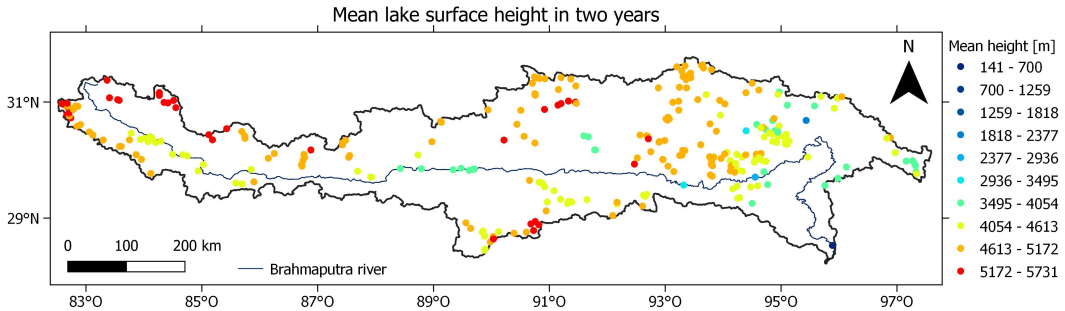

Figure 5.2: The mean water surface height in two years time of each lake based on the ATL13 measurements of ICESat-2 with respect to the geoid EGM2008.

Interpretation
The high spatial resolution of ICESat-2 is at the cost of the amount of passings per lake. Only 13 of the 621 lakes are passed at least eight times in a period of two years. Therefore, for most of the lakes a generic water surface height curve will be difficult to determine based on the ICESat-2 data. However, the ICESat-2 measurements of these lakes do give information about the height of these lakes. Figure 5.2 shows some clusters of elevations. In the western part of the basin a clear distinction is visible between the lakes at the edge of the basin and the lakes near the river.

Amount of passings per month
Only the ICESat-2 passings resulting in a water surface height measurement are taken into account. It is possible that ICESat-2 passes a lake, but due to cloud cover or due to too large standard deviations, no water surface heights are determined. The amount of passings by ICESat-2 resulting in a water surface height measurement are determined per month and is shown in Figure 5.3.

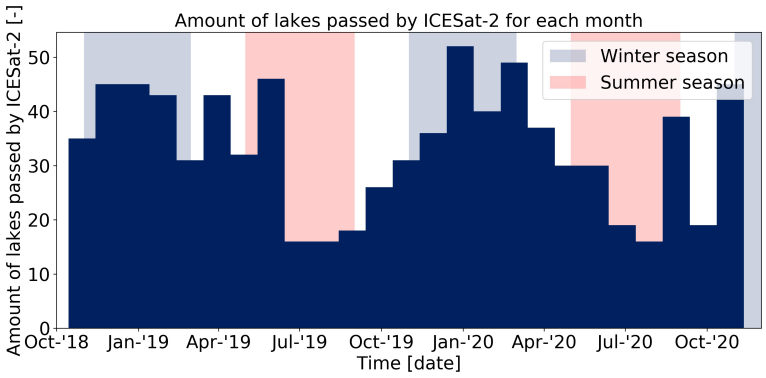

Figure 5.3: Amount of lakes passed by ICESat-2 for each month.

Interpretation
The high spatial resolution of ICESat-2 is an advantage of this mission. However, a drawback of a laser mission is that it is not possible to penetrate through clouds resulting in less measurements during cloudy months. This effect is visible in Figure 5.3. The figure shows a distinction between the months January and July. In the months around January more lakes are passed by ICESat-2 compared to the months around July. In both 2019 and 2020 a minimum around the months of July is visible in the amount of lakes passed by ICESat-2. This could have been caused by cloud cover. During the summer monsoon (May - September) the area will be largely covered by clouds resulting in less successful water surface height measurements.

Conclusion about the amount of passings of ICESat-2
Based on the amount of ICESat-2 passings, ICESat-2 is thus a suitable mission of determining water surface heights for an high amount of lakes due to its high spatial resolution, but seems less suitable for determining a generic water surface height curve due to its low amount of passings per lake.

5.1.2. Error of ATL13 lake surface height measurements
This section discusses the error of the lake surface heights. First the precision per beam is evaluated, followed by the evaluation of the error per ICESat-2 passing.

Precision per beam
In total 1902 beams pass a lake in the study area. From the total amount of beams passing a lake, 888 beams are weak and 1014 are strong. For each individual beam the MAD values are computed to evaluate the precision of the beams. The precision per beam is defined as how close the ATL13 observations are to each other. The method is discussed in Section 4.3. Figure 5.4a and Figure 5.4b show histograms of the MAD values. The colours in Figure 5.4a indicate the lake area for which the MAD is computed and the colours in Figure 5.4b indicate the the weak and strong beams. Note that there is no distinction between lakes or location. Of the total amount of beams 90% have a MAD value of lower than 0.05 meters and 98% of the beams have a MAD value of lower than 0.1 meters. The smaller the MAD value, the smaller the spread of the ATL13 observations,

the higher the precision of the ATL13 measurements. A significantly small amount of beams have a MAD value of larger than 0.2 meters, these are not shown in the figures.

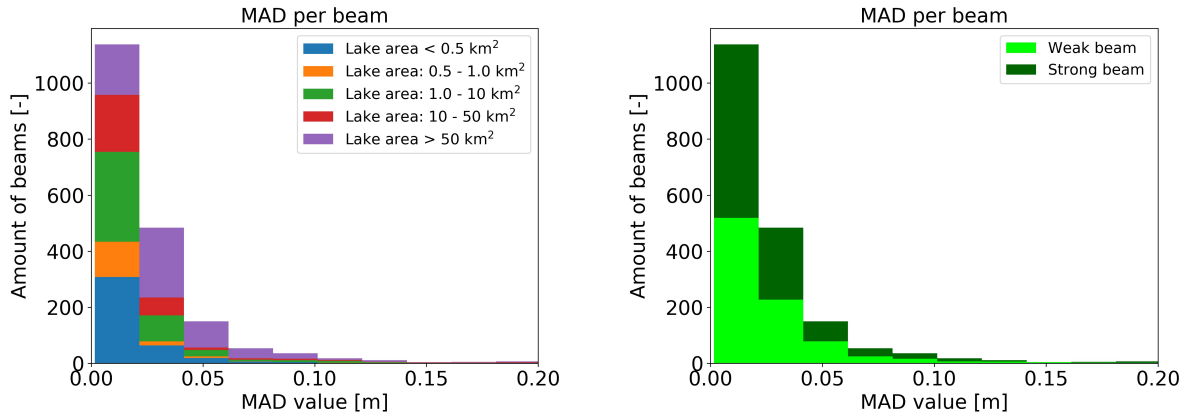

(a) (b)

Figure 5.4: (a) Histogram of the MAD value per beam. The colours indicate the lake area size of which the water surface height is computed. It should be noted that larger sized lakes will be passed by more beams than smaller sized lakes. (b) Histogram of the MAD value per beam. The colours indicate the weak or strong beams.

Interpretation

Figure 5.4 shows that the larger the MAD values are, the larger the contribution of the beams from a lake with an area larger than 50 km^2 is, applying only for MAD values until 0.2 meters. This suggest that the larger sized lakes will have a larger error compared to the smaller sized lakes. The MAD values do not show any dependency for the weak or strong beam. The MAD values of higher than 0.2 meters do not show a dependency on the lake area or for the weak or strong beam. Reasons for these larger MAD values could be wind set-up or geoid influences resulting in slopes in the water surface. Another reason for these large values is due to that some lakes in the lake mask are part of rivers and often have a length of more than 1 kilometer. As was explained in Section 4.4, the river surface heights should be determined differently due to the presence of a slope and the possible bars within the river bed.

Thus, the MAD values for 90% of the total amount of beams have a MAD value of lower than 0.05 meters and 98% of the beams have a MAD value of lower than 0.1 meters. These values indicate that the precision for most of the beams is 0.1 meters.

Error of the ATL13 measurement per ICESat-2 passing

Section 4.3 discussed the method for the computation of the error for each ICESat-2 passing. Figure 5.5 shows the errors per ICESat-2 passing. The colours of Figure 5.5a indicate the lake area size. Figure 5.5b shows the same error per ICESat-2 passing but shows the dependency on the amount of beams per ICESat-2 passing. A significantly small amount of ICESat-2 passings have an error of larger than 0.2 meters, these are not shown in the figures.

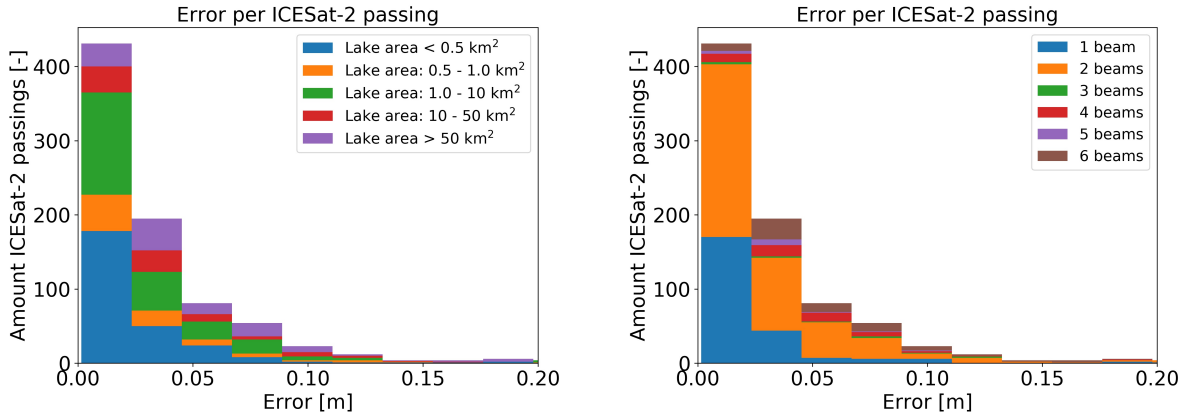

(a) (b)

Figure 5.5: (a) Histogram of the error per ICESat-2 passing. The colours indicate the lake area size of which the water surface height is computed. It should be noted that larger sized lakes will have more ICESat-2 passings than smaller sized lakes. (b) Histogram of the error per ICESat-2 passing. The colours indicate the amount of beams over which the water surface height is computed.

Both Figure 5.5a and Figure 5.5b show a large peak at an error between 0.0-0.1 meters. This peak consists of 92% of the amount of ICESat-2 passings of all sized lakes. The errors larger than 0.1 meters do not contain one particular sized lake.
Besides the error per ICESat-2 passing, it is also important to get an insight into the accuracy of the water surface height measurements of ATL13. Accuracy is defined as how close the result is to the true value. Due to the mountainous area, lakes are difficult to reach for in-situ measurements resulting that a conclusion of the accuracy of the water surface height measurements is hard to make. However, the error and the amount of the beams for each ICESat-2 passing could give an indication of the accuracy. The larger the amount of beams over which the water surface height is computed for one ICESat-2 passing, the more it will state over the accuracy of the ICESat-2 passing. If all the beams of one ICESat-2 passing are close too each other it will result in a low error and this will suggest a relatively high accuracy. If all the beams of one passing are spread more widely resulting in a larger error, it will suggest a relatively low accuracy. A lower amount of beams over which the water surface height per ICESat-2 passing is computed, will state less about the accuracy of one ICESat-2 passing. Figure 5.6b shows the amount of beams per ICESat-2 passing. Mostly ICESat-2 passes a lake with only one or two beams. Since the larger amount of beams can give an indication of the accuracy, an histogram with only the errors computed over five or six beams is shown in Figure 5.6b.

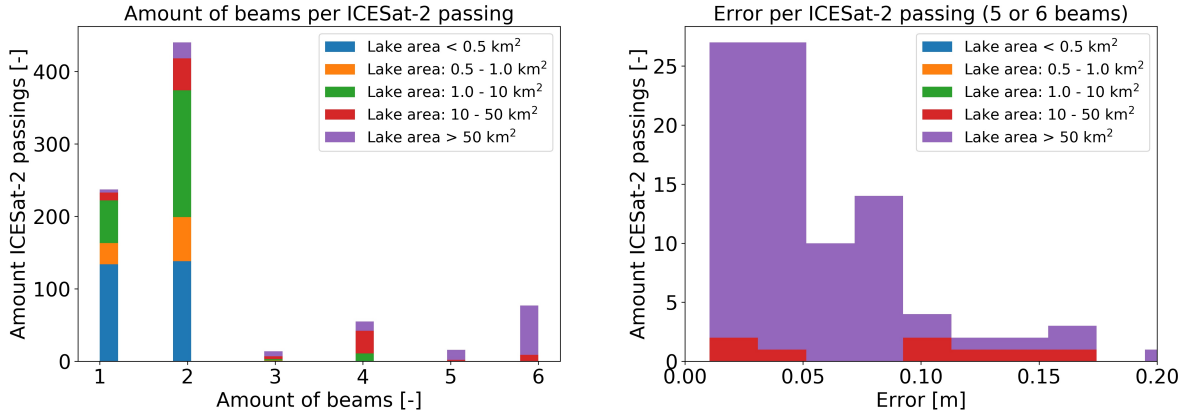

(a) (b)

Figure 5.6: (a) Amount of beams per ICESat-2 passing. ICESat-2 is operating in total with six beams. The amount of beams passing a lake is depended on the size of the lake. (b) Histogram of the error per ICESat-2 passing with five or six beams. The colours indicate the lake area size of which the water surface height is computed.

Interpretation
Figure 5.5a and Figure 5.5b show that the bins of the histograms of the errors do not contain one particular size lake, suggesting that the lake area is not correlated with the lake area size, although a larger error per ICESat-2 passing for a larger sized lake was expected and was found in the MAD values. Also no dependency on the amount of beams could be obtained from Figure 5.5b. A significantly small amount of errors is found to be larger than 0.2 meters. Possible explanations for these large errors are river parts which are marked as lake or a part of a lake that may not contain water during the whole year. An improvement of the lake mask will results that this amount will be reduced. So, beside the outliers in the error per ICESat-2 passing, it can be concluded that most of the water surface heights based on ATL13 have a precision of 0.1 meters.
Figure 5.6a indicates that the amount of beams per ICESat-2 passing per lake and the lake area size are correlated. This is logical because a larger sized lake could be passed by a higher amount of beams per passing than a smaller sized lake. This would also indicate that for a larger sized lake, it will be possible to give an indication of the accuracy of the water surface heights. Figure 5.6b shows that for 75% of the water surface height measurement based on five or six beams the error is smaller than 0.1 meters, indicating a small spread within these five or six beams and therefore also indicating a relatively good accuracy.

Conclusion about the error of the ATL13 lake surface height measurements
Taking all these findings into consideration, it can be concluded that the precision of ATL13 is 0.1 meters. Besides this, for the ICESat-2 passings based on five or six beams a relatively good accuracy is indicated. However, to state something specific about the accuracy in-situ measurements are needed.

5.1.3. Comparison of the lake surface heights with Hydroweb data

Besides evaluating the beams of the lakes, the ATL13 lake surface height measurements for one lake are compared to lake surface height measurements of Theia Data and Services centre for continental surfaces from Hydroweb. The Hydroweb data is created by French institutions involved in Earth observation and environmental sciences (Crétaux et al., 2011). The water surface heights extracted from Theia are processed by the LEGOS (Laboratoire d'Etudes en Géophysique et Océanographie Spatiales) laboratory. The data are composed from multiple satellites (ERS-1, Topex/Poseidon, ERS-2, GFO, Jason-1, Envisat, Jason-2, Saral/Altika, Sentinel-2A, Sentinel-2B) from 1992 to present and has been corrected for solid Earth tide, pole tide, ionospheric delay, wet and dry tropospheric delay and altimeter biases.

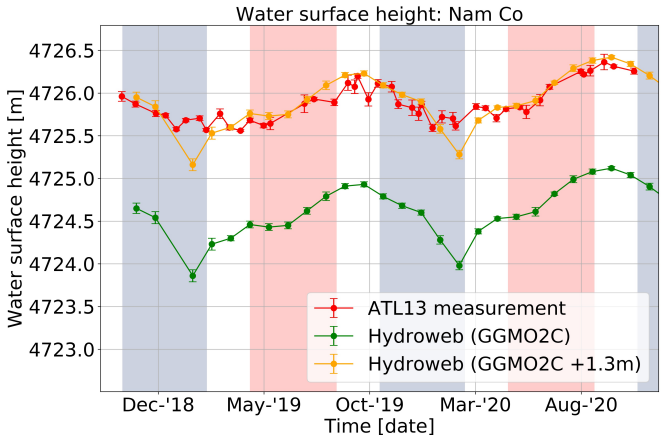

Figure 5.7: Comparison of water surface height measurements of ICESat-2 with LEGOS measurements from Hydroweb.

Theia Data Services has data for the largest lake in the study area: lake Nam Co. The water surface heights from Hydroweb are shown in Figure 5.7 for the lake Nam Co. It should be noted that the reference of the measured water surface height is GGMO2C, a global gravity model, whereas the ATL13 water surface height measurement have a reference with respect to Geoid EGM2008. This results in a difference in height. The exact difference between the global gravity model and the geoid model is hard to compute, so a rough number of 1.3 meters is used to shift the original lake surface heights of Hydroweb (green) approximately to the same height as the lake surface heights of ATL13 such that the water surface heights overlay each other and the variation of the different sources can be compared.

Interpretation
It is found that the variation found by ATL13 water surface height measurements follows the variation of the Hydroweb data. The Hydroweb measurements roughly match the ATL13 measurements, although the Hydroweb measurements are smoother. An important note is that the measurements of Hydroweb are not from water gauges, but are measured by satellites, meaning that this comparison could not say something about the accuracy. But the comparison shows a similar variation of the water surface height which indicates that the variation measured by ICESat-2 is most probably real.

5.1.4. Seasonal variation of lake surface heights

As stated in Section 5.1.1, ICESat-2 will be less suitable for determining a generic water surface height curve, but a seasonal variation might be visible by determining the difference in water surface height between February and August. For each lake the difference in water surface height between February and August is determined for the years 2019 and 2020. The chance that ICESat-2 passes a lake exactly in both these months is small, therefore only for a few lakes could be considered. The results of differences in water surface heights for 2019 are shown in Table 5.2 and for 2020 in Table 5.3. The water surface height in August is expected to be larger than in February due to the contribution of snow melt, glacier melt and precipitation of the summer monsoon.

Table 5.2: Water Surface Heights (WSH) for February and August in 2019. The Water Surface Height differences are found to be the largest for the largest sized lake. It shows a minimum difference in Water Surface Height for several lakes.

Lake ID [-]	**Area [km^2]**	**February 2019**		**August 2019**		**ΔWSH 2019**
		WSH [m]	Beams [-]	WSH [m]	Beams [-]	
149 (Nam Co)	1963.82	4725.57	5	4725.89	6	0.32
1473 (Yamdrok)	566.97	4438.10	6	4438.44	6	0.34
1380253	0.35	4889.52	2	4889.61	2	0.09
1379893	0.34	4642.21	1	4642.46	1	0.26

Table 5.3: Water Surface Heights (WSH) for February and August in 2020. The Water Surface Height differences are found to be the largest for the largest sized lake. It shows a minimum difference in Water Surface Height for several lakes.

Lake ID [-]	**Area [km^2]**	**February 2020**		**August 2020**		**ΔWSH 2020**
		WSH [m]	Beams [-]	WSH [m]	Beams [-]	
149 (Nam Co)	1963.82	4725.62	4	4726.26	2	0.65
15336	40.50	4571.18	4	4572.61	2	1.42
15337	20.77	4974.81	4	4974.82	2	0.01
15386	13.61	4617.62	2	4617.67	2	0.05
176195	4.04	4572.93	2	4573.06	2	0.13
176193	1.00	4571.85	1	4572.29	2	0.43
1378755	0.92	4291.09	2	4291.76	1	0.67
1377265	0.45	4757.84	1	4758.15	1	0.31
1377280	0.21	4754.73	2	4755.21	2	0.48
1379757	0.19	5076.57	2	5077.15	1	0.58
1377761	0.19	5190.19	1	5190.27	2	0.08
1377790	0.17	4736.72	1	4737.20	1	0.48

Interpretation
Table 5.2 and Table 5.3 show that the amount of lakes passed in February and August is limited. Due to low amount of passings per lake, the chance is low that ICESat-2 passes exactly within these months. The chance that ICESat-2 passes at the moment of minimum water surface height or the maximum water surface height is therefore also low, resulting that the seasonal variation based on ICESat-2 will be difficult to assess. An attempt is discussed by the difference in water surface height between February and August.
Four lakes in 2019 and twelve lakes in 2020 were passed in the months February and August. Nam Co is the only lake which has a difference in water surface height in both 2019 and 2020. The difference in water surface height of Nam Co for 2020 is twice as large as for 2019. However, Figure 5.7 shows that the difference in water

surface height between 2019 and 2020 does not vary that much as computed. Thus, it can be concluded that the computed differences between February and August do not match with the seasonal variation. However, the computed differences do show a minimum seasonal variation of that particular year. If this difference is larger than twice the error of ATL13 of ICESat-2 (0.1 meters), it could be stated that the water surface height indeed increased in August, but the exact seasonal variation will be unknown.
The difference in water surface heights within one year varies from 0.01 meters until 0.67 meters with one outlier of 1.42 meters. This outlier corresponds to the lake with ID 15336. By investigating the google satellite images and the lake mask, it became clear that this lake is actually a part of the river. This was also reason for the higher errors found in Section 5.1.2. It is expected that the larger the area of a lake, the smaller the computed difference. Since larger lakes will need a larger water volume to obtain an increase in water surface height. However, the results do not follow this expectation. Most of the smaller sized lakes, have a smaller difference in water surface height than the larger sized lakes. But as already concluded, the computed values do only show a minimum difference in water surface height meaning that the differences in water surface heights of the smaller sized lakes could be higher than these results show.

5.1.5. Examples of lakes

Three lakes are evaluated in more detail to show the differences in results between different sized lakes. A small, medium and large sized lake are evaluated. First, the small sized lake Langbu Co is analysed. Thereafter the medium sized lake, Baiju Co is analysed. Finally, lake Puma Yumco, which is the third largest lake in the study area. All these three lakes are located in the centre of the study area in longitudinal direction and latitude direction close to the south boundary. The locations of the lakes are earlier marked in Figure 5.1.

Lake: Langbu Co (area of 0.88 km^2)
A small sized lake is Langbu Co which is passed three times by ICESat-2 in two years time. Each individual passing beam over the lake is shown in Figure 5.8a and the timeseries are given in Figure 5.8b. Each colour in Figure 5.8a indicates a different passing beam, several beams are overlaying each other in the figure, but note that this is not the case if the figure is zoomed in more closely.

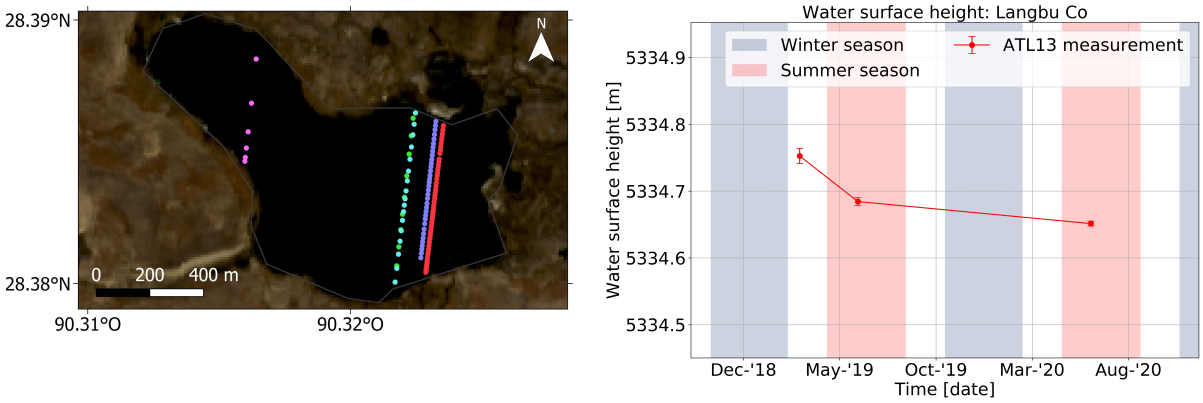

(a) (b)

Figure 5.8: (a) Passing beams over lake Langbu Co. (b) Timeseries of Langbu Co.

Interpretation
This lake is passed only three times by ICESat-2. The errors of the individual ICESat-2 passings are all below 0.02 meters, which is relatively small compared to the found error of the ATL13 measurements in Section 5.1.2. Between the water surface height measurement of June 2019 (second measurement) and the water surface height of June 2020 (third measurement) a gap of one year is visible, resulting in missing several extreme water surface heights. So for this lake a seasonal variation will be difficult to assess and a generic water surface height curve will not be possible to create.
So it can be concluded that the computed errors of the water surface heights of this lake are small. Besides, a seasonal variation for this lake will be difficult to assess, even with longer timeseries due to the large time gaps.

Lake: Bajiu Co (area of 11.7 km^2)
Bajiu Co lake is a medium sized lake. In two years time, this lakes is passed 11 times by ICESat-2 resulting in 29 beams. Each individual passing beam is shown in Figure 5.9a. The timeseries of the measured water surface height by ICESat-2 is shown in Figure 5.9b.

Interpretation
The timeseries of this lake in Figure 5.9b consist of more ATL13 measurements than the previous lake. The error of the ATL13 measurements are all below 0.05 meters, except for the ATL13 measurement in May 2019 where the error is approximately 0.1 meters. This error is caused by a slope in the water surface height. The slope could be caused by wind set-up or geoid fluctuations. Since the other ATL13 measurements have a smaller error indicating that the error is not regular, wind set-up will in this case be more likely.
Although this lake consists of more ATL13 measurements than the previous lake, still a significant gap between May 2019 (sixth measurement) and February 2020 (seventh measurement) is present, which could mean that extreme water surface heights are missing in the data resulting in that a seasonal variation is difficult to assess. Although one sees from the figure that the highest water surface heights occur in the winter season and the lowest water surface heights in the summer season. A difference of approximately 0.25 meters in water surface height between the first winter and summer season is obtained. This difference is larger than the errors of the ATL13 measurements indicating that the water surface heights in the winter season are indeed larger than the summer season.

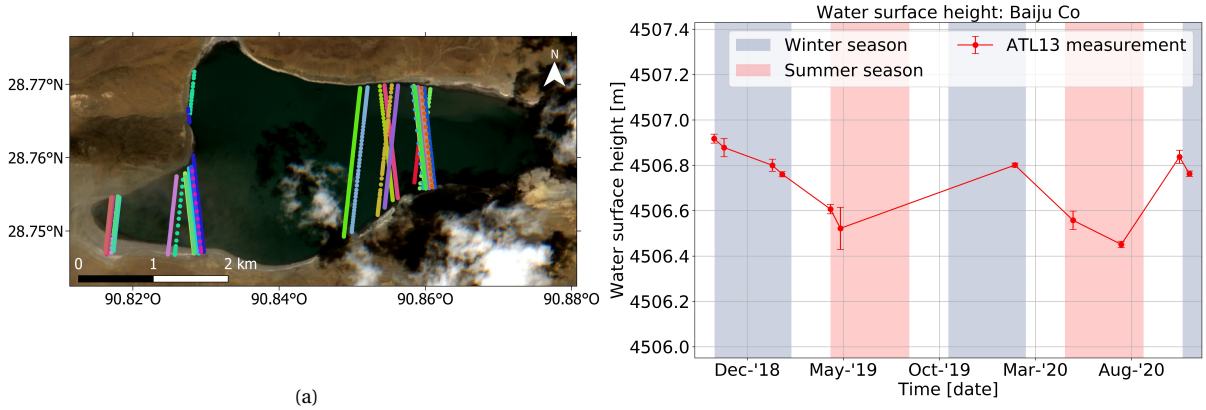

(a) (b)

Figure 5.9: (a) Passing beams over lake Baiju Co. (b) Timeseries of Baiju Co.

Thus, the ATL13 measurements have a relatively small error which indicates a good precision of the water surface heights measurements by ATL13. Due to the large time gaps between some ATL13 measurements, the extreme water surface heights and therefore the seasonal variation will be difficult to assess. But, since the time gaps are not always large, a seasonal variation might be possible to detect, but then longer timeseries are needed.

Lake: Puma Yumco (area of 283 km^2)
Puma Yumco lake is the third largest lake in the study area. In two years time, the lake is passed 18 times by ICESat-2 resulting in 80 beams. The passing beams and the timeseries are shown in Figure 5.10.

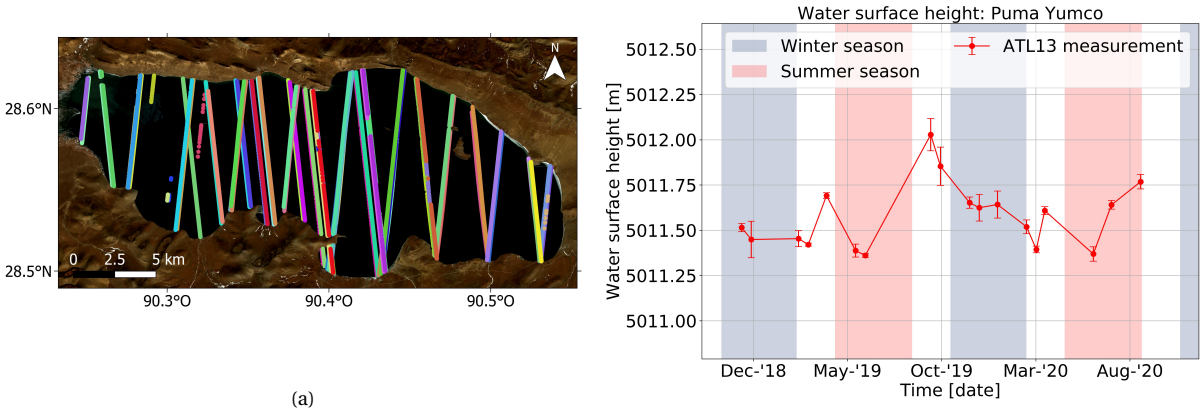

(a) (b)

Figure 5.10: (a) Passing beams over lake Puma Yumco. (b) Timeseries of Puma Yumco.

Interpretation

The timeseries in Figure 5.10b shows a larger amount of ATL13 measurements than both previous lakes. Although, still a relatively large gap between July 2019 and October 2019 is visible compared to the other gaps. A reason for this relatively large gap is the higher chance of cloud cover due to the summer monsoon during the summer season.

The figure shows that the water surface heights are the highest just after the summer season and are the lowest just after the winter season with an approximate difference of 0.6 meters. This difference is larger than the errors of the ATL13 measurements resulting that the water surface height is indeed higher just after the summer season. However, after the second summer season no measurements are present and therefore it is not possible to compare the differences between the winter and summer season.

Thus, this lake consists of more ATL13 measurements than both previous lakes, which is caused by its larger size. Also the amount of beams per passing will therefore be larger. As stated in Section 5.1.2 a larger amount of beams could also state more about the accuracy of the measurements. The errors of the ATL13 measurements for this lake varies from 0.05 up to 0.23 meters. The ATL13 measurements with an error of 0.23 meters will have a lower precision and accuracy than the ATL13 measurements with an error of 0.05 meters.

So taking all these findings into account, a seasonal cycle for this lake might be possible to detect since relatively small time gaps between the passings of ICESat-2 occurred, but a longer timeseries is needed.

Comparison of the three discussed lakes

Table 5.4 shows the results of the three discussed lakes. The table shows that the larger the area, the larger the maximum error of the water surface heights. Explanations for these errors are that for larger lakes the influence of wind set-up and the geoid fluctuations on the water surface height are larger. Thereafter, the table shows that the larger the area, the larger the amount of passings which corresponds to the conclusion in Section 5.1.1. The more ICESat-2 passed within two years time, the smaller the time gaps, the higher the chance the extremes are measured by ICESat-2. For all three discussed lakes, no seasonal variation is possible to determine based on these data due to the high chance of missing the extreme water surface heights, but for lake Baiju Co an Puma Yumco a seasonal variation and therefore a generic water surface height curve may be possible, but a longer timeseries is required.

Table 5.4: Comparison of the three discussed lakes.

Lake name	**Area [km^2]**	**Passings [-]**	**Max error [m]**	**Time gaps [-]**	**Generic WSH curve [-]**
Langbu Co	0.88	3	0.02	Large	No
Baiju Co	11.65	11	0.1	Relatively small	Maybe
Puma Yumco	283.19	18	0.23	Relatively small	Maybe

Conclusion about lake surface heights

Thus, ICESat-2 is capable of measuring the water surface height of 48% of the lakes due to its high spatial resolution. The water surface heights of the lakes have a precision of 0.1 meters. The high spatial resolution is at cost of the amount of passings per lake resulting in relatively large time gaps. Since most of the lakes are

only passed once by ICESat-2, creating a generic water surface height curve for these lakes will be difficult. However, the water surface height of these lakes do give information about the height of these lakes. But also for the lakes which are passed more than once by ICESat-2, a generic water surface height curve could be difficult. Due to the low repeat of ICESat-2, large time gaps will be present in the timeseries, resulting that creating a generic curve will be difficult. As seen in this section, the larger lakes (>10 km^2) will have more passings by ICESat-2 and will have less large time gaps. If at least one ICESat-2 passing is available every two months and longer timeseries are available, a generic curve might be possible to fit resulting in knowledge about the lake surface height during the years and finally may even a relation between the different waterbodies can be found.

5.2. Results of river surface heights based on ATL13

As seen in Chapter 4, determining river surface heights from ICESat-2 data requires more additional steps than for lakes. This section shows the total amount of locations in the river measured by ICESat-2, the error of river surface heights by ATL13, a comparison of the river surface heights with Hydroweb data, seasonal variation in water surface heights and two more detailed examples of timeseries of river locations.

5.2.1. Total amount of locations in the river measured by ICESat-2

In total 2440 beams of ICESat-2 passed the upper Brahmaputra in two years time. Due to the several requirements (e.q. clustering, small slope, see Section 4.4 for a more detailed explanation), this amount is lowered to 127 locations with at least two ICESat-2 passings. All the locations in the river passed at least two times by ICESat-2 are shown in Figure 5.11. The colours in the figure indicate the amount of passings of ICESat-2 and the locations with at least 4 passings are labelled with their ID.

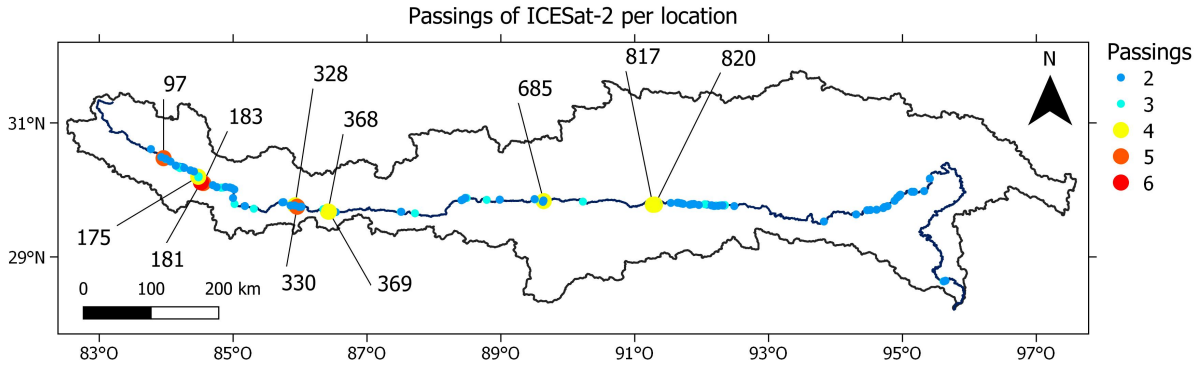

Figure 5.11: All the locations with at least two ICESat-2 passings and a maximum distance of 200 meters between the beams. The locations with at least four times passed by ICESat-2 are indicated with their ID.

Interpretation

The upper Brahmaputra is passed by 2440 beams in two years time. This research determined the locations in the river where ICESat-2 passed more than once and determined timeseries of the river surface heights for these locations. As a result, several passing of ICESat-2 are not used in any timeseries (e.q. only one ICESat-2 passing on a particular location in the river). These ICESat-2 passings may not contribute to a timeseries, but does give information about the river surface height on that moment at that location. Due to the small ground-track spacing, 127 locations in the river are found where the water surface height could be determined. This amount is expected to be the largest amount compared to the other satellite missions, which all have a larger ground-track spacing.

Amount of passings per month

The amount of passings by ICESat-2 resulting in a water surface height measurement are determined per month. This result is shown in Figure 5.12.

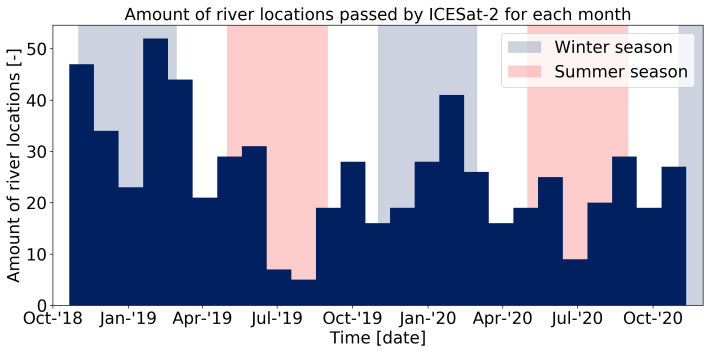

Figure 5.12: Amount of river locations passed by ICESat-2 for each month.

Interpretation
As for lakes, the amount of river locations passed by ICESat-2 per month show a minimum around the month July and a maximum around Janaury, indicating the presence of the summer monsoon. The amount of passing in 2020 is smaller than the amount of passing in 2019, this could indicate that more clouds were present in 2020, although this is not visible in Figure 5.3.

5.2.2. Error of ATL13 river surface height measurements

This section discusses the errors of the river surface heights. First the precision per beam is evaluated, followed by the error per ICESat-2 passing.

Precision per beam
In total 2440 beams passed the upper Brahmaputra. For each individual beam the MAD values are computed to evaluate the error of the beams (see Section 4.4). However, this value is harder to determine with the method for determining river surface heights than for lake surface heights, since only the ATL13 observations within a range of 0.1 meters are used, resulting that the MAD values will never be larger than 0.1 meters and are therefore unrepresentative. The error per beam could only be determined by comparing the results with in-situ measurements or other available river surface heights. Since these are not available for this study area, the error per beam could not be determined.

Error of the ATL13 measurement per ICESat-2 passing
Section 4.3 discussed the computation of the error for each ICESat-2 passing. Figure 5.13 shows the errors per ICESat-2 passing for 127 locations shown in Figure 5.11. The colours of Figure 5.13 indicate the amount of beams.

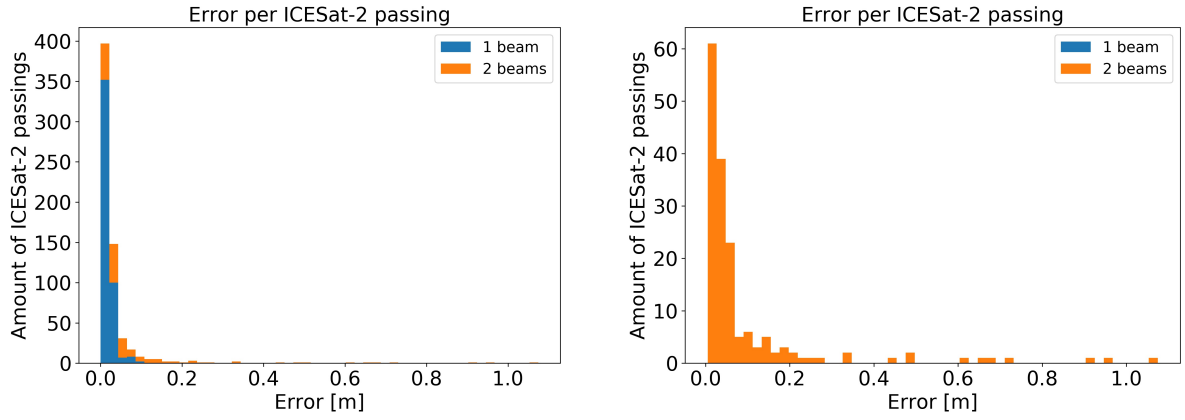

Figure 5.13: (a) Histogram of the error per ICESat-2 passing. The colours indicate the amount of beams over which the river surface height is computed. (b) Histogram of the error per ICESat-2 passing and passed by two beams.

Interpretation
Figure 5.13a shows that most of the computed errors per ICESat-2 passing for 127 locations which are passed at least two times by ICESat-2 is below 0.1 meters. As discussed for lakes, the amount of beams also indicate the accuracy of the measurement. Especially for river surface heights where the method for determining the river surface height is more prone to errors. For the river locations the maximum amount of passing beams is two, this has to do with the maximum length of 200 meters for each river location (see Section 4.4). The errors are based on the MAD values in case this value is smaller than the spread of the beams or in case the river location is passed by only one beam. Since the MAD value is unrepresentative for the river locations, the errors based on only one beam are unrepresentative. It is thus important to know the amount of beams over which a water surface height is computed.
Figure 5.13b shows the errors of the ICESat-2 passing which consist of two beams. 79% of the ATL13 errors is below 0.1 meters indicating a relatively good precision of the ATL13 measurements. However, multiple errors are found to be larger than 0.1 meters. These errors could have different causes. The errors can be caused by detecting of a side channel instead of the main channel (Section 5.2.5 discusses this problem in more detail), detecting shorelines, subsurface or missing data in the ATL13 observations. Even if the location is measured by two beams and the error is small, it is not completely sure whether the river surface heights is measured, since both beams could by coincidence measure for instance the same side channel. The method used in Section 4.4 brings its uncertainties, therefore it is recommended to improve this method by using for instance Sentinel-2 images. Most of the errors by ATL13 will be prevented if only one main channel is present, then the chance of obtaining river surface heights with a better precision is higher. However, side channels are highly present in upstream parts of rivers. Measuring downstream parts will therefore result in smaller errors of ATL13 with this method.
Thus, it can be concluded that most of the ATL13 measurements have a precision of 0.1 meters. However, the used method has its uncertainties due to especially the presence of side channels.

5.2.3. Comparison of the river surface height with Hydroweb data

A comparison is made with water surface height measurements of Hydroweb available at Theia Data and Services (Normandin et al., 2018; Santos da Silva et al., 2010). In the whole upper Brahmaputra river 35 virtual locations are present which are all measured by Sentinel-3, so Sentinel-3 is also capable of measuring relatively small rivers. Section 3.3 showed that the ground-track spacing of Sentinel-3 is 52 kilometers, resulting in the possibility of having multiple virtual locations. The water surface heights of the upper Brahmaputra river are present in the database, but no papers about the water surface heights of the upper Brahmaputra river were found. By comparing both measurements, it should thus be taken into account that the water surface heights measurements of Hydroweb are also acquired by a satellite and should not be seen as water gauge data. Of the 35 virtual stations in the upper Brahmaputra river only the virtual stations which are closer than 3 kilometers to a river location are taken into account resulting in only one virtual stations which is 1.5 kilometers downstream of location 817 and 2 kilometers upstream of location 820. This is illustrated in Figure 5.14a.

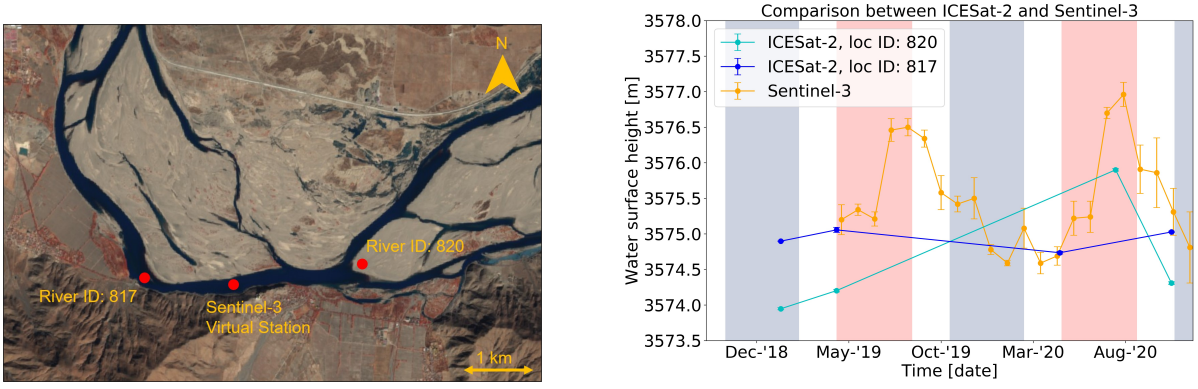

(a) (b)

Figure 5.14: (a) The location of the virtual station of Sentinel-3 available on Hydroweb. (b) Comparison between ICESat-2 and Sentinel-3 measurements. The Sentinel-3 measurements have been acquired from Hydroweb (Crétaux et al., 2011).

Interpretation
By comparing the Sentinel-3 measurements and ICESat-2 water surface height estimations in Figure 5.14b, it is concluded that Sentinel-3 has more measurements over time than ICESat-2. Sentinel-3 is even capable of measuring the seasonal cycle, which is not possible with ICESat-2. ICESat-2 measures the same river location two times in one year while Sentinel-3 measures the same location 14 times in one year. Since the locations 817 and 820 are both on an distance of 1.5 and 2 kilometers respectively from the location where the Sentinel-3 has measured, the water surface heights result in height differences due to the slope. A good comparison between the water surface height of the two missions is therefore not possible. Although a peak in the water surface height of location 820 is visible when also a peak in the water surface heights of Sentinel-3 is visible. Besides that, the water surface height of location 817 roughly matches the water surface height of Sentinel-3.

5.2.4. Seasonal variation of river surface heights
ICESat-2 will be less suitable for determining a generic water surface height curve, but a seasonal variation might be visible by determining the difference in water surface height between February and August. For each river location the difference in water surface height between February and August is determined for the year 2020, in 2019 no locations were passed in both February and August. The results of differences in water surface heights for 2020 are shown in Table 5.5. As concluded in Section 5.2.2, the water surface height measurements based on two beams are more representative than water surface heights based on only one beam, therefore the amount of beams are also indicated in the table.

Table 5.5: Water Surface Heights (WSH) for February and August in 2020. Besides the water surface heights, the amount of beams are shown since more beams give a better representation of the water surface heights. Two large differences in water surface heights are found, which are such large that they are expected to be unrealistic.

River location ID [-]	**February 2020**		**August 2020**		**ΔWSH 2020**
	WSH [m]	Beams [-]	WSH [m]	Beams [-]	
114	4574.19	2	4574.45	1	0.26
1243	178.60	1	191.807	1	13.21
369	4414.14	2	4414.86	1	0.72
1246	177.471	2	188.775	1	11.30
1093	2925.47	1	2927.65	1	2.19
1096	2922.92	1	2925.85	1	2.94
209	4540.01	2	4541.10	1	1.09
119	4571.17	2	4571.88	1	0.71
326	4457.33	1	4457.49	1	0.16

Interpretation
Figure 3.2 shows that as for lakes a larger water surface height in August is expected than in February due to the contribution of snow melt, glacier melt and precipitation of the summer monsoon. Table 5.5 shows that the difference in water surface heights between February and August vary from 0.16 until 13.21 meters. The differences of 11.30 and 13.21 meters are such large that they are expected to be unrealistic. These large differences can be caused by a wrong measurement in February or August, as for instance detecting shorelines instead of water surface heights. No water surface height in August is measured by two beams, indicating a lower chance of a good water surface height. Therefore, no conclusions are made regarding these results. Although, it can be concluded that the used method for determining river surface heights needs to be improved based on the found differences of 11.30 and 13.21 meters.

5.2.5. Examples of river locations
This subsection discusses two locations (locations with ID 181 and ID 685) in more detail to show the performance of ICESat-2 for river surface heights and its complications. The four different stages of the eleven river locations which are passed at least four times by ICESat-2 are given in Appendix A and their timeseries are given in Appendix B.

River: location ID 181
Figure 5.15 shows the location of river location with ID 181 in four different stages of the year with the approximate ICESat-2 track. Note that the same location is used as an example in Chapter 4. The figure shows that

in February the river is covered in ice, which would mean that the ice will be measured instead of the water surface height. In May, all the ice has melted and has an approximate width of 150 meters, while in August the width of the river is approximately 300 meters. In November both the height and the width of the water dropped.

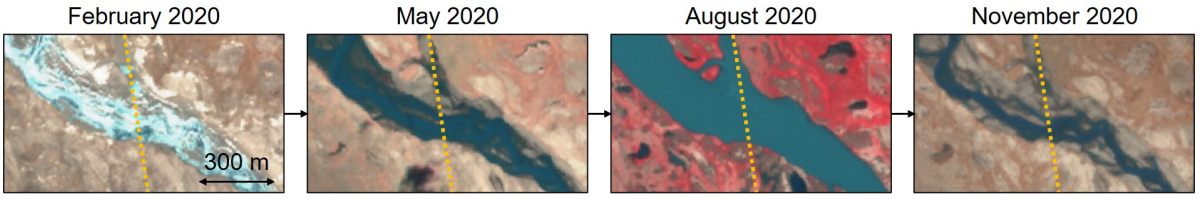

Figure 5.15: Four different stage of cluster location 181. Sentinel-2 images on 20-02-20, 20-05-20, 18-08-20 and 21-11-20 (ESA, NDb). Infrared band (band 8,4 and 3).

This location is six times passed by ICESat-2 in a two year period. Figure 5.16 shows the timeseries of this location and the water surface height values are given in Table 5.6.

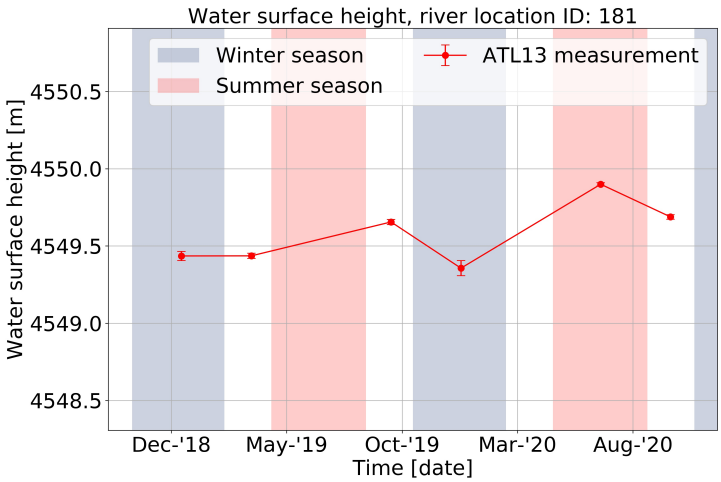

Figure 5.16: Timeseries of the water surface height measurements of river location ID 181 by ICESat-2.

Table 5.6: Water surface heights, errors and amount of beams of river location ID: 181.

Date	Water surface height [m]	Error [m]	Amount of beams
04-01-2019	4549.44	0.03	2 beams
05-04-2019	4549.44	0.02	2 beams
03-10-2019	4549.66	0.02	1 beam
02-01-2020	4549.39	0.05	2 beams
02-07-2020	4549.89	0.01	2 beams
30-09-2020	4549.69	0.01	2 beams

Figure 5.17 shows the ATL13 observations and the photons of the strong and weak beam of January 2019. Figure 5.17a shows the observations of ATL13 and the photons of the strong beam and Figure 5.17b of the weak beam. The MAD interval is shown as a transparent band. Note that the observations in orange were not used for the estimation of the median over the ATL13 observations. The photons have only been visualized in the figure to get a better idea of the cross-section of the river, the photon data is not used in this research for the determination of the water surface heights.

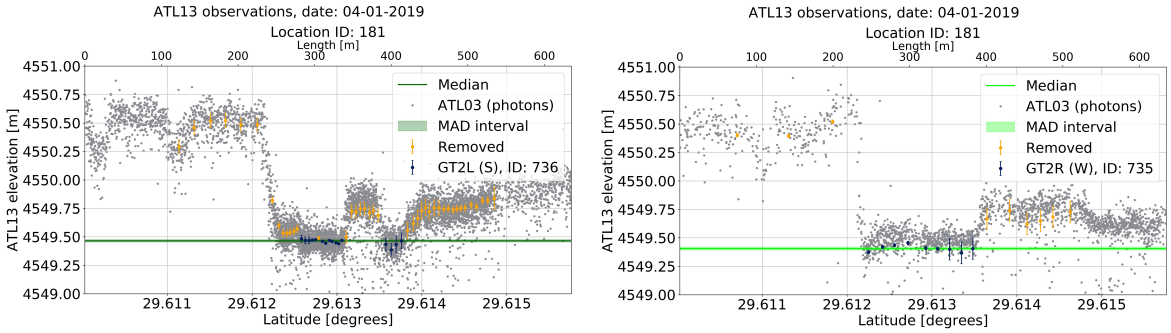

(a) Strong beam

(b) Weak beam

Figure 5.17: ATL13 observations of ICESat-2 of river location 181 on 04-01-19 for both the strong (a) and weak (b) beam. Also the ATL03 photons have been indicated, to get an idea of the cross-section profile of the river.

Interpretation

Figure 5.16 shows that the water surface height in July 2020 is higher than the other measurements. In the second winter season the lowest water surface height has occurred and in the summer season the highest, which follows the expectation. However, it is important to note that in between the measurements the period is too long to conclude something about the seasonal cycle. Especially between April 2019 and October 2019, but also between January 2020 and July 2020 a significant time gap is present. The water surface height in both these time periods could deviate significantly.

From the figure and table, it can be seen that the errors for each ICESat-2 passing are smaller than 0.1 meters. The water surface height measurement in January 2020 (fourth measurement) has the largest error of 0.05 meter. Since four out of five ATL13 measurements are determined of two beams and the errors are small, it is more certain that the correct water surface height is determined. For evaluating this in more detail the observations on January 2019 (first measurement) for both the weak and the strong beam are shown in Figure 5.17. It can be seen that the lowest plateau is used for the computation of the median over the observations. From this river location can be concluded that errors of the water surface heights are low. Although the measurements of ICESat-2 are good, it will be difficult to conclude something about the seasonal variation on this location due to the large time gaps. In case longer timeseries are available, it might be possible to conclude something about the variation in water surface height, but this will need further research.

River: location ID 685

Figure 5.18 shows the location of the river location with ID 685 in four different stages of the year with the approximate ICESat-2 track in orange. This location is not covered with ice in February 2020, nor November 2020. The braiding pattern of the river looks constant over the months February, May and November. In August, the river surface height is higher which leads to more submerged parts of the river, but still some bars are visible in the river and multiple side channels.

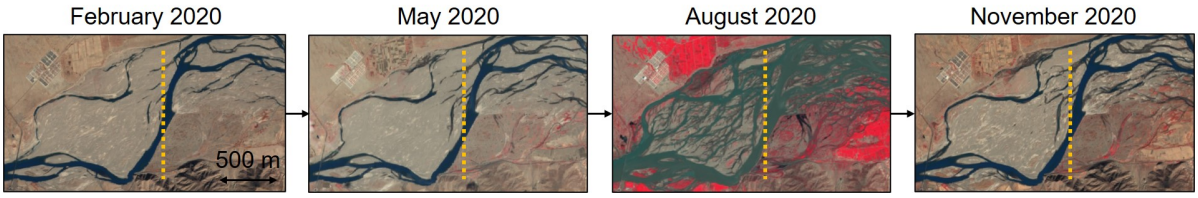

Figure 5.18: Cluster location 685. Sentinel-2 images on 04-02-20, 04-05-20, 07-08-20 and 05-11-20 (ESA, NDb).

The location is passed four times by ICESat-2 in a period of two years. Figure 5.19 shows the timeseries of this location with the water surface height values shown in Table 5.7. For three out of four ICESat-2 passings, the river is measured by only one beam. The fourth measurement (May 2020), is measured by a weak and strong beam.

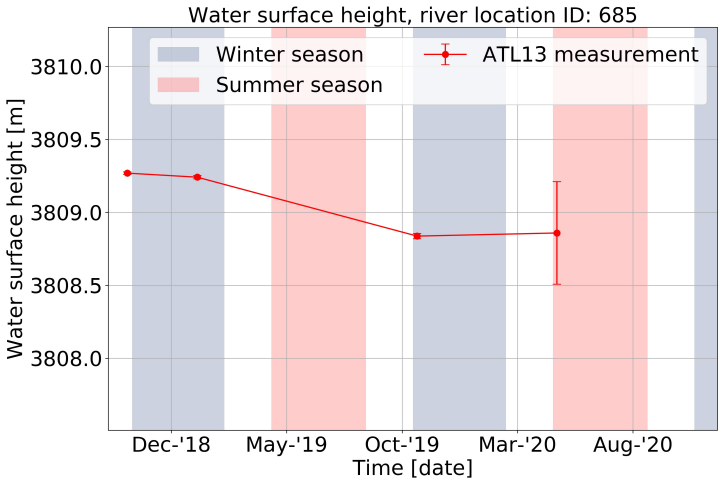

Figure 5.19: Timeseries of the water surface height estimation of river location ID 685.

Table 5.7: Water surface heights, errors and amount of beams of river location ID: 685.

Date	Water surface height [m]	Error [m]	Amount of beams
25-10-2018	3809.27	0.01	1 beam
24-01-2019	3809.24	0.01	1 beam
06-11-2019	3808.84	0.02	1 beam
06-05-2020	3808.74	0.4	2 beams

Figure 5.20 shows the cross-section profiles of May 2020 of the strong and weak beam.

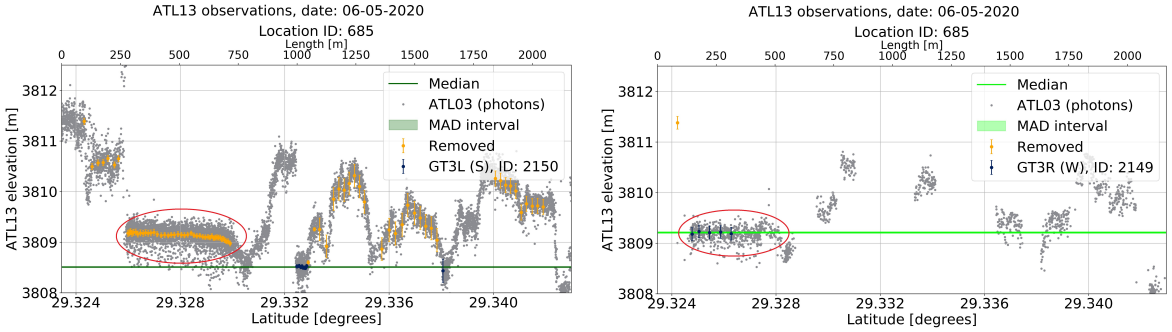

(a) Strong beam

(b) Weak beam

Figure 5.20: ATL13 observations of ICESat-2 of river location 685 on 06-05-20 for both the strong (a) and weak (b) beam. Also the ATL03 photons have been indicated, to get an idea of the cross-section profile of the river. The red circle shows the location of the main channel.

Interpretation

Figure 5.19 shows the timeseries of the water surface height of location ID 685. The last measurement in May 2020 is immediately remarkable due to its large error of 0.4 meters. Since this is the only ATL13 measurement which is based on two beams, this measurement indicates that the computed river surface height is not correct. By evaluating the cross-section profiles of the weak and strong beam of this measurements (see Figure 5.20), it can be concluded that the cross-section profiles vary a lot in height. The blue observations of Figure 5.20a are used for determination of the water surface height, but on the left of the blue observations, also another rather flat plateau is visible (marked by a red circle in Figure 5.20a). Both the strong and weak beam determine the water surface heights over a different plateau. This is the reason of the large error of the water surface height. By taking Figure 5.21 into account which shows a Sentinel-2 image with the corresponding ATL13 observations. The blue dots in this figure represents the ATL13 observations over which the water surface height is determined. It can be obtained that the strong beam consists of ATL13 observations of the side channels and the weak beam contains the ATL13 observations of the main channel.

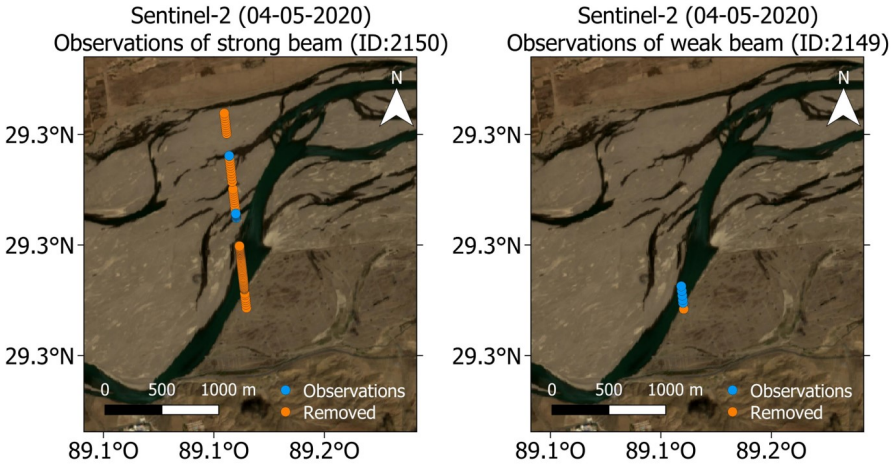

Figure 5.21: Sentinel-2 image of 04-05-2020 with the ATL13 observations of 06-05-2020.

Thus, from these results can be concluded that the method used in this research does not always results in the correct water surface heights. The error of the water surface height could give an indication whether the computation went wrong, but for this two beams are needed. This problem will mainly happen in upstream parts of a river where rivers are braiding and are small in width. The river surface heights for rivers that are not braiding or wider will therefore be easier to determine.

Conclusion about river surface heights
One main conclusion is that the amount of ICESat-2 passings is too low leading to large time gaps. This will again result in missing extreme water surface heights which will make it difficult to generate a generic water surface height curve on the river locations. Although, with a longer timeseries it might be possible to fit a curve through the ICESat-2 measurements, but this will need further research. Another important finding is that the method used for determining river surface heights in this research does not always lead to the correct river surface height. It is important to know that this is not always visible from the water surface heights. In case the river location is only measured by one beam, it could be the case that that one beam has measured the side channel instead of the main channel. Also if the river location is measured by two beams which both measure the same side channel and not the main channel it will not be visible in the water surface height measurements. For this reason it is recommended to improve this method by using for instance Sentinel-2 images and create a river mask of only the main channel, which is present during all the seasons of the year. With this river mask it will not be possible to measure a side channel instead of the main channel. For downstream parts where the rivers are wider and not braiding, it is expected that this problem will not occur. Also shorelines will not be a problem in case of a wider rivers, since the shorelines in a wider river will only be a small part of the complete cross-section, resulting that the shorelines will not be taken into account by determining the median of the observations. Thus, it is possible to determine river surface heights with ATL13 of ICESat-2 for upstream parts of river, but for the locations where the river is braiding the method should be improved to only determine the water surface height of the main channel.

5.3. Case studies

This section discusses three different cases. These cases are done to analyse the relation between the waterbodies based on the ATL13 measurements. First a comparison between a lake in the Brahmaputra basin and Nam Co basin is done, followed by a comparison of the water surface height timeseries between a river location and a nearby lake. Finally, the timeseries of lake is discussed which is neighbouring a glacier.

Case: comparison between lakes in the Brahmaputra basin and Nam Co basin
This case compares a lake in the Brahmaputra basin and the lake Nam Co. The lakes Nam Co and Puma Yumco are chosen for comparison, because these lakes are large and have therefore a higher potential to conclude something about the seasonal variation due to their higher amount of passings compared to other lakes. Lake Nam Co is the largest lake in the study area with an area of 1964 km^2. It is a salt lake and thus endorheic, and not connected to a river or ocean. As a result this lake is a good indicator for climate change

and glacier melt. Figure 5.22a shows that Nam Co lake is located near a large glacier. Lake Puma Yumco is the third largest lake in the study area with an area of 283 km^2. Figure 5.22b shows that also Lake Puma Yumco is located near a glacier which is part of the Himalaya.

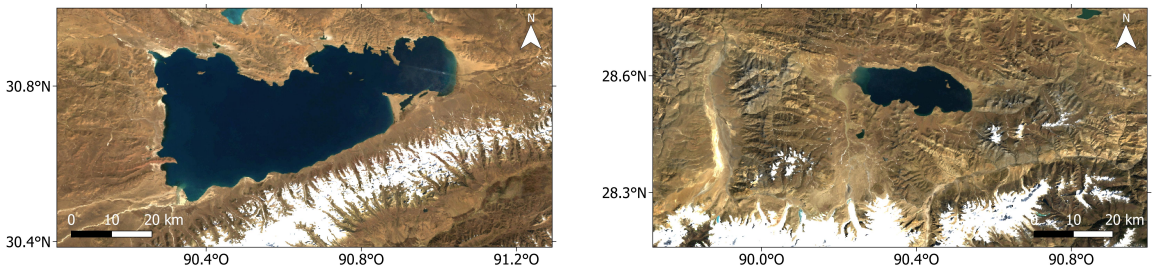

(a) (b)

Figure 5.22: Landsat image of lake Nam Co (a) and Lake Puma Yumco (b) visualized by Google Earth Engine (Vermote et al., 2016).

The corresponding timeseries of the ATL13 measurements of these lakes are shown in Figure 5.23.

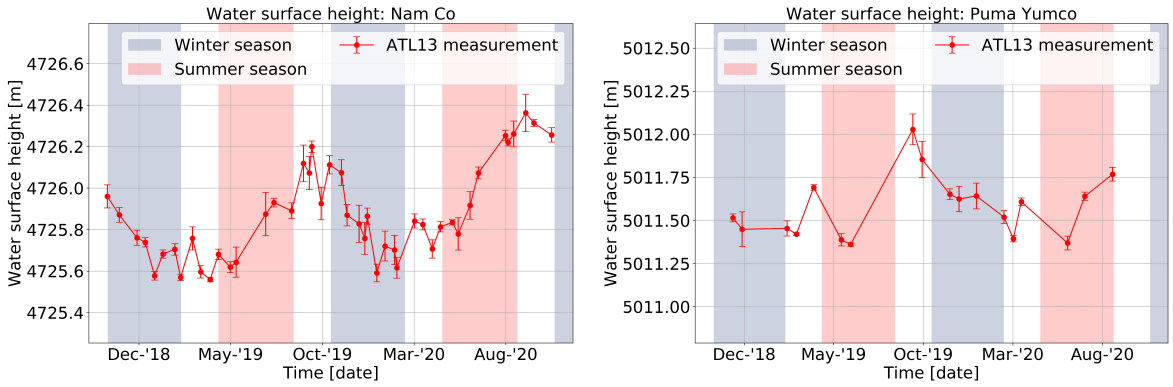

(a) (b)

Figure 5.23: (a) Water surface height of lake Nam Co by ATL13. (b) Water surface height of lake Puma Yumco by ATL13.

Interpretation

The water surface heights of Nam Co by ATL13 are shown in Figure 5.23a. The ATL13 measurements shows a clear variation over time. Just after the summer season the water surface height in lake Nam Co is on its maximum. The water surface height is the lowest at the end of the winter season. It is remarkable that the peak near August 2020 is significantly larger than the peak near August 2019.
Figure 5.23b shows the water surface height of lake Puma Yumco. By comparing lake Puma Yumco with lake Nam Co, it is seen that the timeseries of lake Puma Yumco shows a less clear variation of its water surface height than lake Nam Co, which is mainly caused by the less amount of ICESat-2 passings. Although, a peak September 2019 is visible. The water surface height in the second summer season is also increasing, but no ICESat-2 passings are available after August 2020, where may a peak would have been visible. Overall, the timeseries of this lake are too short to conclude something about a possible trend in the water surface height.

Both lake surface heights are discussed in papers (see Table 5.8). The table shows for two of the three papers a significant trend for Nam Co. This trend of 0.23 meters and 0.25 meters is almost similar as the difference of 0.18 meters between the peak in August 2019 and the peak in August 2020, which can be seen in Figure 5.23a. The trend found by Kleinherenbrink et al. (2015) does not corresponds to the found difference in height in Figure 5.23a. For lake Puma Yumco small decreasing trends are found. This decreasing trend from Table 5.8 is not visible in 5.23b. As stated the timeseries of lake Puma Yumco is too short to derive a trend for the water surface heights.

Table 5.8: Papers which discussed the lake surface heights of Nam Co and Puma Yumco. For each of them the trend and error is shown.

Authors of paper	**Satellite**	**Year**	**Nam Co**		**Puma Yumco**	
			Trend [m/y]	Error [m]	Trend [m/y]	Error [m]
Zhang et al. (2011)	ICESat-1	2003-2009	0.25	0.12	-0.03	0.09
Phan et al. (2012)	ICESat-1	2003-2009	0.230	0.388	-0.039	0.241
Kleinherenbrink et al. (2015)	CryoSat-2	2012-2014	-0.02	0.04	-	-

Taking all these things into consideration, an increasing trend is visible in the water surface height measurements of lake Nam Co indicating an increase of glacial melt, while no trend is visible in the water surface height measurements of lake Puma Yumco due to the short timeseries.

Case: Lake close to the river

For the relation between lakes and the main river, a location is evaluated in more detail where a lake and river are located close to each other. Figure 5.24a shows the location considered that is considered. The lake with ID 176297 is located close to both river location ID 181 and river location ID 183. The figure shows a small water stream of the lake into the river in between those two river locations. The lake is on approximately 2.5 kilometers distance from the river. The timeseries of the lake is shown in Figure 5.24b and the timeseries of the two river locations are shown in Figure 5.25.

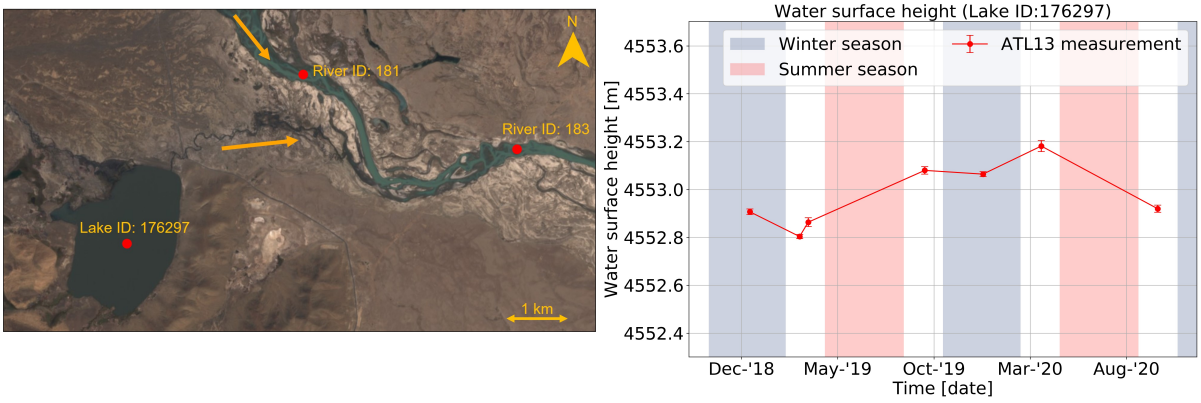

(a) (b)

Figure 5.24: (a) A lake in the upper Brahmaputra basin close to the upper Brahmaputra river. Sentinel-2 image from 13-10-19 (ESA, NDb). (b) Water surface height of lake ID:176297 by ATL13.

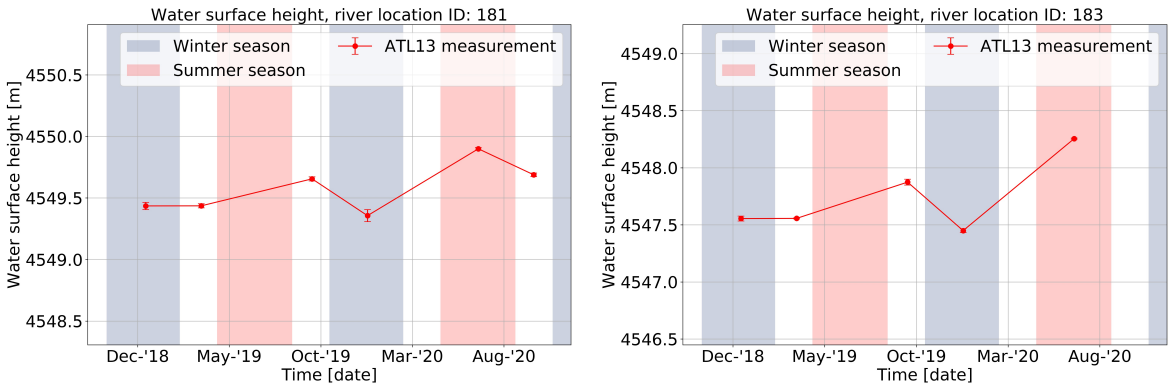

(a) (b)

Figure 5.25: Water surface heights of river location ID 181 (a) and river location ID 183 (b) by ATL13.

Interpretation
Figure 5.24a shows the water surface height of the nearby lake. This lake is passed seven times by ICESat-2, and has no passing of ICESat-2 in any of the two summer seasons, resulting in missing peaks in timeseries of the water surface height in this lake.
River location ID 181 is already in more detail discussed in Section 5.2.5, but is not yet compared with the nearby river location ID 183. Figure 5.25 shows the timeseries of the water surface heights for both locations. The figure shows that water surface height have a similar variation. Both locations have a minimum in the second winter season and a maximum in the second summer season. The difference between the water surface height measurements in January 2020 and July 2020 is 0.5 meters for location ID: 181 and 0.8 meters for location ID: 183. This difference in water surface height could be caused by the input of water from the lake. However, since no ATL13 measurements in the second summer season are present for the lake, it is hard to compare the lake surface height with the river surface heights.
Taking those findings into account, it can be concluded that the nearby river locations show a similar variation in time. The difference in water surface height between the second winter season and second summer season indicates input of water from the lake. But a comparison between the nearby lake and the river locations is difficult to assess due to the low amount of ATL13 measurements.

Case: Lake neighbouring a glacier
This section evaluates the results of the timeseries of the water surface heights determined based on ATL13 of a lake neighbouring a glacier. Figure 5.26a shows the considered lake neighbouring the glaciers of the Himalaya. The area of this lake is approximately 5.2 km^2.

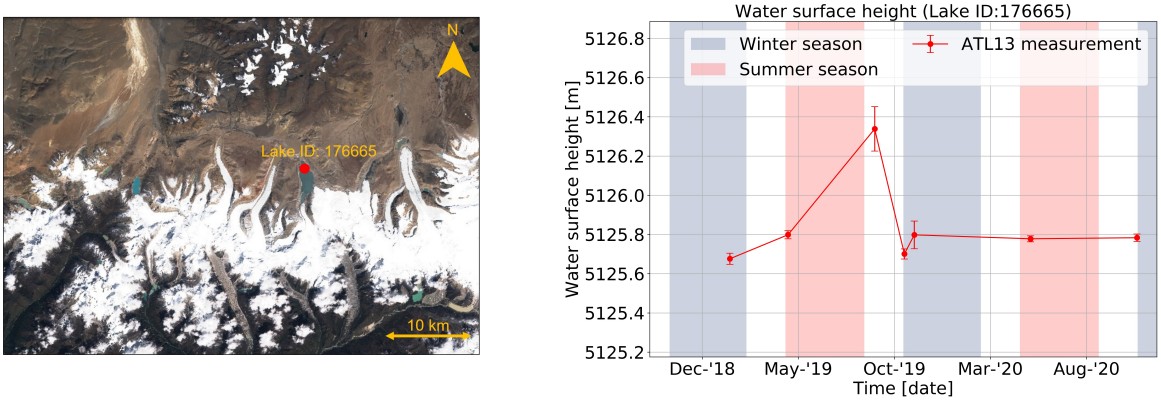

(a) (b)

Figure 5.26: (a) A lake neighbouring a glacier of the Himalaya. Sentinel-2 image from 13-10-19 (ESA, NDb). (b) Water surface heights of lake ID:176665 by ATL13.

Interpretation
Figure 5.26b shows the water surface height of the lake neighbouring a glacier. The timeseries of the water surface height is quite stable, except for one peak after the first summer season. For both winter seasons and the second summer season maxima and minima are expected but are not present in the timeseries. So also this lake does miss several extremes due to the relatively low amount of ICESat-2 passings.

Conclusion of case studies
Taking all the case studies into consideration, it can be concluded that the amount of ICESat-2 passings is too low and the timeseries too short to conclude something about the relation between the lake and river surface heights and about the lakes neighbouring glaciers. For the largest lake in the study area it was possible to see a trend through the water surface heights indicating that ICESat-2 could have a contribution for water surface heights, but mainly for large enough waterbodies such that the waterbodies are passed enough times by ICESat-2.

6

Discussion

This chapter discusses the strengths and limitations of ICESat-2 in Section 6.1 and Section 6.2 respectively. The limitations based on the water mask are discussed in Section 6.3, followed by the limitations of the method used in this research in Section 6.4. Finally, Section 6.5 discusses the possibility of determining water surface heights on other locations.

6.1. Strengths of ICESat-2

High spatial resolution of ICESat-2

Section 3.3 already indicated the high spatial resolution of ICESat-2 compared to the other missions. This research confirms the high spatial resolution of ICESat-2. ICESat-2 was capable of finding 299 lakes in a period of two years in the study area, while ICESat-1 was only capable of finding six lakes in the area, indicating the better spatial resolution of ICESat-2 compared to ICESat-1. The main cause of this high spatial resolution is the small ground-track spacing, which is the smallest for ICESat-2 compared to the other discussed satellite missions.

Side branches

The data product ATL13 of ICESat-2 consist of smaller sized rivers as well. All the rivers are shown in Figure 6.1. The main river (upper Brahmaputra) is shown in dark blue and is used in this research. The green rivers are side branches of the main river and are also provided in data product ATL13. However, it should be noted that not all small rivers or side branches are provided in the data product ATL13. The smaller rivers, shown in light blue are not provided in ATL13.

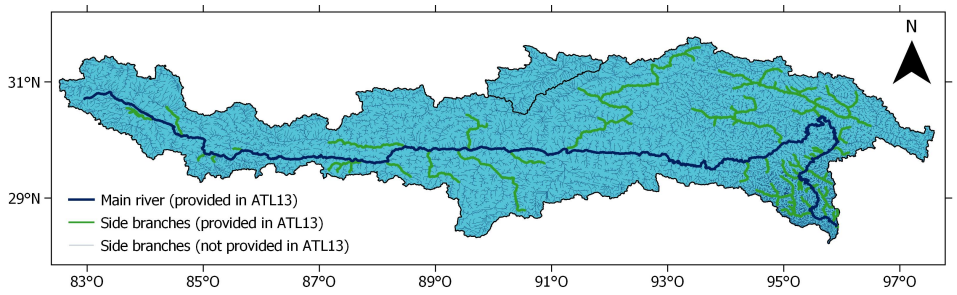

Figure 6.1: The main river (upper Brahmaputra) is shown in dark blue. The green rivers are side branches of the main river and are also provided in data product ATL13. The smaller rivers, shown in light blue are not provided in ATL13.

The smaller rivers could be detected based on the photon data of ATL03. This would mean that the water surface heights for smaller rivers than the upper Brahmaputra river might be possible to measure as well. However, it is important to note the the smaller rivers are mostly also the more upstream rivers which have a larger slope resulting in even less ICESat-2 passings than for the main river. Thereafter, the depth of these rivers will be lower resulting that it might be more difficult to distinguish the bottom with the top of the water surface.

Relatively good precision
The results show that the lake surface heights and river surface heights based on ATL13 of ICESat-2 both have a relatively good precision of lower than 0.1 meters. Although, the method for determining river surface heights need to change a bit which can result in another precision.

6.2. Limitations of ICESat-2

Low repeat of ICESat-2
In total 299 lakes in the study area are passed by ICESat-2 and only 64 of these lakes are passed at least four times by ICESat-2. Of the 127 river locations, only eleven of these locations are passed at least four times. However, even four water surface height measurements in time by ICESat-2 in a two year period will lead to missing extreme water surface heights. The results for both lakes and river show that the repeat of ICESat-2 is too low with 8 cycles of 91 days, especially for lakes with an area smaller than 10 km^2 and the evaluated locations in the river, to create a generic water surface height curve for each lake or river location. Due to the cycle of 91 days, more than 3 months of data may be missing within two water surface height measurements of ICESat-2, leading to missing the extreme water surface heights resulting in a misconception of the water surface heights. Although, for larger lakes which are defined with a size larger than 10 km^2, as for example lake Puma Yumco, more than one water surface height is estimated within 91 days. Due to their size, one cycle passes the large lakes more than once, resulting in more than one water surface height measurement within one cycle. For the larger lakes, it thus might be possible to extract some extreme water surface heights and thus might be possible to even see a seasonal cycle. If ICESat-2 is operating for a longer time, a generic water surface height curve might be estimated for those lakes. However, the study area consist of 85% of lakes with an area of smaller than 1 km^2. For these lakes and the evaluated river locations one cycle does not pass them more than once, resulting in a low amount of ICESat-2 passings. The smallest lakes which have an area of 1 km^2 or smaller that are passed by ICESat-2 in two years time are not even measured for every cycle of ICESat-2, resulting in even more gaps. Creating a generic water surface height curve for these lakes and the river locations will be difficult to assess with ICESat-2.
The low amount of ICESat-2 passings will also result that the computed difference between the water surface height of February and August will not represent the seasonal difference (see Section 4.5). ICESat-2 should pass on the exact moment in time when the water surface height is on its maximum to determine this difference, but this chance is very low.

Only profile cross-sections of the waterbodies
ICESat-2 is a laser satellite and is only capable of measuring cross-sections of lakes and rivers. The estimated water surface heights are thus depended on these cross-sections.

Cloud cover disrupts measurements
A laser could not penetrate through a cloud cover, resulting in unsuccessful measurements during cloudy days. Figure 5.3 and Figure 5.12 show that around July less amount of successful measurements are present. A possible explanation for this is the cloud cover during the summer monsoons. This will result in larger time gaps during the summer monsoons.

6.3. Limitations of the water masks

Man-regulated lakes and river parts in the lake mask
The HydroLAKES database of WWF (Messager et al., 2016) consists of a variable which indicates whether a lake is a natural lake, reservoir or a natural lake with a regulation structure. Although, the default type is a natural lake, indicating that if the type of lake is unknown, it is marked as a natural lake resulting in more natural lakes than in reality. By visual inspection of Sentinel-2 images of the lakes which are passed at least four times by ICESat-2 in two years, it became clear that already three lakes are reservoirs (human-regulated lakes), meaning that in the complete study area more man-regulated lakes could be found. Man-regulated lakes do not behave naturally and would thus not be interesting for analysing the natural behaviour of lakes, but could be interesting for other purposes. This distinction could be made by visual inspection from satellite images, although inspection of all the 621 lakes will be very time consuming.
Besides man-regulated lakes also river parts which are marked as lakes are present in the in the lake mask. By zooming into the lakes with at least four passes by ICESat-2, it is seen that some lakes are part of rivers and often have a length of more than 1 kilometer. An example of a river part in the lake mask is shown in

Figure 6.2. It is found that at least four of the 64 lakes which are passed at least four times by ICESat-2 are part of a river and should therefore be excluded from the analysis of the lake surface heights. As explained in Section 4.4, the river surface heights should be estimated differently due to the presence of a slope and the possible bars within the river. So the river parts in the lake mask will result in distortion of the estimation of the water surface heights. In the lake mask of the complete study area more man-regulated lakes and river parts marked as lakes are present and are not removed in this research. For better results of the timeseries of all the lakes in the study area, it would be recommended for further research to check with a certain method whether a lake is man-regulated or not. This will finally result in a better determination of the water surface height behaviour in the study area.

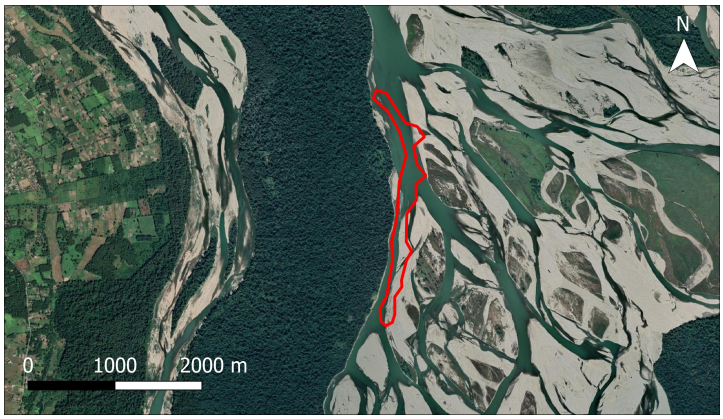

Figure 6.2: The red line shows the boundary of an object in the lake mask. Some lakes in the lake mask turn out to be parts of a river, water surface heights for rivers should be determined with a different method.

River mask based on average discharge

The width of the river mask used for this research is based on the average discharge of the river as explained in Section 4.1. In case the river discharge is lower than the average discharge, the width of the river is smaller than the the width used for the river mask. This would mean that during lower discharges more side channels or bars are visible resulting in more variation in the river cross-section measured by ICESat-2. By creating a river mask which is based on the lowest discharge, this problem will be avoided. A remark for this recommendation is that it should be studied whether the main channel is not moving too much over time.

6.4. Limitations of the method used in this research

Sensitivity analysis of the maximum distance between the beams

Section 4.4 described in *Step 2* the clustering of passing beams based on a maximum allowed distance. It was chosen to use a distance of 200 meters, since a distance of 100 meters would result in significantly less amount of measurements and the distance of 500 meters may would result in large slopes resulting in larger errors. Figure 6.3 shows the errors per ICESat-2 passings for each of those discussed distances. It should be noted that the shown errors are only based on two beams since this will give a better representation of the error as discussed in Section 5.2.2.

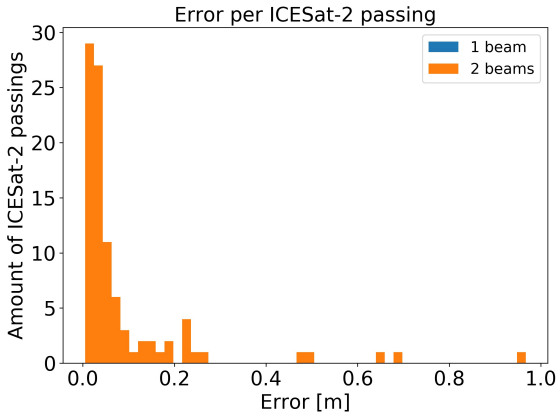

(a) 100 meters

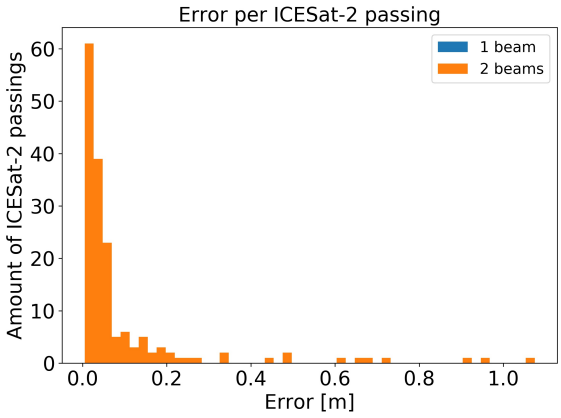

(b) 200 meters

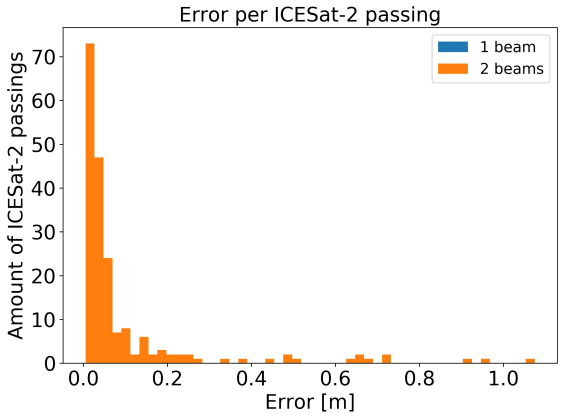

(c) 500 meters

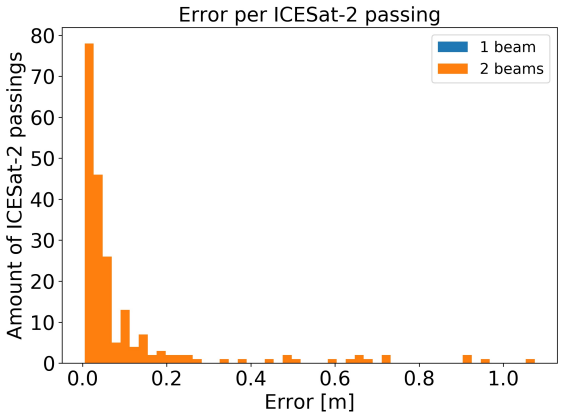

(d) 1000 meters

Figure 6.3: Histogram of the error per ICESat-2 passing and passed by two beams. The four figures all show a different maximum distance between the beams: (a) 100 meters, (b) 200 meters, (c) 500 meters and (d) 1000 meters.

The figures show that a larger maximum allowed distance between the beams does not lead to significantly larger errors. This is may the result of *step 3* where the locations with too steep slopes are removed. These figures indicate that a maximum distance of 200 meters between the beams may be increased. Although, for determining cluster locations a maximum distance should be set.

Determination of the slope in the river

Step 3 of Section 4.4 determines the slope of the river based on SRTM data. The slope on multiple locations is determined with least squares estimates, however due to the low vertical accuracy of 16 meters, the estimated slope may not represents the slope in reality. The slope of the river is possible to determine, but would only give an indication of the real river slope. Only the locations which have a slope of smaller than 0.0001 meter/meter are used further in this research. Although, it is thus possible that some of these locations have a larger slope than this threshold value and should not be further analysed. Another possibility is that on some locations the slope is smaller in reality than estimated, resulting that these locations will be incorrectly removed.

Thus, it is assumed that slopes larger than 0.0001 meter/meter will result in a larger error. Therefore, the difference between the errors per ICESat-2 passing with the requirement that the slope should be smaller than 0.0001 meter/meter and without the requirement is determined. Figure 6.4 shows the results.

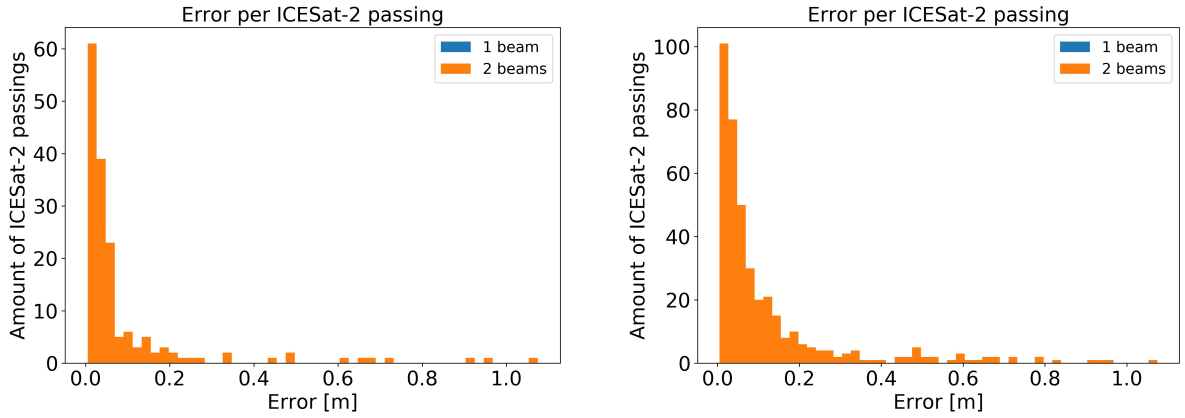

(a) with the requirement of a slope < 0.0001 meter/meter

(b) without the requirement of a slope < 0.0001 meter/meter

Figure 6.4: Histogram of the error per ICESat-2 passing. Only the ICESat-2 measurements based on two beams are included. (a) Histogram of the errors per ICESat-2 passing with the requirement of a slope < 0.0001 meter/meter, (b) Histogram of the errors per ICESat-2 passing without the requirement of a slope < 0.0001 meter/meter

The figure shows that without the requirement of the slope, more ICESat-2 passings are found. All the bins of the histogram increased in Figure 6.4b compared to 6.4a, especially more errors between 0.1 and 0.4 meters are found. Therefore, it can be concluded that the requirement for the removal of locations which have a too large slope results in less ICESat-2 passings for both small (errors < 0.1 meters) and larger (error > 0.1 meters) errors, but especially some larger errors are prevented.

Side channels and bottom observations

Also river surface heights are possible to determine with ICESat-2 due to its large spatial resolution. Although the determination of river surface heights is more complicated than the determination of lake surface heights due to the slope in the river and the spatially varying width of the river. The river cross-section profiles of ICESat-2 show a large variation in height, caused by shorelines or bars. For this reason an extra step is added to determine only the water surface height over the water surface observations. The water surface is assumed to be the lowest in the whole river cross-section profile. For extracting only the lowest observations in the river cross-section profile, a histogram is created of the ATL13 observations. This results in a histogram with on the x-axis the height of the ATL13 observations and on the y-axis the frequency of the amount of ATL13 observations. Since the lowest observations are assumed to be the water surface observations, the observations in the lowest bin are used for the estimation of the water surface height. It is possible that outliers are present which are likely the subsurface or the bottom that were not removed by their Subsurface Anomaly Quality Flag. If the lowest bin consist of only one observation or the two following bins do not contain any observation, the next not empty bin is used for estimating the median over the ATL13 observations. This is repeated till a bin is found which follow these two condition. Although these requirements, it is still possible that observations from the subsurface or another side channel are used for the estimation of the water surface height. This is the case for the locations 97 and 685 (see Section 5.2.5), their timeseries are shown in Figure 6.5. At these river locations the weak and the strong beam differ in a range of 0.7 meters, while the weak and strong beam should estimate approximately the same water surface height.

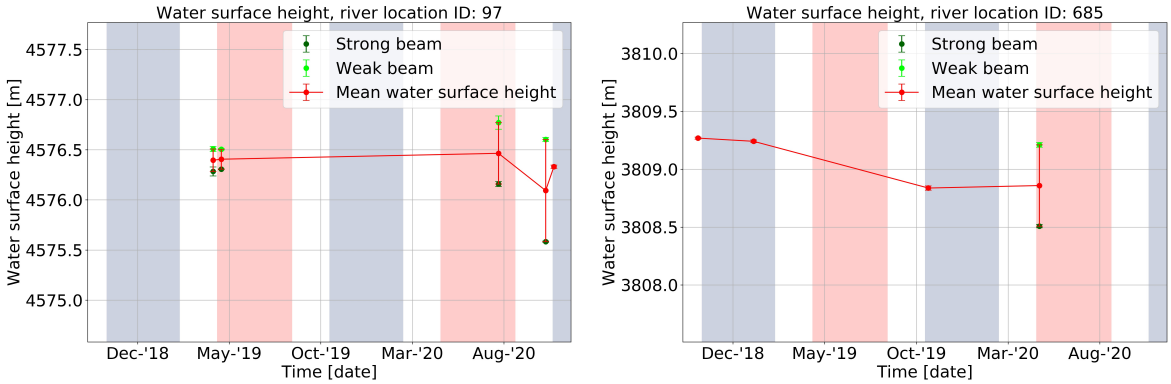

(a) (b)

Figure 6.5: Timeseries of river locations ID:97 and ID:685 with the strong and weak beam.

So for these two locations it is clear the final determination of the water surface height (red) is uncertain and other side channels or the bottom is measured instead of the main channel, but in case the river is only passed by one beam, no comparison between the beams could be made and thus also no indication is given whether the estimated water surface heights are correct. Although, it is still possible that in case a river location is measured by two beams, both beams measure the bottom or a side channel. So, a recommendation for further research will be to overlay ATL13 observations over the optical imagery of for example a Sentinel-2 image of that moment and to use only the ATL13 observations which overlay the main channel. Another possibility is to create another river mask as discussed in Section 6.3: *River mask based on average discharge.*

Geoid influence in large lakes

Remarkable is that in some passing beams over large lakes a slope is visible, as could be seen for lake Puma Yumco (area of 283 km^2) in Figure 6.6. The ICESat-2 observations of Figure 6.6 follow a slope from left to right. On the left the ATL13 elevation is approximately 5011.5 meters and on the right the ATL13 elevation is approximately 5011.7 meters, resulting in a difference of 0.2 meters. Since the surface of the lakes are assumed to be flat, this event is further analysed.

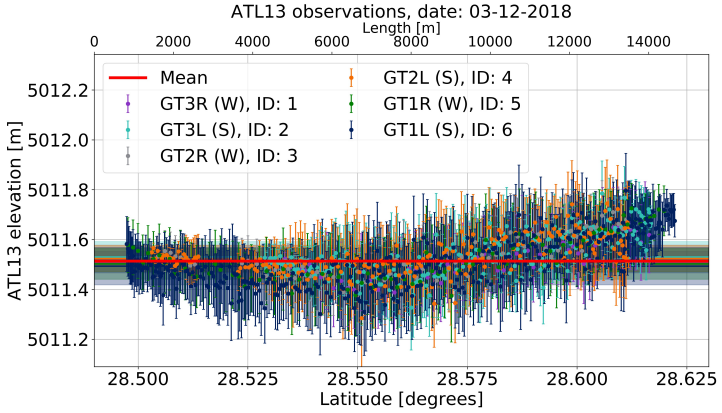

Figure 6.6: ATL13 observations of six beams passing Puma Yumco on the 3rd of December. The six beams each have a different colour. The MAD interval is shown as transparent band. A clear slope from left to right is visible.

This event has appeared in multiple studies. Also Kleinherenbrink et al. (2015) encountered this problem and found that this was caused by the low resolution geoid model or might be caused by wind set up. Since the slope in the water surface heights is regularly visible, the most likely cause of the slope is the influence of the geoid. The low resolution geoid model EGM2008 (reference of the ICESat-2 observations) does not include high resolution geoid fluctuations, which is mainly the problem in mountainous areas as the Himalayan (Pavlis et al., 2012).

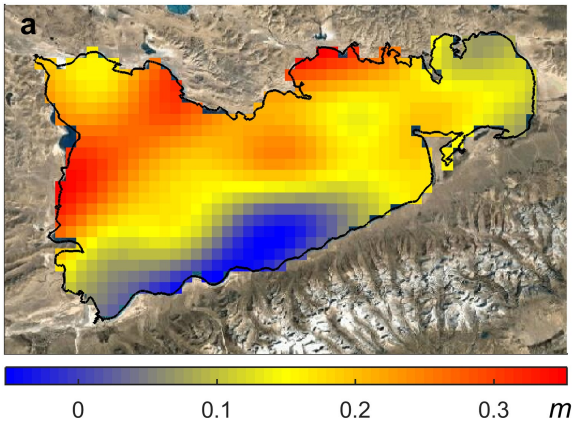

Figure 6.7: Geoid difference between EGM2008 and GOCO05c in Nam Co lake (Jiang et al., 2019).

The geoid differences of two regularly used geoid models EGM2008 and GOCO05c are evaluated in an earlier research for the Nam Co lake. A geoid difference of -0.05 till 0.35 m within the lake was found (Jiang et al., 2019) (see Figure 6.7). Nam Co is the largest lake in the study area with an area of 1964 km^2, which means that the effect of the geoid fluctuations on the ICESat-2 observations will be the largest. The ICESat-2 observations of one passing beam on 31st of October 2018 is shown in Figure 6.8. The lower latitudes show a water surface height of approximately 4726.2 meters and the higher latitude show a water surface height of approximately 4726.0 meters, resulting in a difference of 0.2 meters. It could be obtained that the lower latitude observations correspond to the blue area in Figure 6.7, while the higher latitude observations correspond to the orange/yellow area in Figure 6.7. The difference in geoid from Figure 6.7, is in the same order as the difference obtained from the ICESat-2 observations. Therefore, it is supposed that the difference in water surface height in larger lakes is caused by the low resolution geoid.

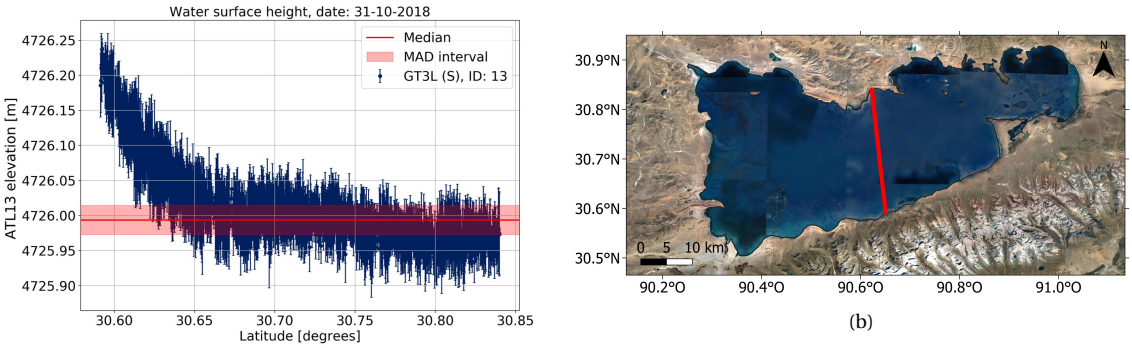

Figure 6.8: A steep slope is visible in lake Nam Co. (a) ATL13 observations of one beam passing Nam Co on the 31st of October. The MAD interval is shown as transparent band. A clear slope from left to right is visible. (b) Location of the passing beam over Nam Co.

An approach to reduce the influence of the slope on the water surface height measurements which is caused by the geoid, is to use a single reference latitude for each lake and reference all the observations to this latitude (Kleinherenbrink et al., 2015). In another study it is found that CryoSat-2 and SARAL are capable of finding high resolution geoid information (Jiang et al., 2019). By using the measurements of CryoSat-2 and SARAL an interpolated local geoid map is created. This is done by first computing the water surface height anomalies by subtracting the along-track mean value of the observations where the outliers are removed, resulting in an anomaly for each individual track. Finally all the anomalies are interpolated and filtered spatially leading to an interpolated local geoid correction map. Using this geoid map the water surface height measurements for CrySat-2, ICESat-1, SARAL and Sentinel-3 were corrected. The correction improved the uncertainty of the measurements of the missions with 8 to 37% (Jiang et al., 2019).
These geoid corrections were not applied in this research, which may results in a lower precision of the water surface heights of ICESat-2 for the larger lakes. For the larger lakes it would thus be recommended to apply a geoid correction for a better precision of the water surface heights.

6.5. Other locations

ICESat-2 for other locations

This research determined the water surface heights of lakes and rivers with ICESat-2 in the upper Brahmaputra and Nam Co basin. Earlier research already showed that ICESat-2 can measure 460.000 reservoir globally (Cooley et al., 2021). Although, this research has found that lakes with a size smaller than 10 km^2 will have a too low amount of measurements in time to generate a generic water surface height curve. ICESat-2 is not used in earlier research for determining river surface height measurements. Due to the slope in the upper Brahmaputra, only beams which are closer than 200 meter to each other are used for the determinations. This resulted in a low amount of measurements with significant time gaps and missing extreme water surface heights. For this reason it would not be recommended to use ICESat-2 for water surface heights in a river with a slope larger than 0.0001 meters/meters. More downstream rivers often have a smaller slope, the closer to the mouth of the river, the smaller the slope. This would mean that the maximum allowed distance between the passing beams could be increased, resulting in more passing beams on the same location. This is illustrated in Figure 6.9.

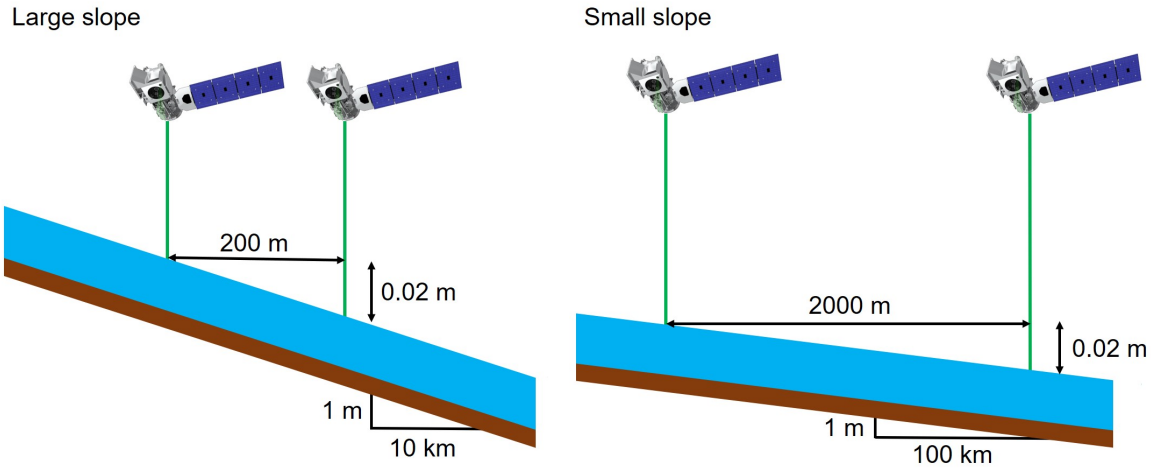

Figure 6.9: The maximum possible distance between the beams can be larger for smaller slopes. Note that this illustration represent not the right scales.

7

Conclusions and recommendations

7.1. Conclusions

The purpose of this report is to present the value of ICESat-2 for measuring waterbodies in the upper Brahmaputra and Nam Co basin located on the Tibetan Plateau. The main research question is split up in three parts with sub-questions. The found answers on the sub-questions are described below:

A. **Motivation**

A.1 *Why is it important to monitor waterbodies in the upper Brahmaputra and Nam Co basin?*
The upper Brahmaputra and Nam Co basin are located on the Tibetan Plateau which consists of a large amount of glaciers. The glaciers are the water source for big rivers as the Brahmaputra which stream towards the most densely populated area on Earth. Due to climate change, the temperatures increase and the glaciers are melting and the water storage of the most densely populated area is decreasing. In short term the river surface heights are increasing due to the melting glaciers, but in long term the river surface heights will decrease due to the decreased amount of glaciers. Monitoring of these waterbodies could indicate climate change and could help determining the water storage in this area. However, literature showed that the upper Brahmaputra basin, which is located in the south of the Tibetan Plateau, is behaving differently than the north of the Tibetan Plateau. Instead of an increase in water surface height, a decrease in water surface height is found. Although, the decrease is significantly smaller than the increase in water surface height of the north of the Tibetan Plateau. Literature discussed that the water surface heights are not only influenced by melting glaciers, but also precipitation plays a big role in the water surface height variations in the lakes and rivers in the upper Brahmaputra basin.

B. **ICESat-2**

B.1 *What data products of ICESat-2 can be used for monitoring changes in waterbodies and what are their properties?*
ICESat-2 provides several data products. The main data of ICESat-2 are all the geolocated photons, which forms the basis of the higher order surface height data products and are provided by data product ATL03 (see Section 3.4). The data product used in this research for determining surface heights of waterbodies is ATL13 (Inland Water Elevation). ATL13 consists of water surface height observation for lakes and rivers and is constructed by estimating the mean height of short segments varying from 30 till 100 meters for each beam over signal photons from ATL03. ICESat-2 has a ground-track spacing of 3.6 kilometers, which is small compared to other satellite missions (Section 3.3). However, this small ground-track spacing is at the cost of the temporal resolution of ICESat-2. ICESat-2 has a 91-day repeat orbit and returns to the same location after two years.

B.2 *What processing steps should be applied to ICESat-2 data to be able to estimate water surface heights?*
In this research the ATL13 data of ICESat-2 is processed to determine water surface heights for lakes and rivers. Both waterbodies are processed differently due to the fact that rivers have a slope and are spatially varying over the year. The complete method for determining the water surface heights is described in Chapter 4.

C. **Waterbody surface heights**

C.1 *What is the precision of the measured water surface heights by ICESat-2?*
The accuracy of the ICESat-2 measurements is not possible to determine since no hydrological stations in the lakes or river in the study area are present or are unavailable. The mountainous area makes it difficult to reach locations in the study area for in-situ measurements, which makes satellite observations even more important. Earlier studies have found that the accuracy of ATL13 of ICESat-2 varies between 2 and 34 centimeters. Even though no accuracy could be assigned to the measured water surface height measurements of this research, the precision of the measured water surface heights are examined. For both the lakes and main river in the study area, it turned out that the precision of the measured water surface heights by ATL13 of ICESat-2 in this study area is 0.1 meters. However, the method for determining river surface heights should only be used for non-braiding rivers. The water surface heights and errors on the locations in the river which are braiding are also possible to determine with ATL13, but then the discussed method should be improved. For both lakes and rivers the error by ATL13 is discussed in more detail in Section 5.1.2 and Section 5.2.2.

C.2 *What are the seasonal variations in water surface heights of the waterbodies in the upper Brahmaputra and Nam Co basin?*
The water surface height differences between February and August are determined for both years 2019 and 2020 (see Section 5.1.4 and 5.2.4). However, the chance that ICESat-2 passes the same waterbody exactly in both months is small due to its low temporal resolution. The found differences in water surface height only show a minimum difference, since the assumption that the lowest water surface height will occur in February and the highest water surface height will occur in August would not always be correct. Beside that, the chance that ICESat-2 passes a lake or river on the moment of the maximum of minimum water surface height is small and therefore determining a seasonal variation will be difficult to assess. Only the larger lakes (>10 km^2) will have more passings by ICESat-2 (at least eight in a period of two years) and will have less large time gaps, but this is only 2% of the total amount of lakes in the study area. If at least one ICESat-2 passing is available every two months and a longer timeseries is available a generic water surface height curve might be possible to fit resulting in knowledge about the seasonal variation of the lake surface height during the years.

C.3 *What can be concluded from the water surface height measurements of ICESat-2?*
From this research it can be concluded that it is possible to measure water surface heights of lakes and upstream rivers with ICESat-2. For the locations where the river is braiding the method should be improved. ICESat-2 has passed in total 127 locations in the Brahmaputra river and 299 lakes in the upper Brahmaputra and Nam Co basin in two years time due to its high spatial resolution. However, due to its low repeat it is difficult to assess the seasonal variation of the waterbodies. For assessing the seasonal variation in the waterbodies, at least one ICESat-2 measurement in two months and longer timeseries are needed. Over a longer time period it might then be possible to fit a generic water surface height curve through the water surface heights and finally something about the seasonal variation could be concluded. But this requires further research.

Thus, taking also those sub-questions into account the main research question can be answered.

What is the contribution of ICESat-2 for measuring waterbodies in the upper Brahmaputra and Nam Co basin located on the Tibetan Plateau?

This research found that ICESat-2 can have a contribution for determining lake and river surface heights due to its relatively good precision and its high spatial resolution. The ground-track spacing of ICESat-2 is lower than other satellite missions, resulting that ICESat-2 passes the most amount of lakes and river locations. In total the water surface heights of 299 lakes and 127 river locations are determined. However, this small ground-track spacing is at the cost of the temporal resolution resulting in large time gaps in the timeseries of the lakes and river locations. Therefore, a seasonal variation and generic water surface height curve will be difficult to assess. It is possible that ICESat-2 will miss the moments with the extreme water surface heights resulting in a misconception of the water surface heights. But, over a longer time period it might be possible to fit a generic water surface height curve through the water surface heights of lakes larger than 10 km^2 due to its higher amount of ICESat-2 passings.

7.2. Recommendations

This section discusses recommendations for further research. First, recommendations are given to create denser timeseries of the water surface heights, followed by recommendations to acquire the water surface height on locations where the river is braiding. Thereafter, the validation of the water surface heights is discussed and finally other interesting opportunities with ICESat-2 are presented.

Denser timeseries of the water surface height

ATL03 photon cross-section profiles with Sentinel-2

In this research ATL13 observations are used for the estimation of the water surface heights in the river. Another possibility to estimate the river surface heights is to use the photons (ATL03) of ICESat-2 in combination with Sentinel-2 images. A method to use the photon data is to overlay the photon data over the Sentinel-2 image of the day ICESat-2 is passing. The photon data could be used to determine the locations of the most outer banks of the river and to determine the river surface height. The relation between the river surface height and the width of the river could be studied. With this information it may be possible to determine river surface height based on the width of the river from Sentinel-2 images. Since Sentinel-2 has a higher repeat than ICESat-2, smaller time gaps will be present in the timeseries.

Sentinel-3

By comparing the estimated water surface heights of ICESat-2 with the water surface heights of Sentinel-3 from Hydroweb, it is seen that Sentinel-3 is also capable of measuring the upstream rivers like the upper Brahmaputra and is even capable of detecting a seasonal cycle. It is thus highly recommended to examine the performance of Sentinel-3 for the upper Brahmaputra and to study the seasonal cycle of the river and the lakes of the upper Brahmaputra and Nam Co basin.

Combination of timeseries of neighbouring lakes

It is expected that neighbouring lakes have a similar variation in water surface height. Therefore, it would be interesting to combine the timeseries of multiple neighbouring lakes. The timeseries could give an indication of the behaviour of the water surface height in that area.

Braiding rivers

Combination of ICESat-2 and Sentinel-2

Besides bars in braiding rivers, side channels in a braiding river could cause problems as well. Due to braiding rivers the river consist of multiple side channels which are all measured by ICESat-2. It is not (always) the case that the main channel, also represents the lowest plateau in the river profile cross-section, resulting in measuring different channels. A recommendation for further research will be to overlay ATL13 observations over the optical imagery of for example a Sentinel-2 image of that moment and to use only the ATL13 observations which overlay the main channel. Another possibility is to create another river mask. This river mask should contain only the main channel which is present during the whole year, so also when the river surface height is low and the discharge low. In this research a river mask is used which is created out of images which represents the average discharge of the year, so also the average width of the river leading to that during lower discharges more side channels are visible or bars. By creating a river mask which is based on the lowest discharge, this problem will be avoided. A remark for this last recommendation is that it should be studied whether the main channel is not moving too much over time.

Classifying ATL03 photons of ICESat-2

The river observation could be distorted by bars. This problem is tackled in this research by assuming that the lowest plateau of the ATL13 observations consists of the water surface observations. From only the lowest ATL13 observations, the water surface height is estimated. So it is assumed that the lowest plateau represents the water surface, but this assumption is not always correct. Especially in cases where the river is braiding and consist of bars in the river cross-section, therefore the method in this research is mainly applicable for the non-braiding rivers. But for extracting the water surface heights on locations where the river is braiding, further research is recommended to extract only the water surface observations of ICESat-2 and not the bars as well. A possible method to do this by classifying the ATL03 photon data of ICESat-2 for water surfaces. By classifying the photons, the water surface height could be computed from only the observations which are classified as water surface resulting in a more accurate water surface height where no bars are involved.

Validation

Validation of the water surface heights

This research determines the water surface heights on locations where no in-situ measurements are available due to the mountainous area or because these measurements are not easily accessible. Several papers are available about the lake surface heights on the Tibetan Plateau and therefore the lake surface height trends could be compared. River surface heights have not been studied much and it will therefore not be possible to compare the data with others. Since the method discussed in this research has its uncertainties due to the presence of bar, it would be recommended to determine the river surface heights at an upstream location in the river where in-situ measurements are present and easily accessible.

Water surface heights to Hydroweb

Add ICESat-2 water surface heights to Hydroweb

Hydroweb consists of one naturally behaving lake in the study area and 35 virtual locations in the upper Brahmaputra river. This research found the water surface heights of 299 lakes and of 127 locations in the river. This amount is a lot more than now available on Hydroweb. Therefore, it would be recommended to add these lakes and river locations to Hydroweb. However, since it is concluded that large time gaps are present in the timeseries, it would be recommended to first make denser timeseries for the river locations by using the photon cross-section profiles with Sentinel-2.

Other interesting opportunities with ICESat-2

Side branches in ATL13

The higher order data product ATL13 of ICESat-2 is also capable of measuring some of the side branches of the upper Brahmaputra. These side branches have not been taken into account in this research, but might be interesting for further research. However, this could lead into problems, since the smallest rivers are often the most upstream parts in the river system. The most upstream parts of the river will have the largest slope within the river system. This will mean that the slope of these side branches should be carefully studied. Another important note, is that the side branches and the smallest rivers in the system will have a smaller depth. In case the depth is low, the bed profile might be seen as water surface. This will make it harder to only extract the water observations, leading to more distortion of the river surface height measurements.

Slope between strong and weak beam

The aim of ICESat-2 for carrying a strong and weak beam is to have the possibility to determine the slope between the beams. This property is not used in this research, but might be interesting for further research. With this property it will be possible to compute the slope between the weak and strong beams and to determine the slope of the river on that location. If the slope between the weak and strong beam is too large, that location will not be a location where the water surface heights should be estimated. Another interesting advantage of this property might be that the slope of the whole river could be estimated.
Thereafter, for lakes this property might be interesting to examine the geoid variation within large lakes. For the largest lakes (size > 50 km^2) a slope within the ATL13 observations is present, but also slope over the different beams is visible. By examining the variation within the beams and among the beams, information about the geoid fluctuations might be gained.

References

Allen, G. H. and Pavelsky, T. M. (2018). Global extent of rivers and streams. *Science*, 361(6402):585–588.

Baghdadi, N., Lemarquand, N., Abdallah, H., and Bailly, J. S. (2011). The Relevance of GLAS/ICESat Elevation Data for the Monitoring of River Networks. *Remote Sensing*, 3(4):708–720.

Biancamaria, S., Schaedele, T., Blumstein, D., Frappart, F., Boy, F., Desjonquères, J.-D., Pottier, C., Blarel, F., and Niño, F. (2018). Validation of Jason-3 tracking modes over French rivers. *Remote Sensing of Environment*, 209:77–89.

Boergens, E., Nielsen, K., Andersen, O. B., Dettmering, D., and Seitz, F. (2017). River Levels Derived with CryoSat-2 SAR Data Classification—A Case Study in the Mekong River Basin. *Remote Sensing*, 9(12).

Brun, F., Treichler, D., Shean, D., and Immerzeel, W. W. (2020). Limited Contribution of Glacier Mass Loss to the Recent Increase in Tibetan Plateau Lake Volume. *Frontiers in Earth Science*, 8:495.

Chopde, N. R. and Nichat, M. (2013). Landmark based shortest path detection by using A* and Haversine formula. *International Journal of Innovative Research in Computer and Communication Engineering*, 1(2):298–302.

Consortium, R. (2017). Randolph Glacier Inventory – A Dataset of Global Glacier Outlines: Version 6.0: Technical Report, Global Land Ice Measurements from Space, Colorado, USA. *Digital Media*.

Cooley, S. W., Ryan, J. C., and Smith, L. C. (2021). Human alteration of global surface water storage variability. *Nature*, 591:78–81.

Crétaux, J.-F., Arsen, A., Calmant, S., Kouraev, A., Vuglinski, V., Bergé-Nguyen, M., Gennero, M.-C., Nino, F., Abarca Del Rio, R., Cazenave, A., and Maisongrande, P. (2011). SOLS: A lake database to monitor in the Near Real Time water level and storage variations from remote sensing data. *Advances in Space Research*, 47(9):1497–1507.

Cuo, L., Li, N., Liu, Z., Ding, J., Liang, L., Zhang, Y., and Gong, T. (2019). Warming and human activities induced changes in the Yarlung Tsangpo basin of the Tibetan plateau and their influences on streamflow. *Journal of Hydrology: Regional Studies*, 25:100625.

Duan, S.-B., Li, Z.-L., Li, H., Göttsche, F.-M., Wu, H., Zhao, W., Leng, P., Zhang, X., and Coll, C. (2019). Validation of Collection 6 MODIS land surface temperature product using in situ measurements. *Remote Sensing of Environment*, 225:16–29.

ESA (NDa). Sentinel-3 altimeter coverage. `https://sentinel.esa.int/web/sentinel/user-guides/sentinel-3-altimetry/coverage`. Accessed June 3, 2021.

ESA (NDb). Sentinel playground. `https://apps.sentinel-hub.com/sentinel-playground`. Sinergise Ltd. Accessed May 5, 2021.

Huang, Q., Long, D., Du, M., Zeng, C., Li, X., Hou, A., and Hong, Y. (2018). An improved approach to monitoring Brahmaputra River water levels using retracked altimetry data. *Remote Sensing of Environment*, 211:112 – 128.

Huffman, G., Bolvin, D., Braithwaite, D., Hsu, K., Joyce, R., and Xie, P. (2014). Integrated Multi-satellitE Retrievals for GPM (IMERG), version 4.4. *NASA's Precipitation Processing Center*. Accessed 28 January, 2021.

Jasinski, M., Stoll, J., Hancock, D., Robbins, J., Nattala, J., Pavelsky, T., Morrison, J., B. Jones, M., Parrish, C., and the ICESat-2 Science Team (2020). Algorithm Theoretical Basis Document (ATBD) for Inland Water Data Products, ATL13, Version 3. *NASA Goddard Space Flight Center*.

Jiang, L., Andersen, O. B., Nielsen, K., Zhang, G., and Bauer-Gottwein, P. (2019). Influence of local geoid variation on water surface elevation estimates derived from multi-mission altimetry for Lake Namco. *Remote Sensing of Environment*, 221:65–79.

Jiang, L., Nielsen, K., Andersen, O. B., and Bauer-Gottwein, P. (2020). A bigger picture of how the Tibetan lakes change over the past decade revealed by CryoSat-2 altimetry. *Journal of Geophysical Research: Atmospheres*.

Kelly, O. (2020). The IMERG multi-satellite precipitation estimates reformatted as 2-byte GeoTIFF files for display in a Geographic Information System (GIS). `https://gpm.nasa.gov/sites/default/files/2020-06/IMERG-GIS-Readme_4_22_20.pdf`. Accessed January 28, 2021.

Kleinherenbrink, M., Lindenbergh, R., and Ditmar, P. (2015). Monitoring of lake level changes on the Tibetan Plateau and Tian Shan by retracking Cryosat SARIn waveforms. *Journal of Hydrology*, 521(February):119–131. Available online 3-12-2014.

Kleinherenbrink, M., Naeije, M., Slobbe, C., Egido, A., and Smith, W. (2020). The performance of CryoSat-2 fully-focussed SAR for inland water-level estimation. *Remote Sensing of Environment*, 237(111589).

Koudijs, M., Menenti, M., and Lindenbergh, R. (2008). Using ICESatGLAS laser altimetry for water level estimations in the Mekong River. Master's thesis, University of Technology Delft.

Krishnamurti, T. (2015). Indian monsoon. `https://www.britannica.com/science/Indian-monsoon`. Accessed January 22, 2021.

Lehner, B. and Döll, P. (2004). Development and validation of a global database of lakes,reservoirs and wetlands. *Journal of Hydrology*, 296/1-4:1–22.

Lehner, B. and Grill, G. (2013). Global river hydrography and network routing: baseline data and new approaches to study the world's large river systems. *Hydrological Processes*, 27(15):2171–2186. Data is available at www.hydrosheds.org.

Lehner, B., Verdin, K., and Jarvis, A. (2008). New global hydrography derived from spaceborne elevation data. *Eos, Transactions*, 89(10):93–94.

Liu, G., Schwartz, F., Tseng, K.-H., Shum, C. K., and Lee, S. (2018). Satellite altimetry for measuring river stages in remote regions. *Environmental Earth Sciences volume*, 77(639).

Lutz, A. F., Immerzeel, W. W., Shrestha, A. B., and Bierkens, M. F. P. (2014). Consistent increase in High Asia's runoff due to increasing glacier melt and precipitation. *Nature Climate Change*, 4:587–592.

Markus, T., Neumann, T., Martino, A., Abdalati, W., Brunt, K., Csatho, B., Farrell, S., Fricker, H., Gardner, A., Harding, D., Jasinski, M., Kwok, R., Magruder, L., Lubin, D., Luthcke, S., Morison, J., Nelson, R., Neuenschwander, A., Palm, S., Popescu, S., Shum, C., Schutz, B. E., Smith, B., Yang, Y., and Zwally, J. (2017). The Ice, Cloud, and land Elevation Satellite-2 (ICESat-2): Science requirements, concept, and implementation. *Remote Sensing of Environment*, 190:260 – 273.

Maurer, J. M., Schaefer, J. M., Rupper, S., and Corley, A. (2019). Acceleration of ice loss across the Himalayas over the past 40 years. *Science Advances*, 5(6).

Messager, M., Lehner, B., Grill, G., Nedeva, I., and Schmitt, O. (2016). Estimating the volume and age of water stored inglobal lakes using a geo-statistical approach. *Nature Communications*, 13603.

NASA (NDa). ICESat-2 Ground Tracks. https://icesat-2.gsfc.nasa.gov/science/specs. Accessed December 15, 2020.

NASA (NDb). Observatory graphics. `https://icesat-2.gsfc.nasa.gov/observatory-graphics`. Accessed Februacy 25, 2021.

NASA (NDc). Open altimetry. `https://openaltimetry.org/data/icesat2/`. Accessed March 4, 2021.

Neuenschwander, A., Pitts, K., Jelley, B., Robbins, J., Klotz, B., Popescu, S., Nelson, R., Harding, D., Pederson, D., and Sheridan, R. (2020). Algorithm Theoretical Basis Document (ATBD) for Land - Vegetation Along-Track Products, ATL08, Version 3. *NASA Goddard Space Flight Center*.

Neumann, T., Brenner, A., Hancock, D., Robbins, J., Saba, J., Harbeck, K., Gibbons, A., Lee, J., Luthcke, S., and Rebold, T. (2020a). Algorithm Theoretical Basis Document (ATBD) for Global Geolocated Photons, ATL03, Version 3. *NASA Goddard Space Flight Center*.

Neumann, T. A., Martino, A. J., Markus, T., Bae, S., Bock, M. R., Brenner, A. C., Brunt, K. M., Cavanaugh, J., Fernandes, S. T., Hancock, D. W., Harbeck, K., Lee, J., Kurtz, N. T., Luers, P. J., Luthcke, S. B., Magruder, L., Pennington, T. A., Ramos-Izquierdo, L., Rebold, T., Skoog, J., and Thomas, T. C. (2019). The Ice, Cloud, and Land Elevation Satellite – 2 mission: A global geolocated photon product derived from the Advanced Topographic Laser Altimeter System. *Remote Sensing of Environment*, 233:111325.

Neumann, T. E., Markus, T., Bhardwaj, S., and Hancock, D. W. (2020b). ATL13 product data dictionary. `https://nsidc.org/sites/nsidc.org/files/technical-references/ICESat2_ATL13_data_dict_v003.pdf`. Accessed February 23, 2021.

Normandin, C., Frappart, F., Diepkilé, A. T., Marieu, V., Mougin, E., Blarel, F., Lubac, B., Braquet, N., and Ba, A. (2018). Evolution of the Performances of Radar Altimetry Missions from ERS-2 to Sentinel-3A over the Inner Niger Delta. *Remote Sensing*, 10(6).

NSIDC (ND). ICESat-2 Product Descriptions. `https://nsidc.org/data/icesat-2/products/`. Accessed November 11, 2020.

Pavlis, N. K., Holmes, S. A., Kenyon, S. C., and Factor, J. K. (2012). The development and evaluation of the Earth Gravitational Model 2008 (EGM2008). *Journal of Geophysical Research: Solid Earth*, 117(B4).

Phan, V., Menenti, M., Lindenbergh, R., Scaloni, M., Su, Z., van de Giesen, N., Kropacek, J., Gourmelen, N., and Bastiaanssen, W. (2015). *Observing changes in lake level and glacial thickness on the Tibetan Plateau with the ICESat laser altimeter*. PhD thesis, University of Technology Delft.

Phan, V. H., Lindenbergh, R., and Menenti, M. (2012). ICESat derived elevation changes of Tibetan lakes between 2003 and 2009. *International Journal of Applied Earth Observation and Geoinformation*, 17:12 – 22. Retrieval of Key Eco-hydrological Parameters for Cold and Arid Regions.

Rao, G. D. S. S. (2020). Validation of ICESat-2 Surface Water Level Product ATL13 with Near Real Time Gauge Data. *Hydrology*, Vol. 8(No. 2):pp. 19–25.

Ryan, J. C., Smith, L. C., Cooley, S. W., Pitcher, L. H., and Pavelsky, T. M. (2020). Global Characterization of Inland Water Reservoirs Using ICESat-2 Altimetry and Climate Reanalysis. *Geophysical Research Letters*, 47(17):e2020GL088543. e2020GL088543 2020GL088543.

Sang, Y.-F., Singh, V. P., Gong, T., Xu, K., Sun, F., Liu, C., Liu, W., and Chen, R. (2016). Precipitation variability and response to changing climatic condition in the Yarlung Tsangpo River basin, China. *Journal of Geophysical Research: Atmospheres*, 121(15):8820–8831.

Santos da Silva, J., Calmant, S., Seyler, F., Rotunno Filho, O. C., Cochonneau, G., and Mansur, W. J. (2010). Water levels in the Amazon basin derived from the ERS 2 and ENVISAT radar altimetry missions. *Remote Sensing of Environment*, 114(10):2160–2181.

Shugar, D. H., Burr, A., Haritashya, U. K., Kargel, J. S., Watson, C. S., Kennedy, M. C., Bevington, A. R., Betts, R. A., Harrison, S., and Strattman, K. (2020). Rapid worldwide growth of glacial lakes since 1990. *Nature climate change*, 10:939–945.

Stevens, J., Neuenschwander, A., and Harbeck, K. (2018). ICESat-2 Sees the Trees in Mexico. `https://earthobservatory.nasa.gov/images/144450/icesat-2-sees-the-trees-in-mexico`. Accessed November 20, 2020.

Tan, Q. and Liu, Y. (2020). Spatiotemporal variation and climatic response of water level of major lakes in China, Mongolia, and Russia. *Open Geosciences*, 12(1):1200 – 1211.

USGS and EROS (2015). Digital Elevation - Shuttle Radar Topography Mission (SRTM) 1 Arc-Second Global. `https://earthexplorer.usgs.gov/`. Accessed February 2, 2021.

Vermote, E., Justice, C., Claverie, M., and Franch, B. (2016). Landsat data and associated products courtesy of the U.S. Geological Survey. *Remote Sensing of Environment*.

Wan, Z., Hook, S., and Hulley, G. (2015). MOD11A1 MODIS/Terra Land Surface Temperature/Emissivity Daily L3 Global 1km SIN Grid V006 [Terra]. *NASA EOSDIS Land Processes DAAC*. Accessed 05-02-2021.

Wessel, P. and Smith, W. H. F. (1996). A GlobalSelf-consistent, Hierarchical, High-resolution Shoreline Database. *J.Geophys. Res.*, 101:8741–8743.

Xuan, W., Xu, Y.-P., Fu, Q., Booij, M. J., Zhang, X., and Pan, S. (2020). Hydrological responses to climate change in Yarlung Zangbo River basin, Southwest China. *Journal of Hydrology*, page 125761.

Yuan, C., Gong, P., and Bai, Y. (2020). Performance Assessment of ICESat-2 Laser Altimeter Data for Water-Level Measurement over Lakes and Reservoirs in China. *Remote Sensing*, 770(12(5)).

Zhang, G., Chen, W., and Xie, H. (2019). Tibetan Plateau's Lake Level and Volume Changes From NASA's ICESat/ICESat-2 and Landsat Missions. *Geophysical Research Letters*, 46(22):13107–13118.

Zhang, G., Xie, H., Kang, S., Yi, D., and Ackley, S. F. (2011). Monitoring lake level changes on the Tibetan Plateau using ICESat altimetry data (2003–2009). *Remote Sensing of Environment*, 115(7):1733 – 1742.

Zhang, G., Yao, T., Xie, H., Yang, K., Zhu, L., Shum, C., Bolch, T., Yi, S., Allen, S., Jiang, L., Chen, W., and Ke, C. (2020). Response of Tibetan Plateau lakes to climate change: Trends, patterns, and mechanisms. *Earth-Science Reviews*, 208:103269.

A

Appendix: Cluster locations

In this appendix the river locations have been visualized with Sentinel-2 images in February, May, August and November. Note that the images are not natural colours (bands 4,3,2) but infrared colours (bands 8,4,3).

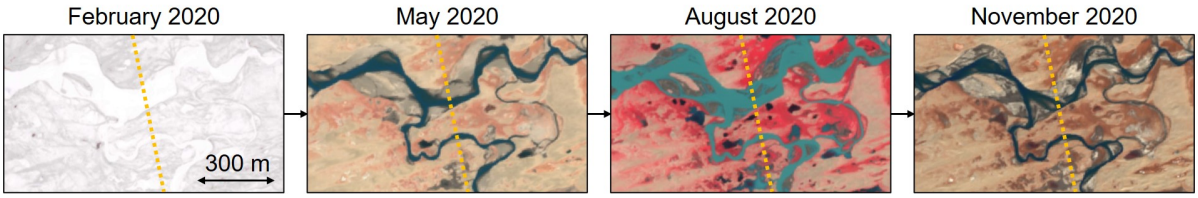

Figure A.1: Cluster location 97. Sentinel-2 images on 08-02-20, 10-05-20, 08-08-20 and 01-11-20 (ESA, NDb).

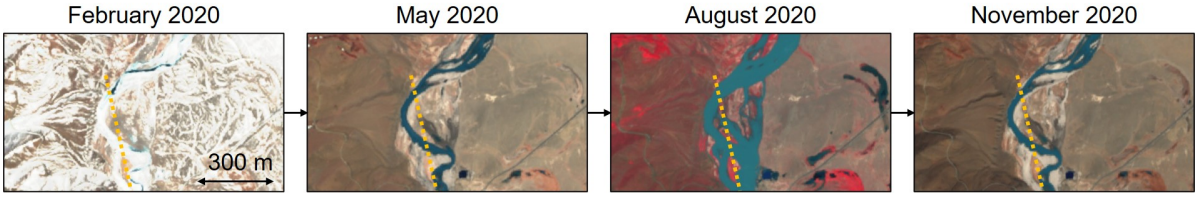

Figure A.2: Cluster location 175. Sentinel-2 images on 10-02-20, 10-05-20, 08-08-20 and 01-11-20 (ESA, NDb).

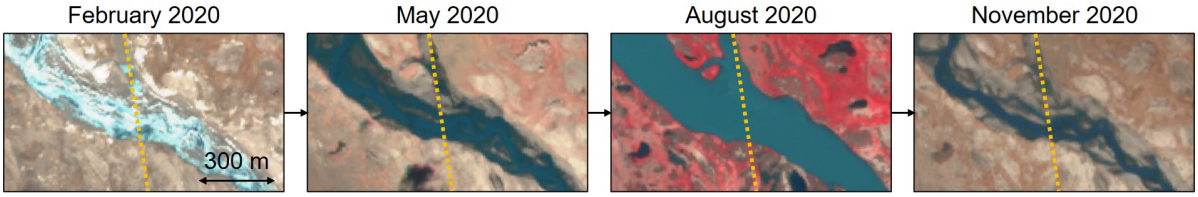

Figure A.3: Cluster location 181. Sentinel-2 images on 20-02-20, 20-05-20, 18-08-20 and 21-11-20 (ESA, NDb).

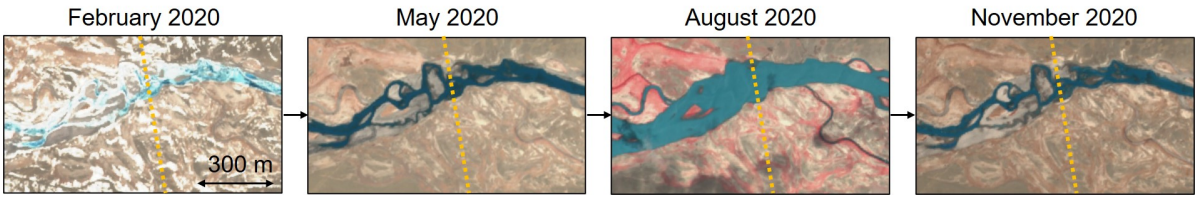

Figure A.4: Cluster location 183. Sentinel-2 images on 10-02-20, 10-05-20, 13-08-20 and 06-11-20 (ESA, NDb).

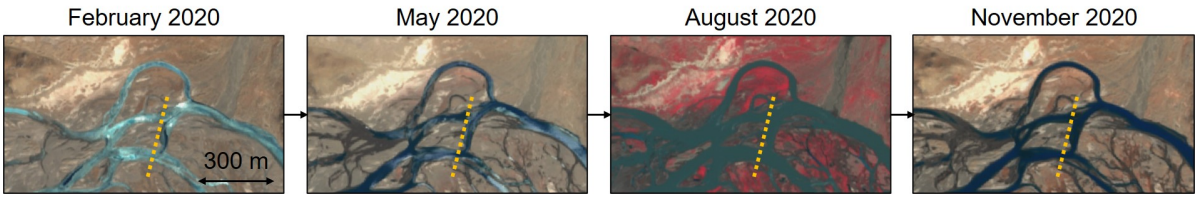

Figure A.5: Cluster location 328. Sentinel-2 images on 05-02-20, 15-05-20, 23-08-20 and 01-11-20 (ESA, NDb).

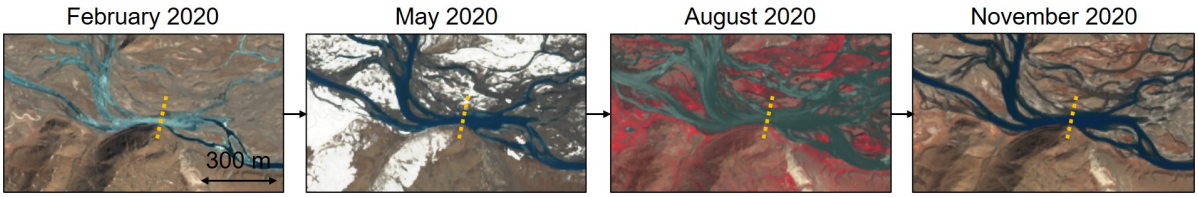

Figure A.6: Cluster location 330. Sentinel-2 images on 05-02-20, 30-04-20, 18-08-20 and 01-11-20 (ESA, NDb).

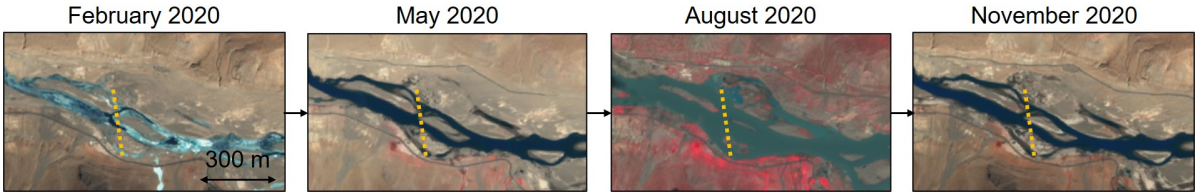

Figure A.7: Cluster location 368. Sentinel-2 images on 05-02-20, 17-05-20, 15-08-20 and 01-11-20 (ESA, NDb).

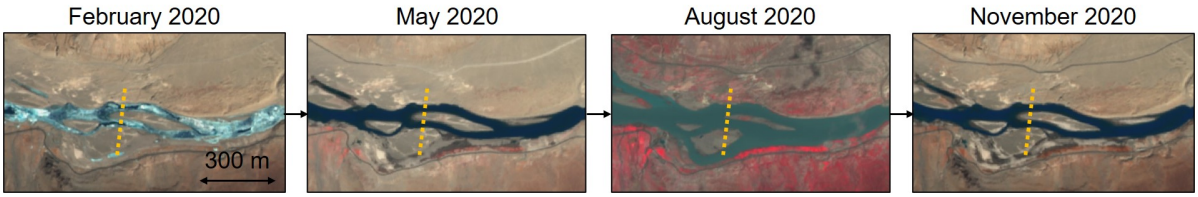

Figure A.8: Cluster location 369. Sentinel-2 images on 05-02-20, 17-05-20, 15-08-20 and 01-11-20 (ESA, NDb).

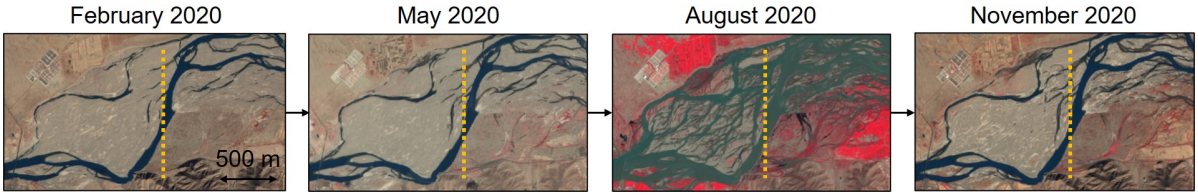

Figure A.9: Cluster location 685. Sentinel-2 images on 04-02-20, 04-05-20, 07-08-20 and 05-11-20 (ESA, NDb).

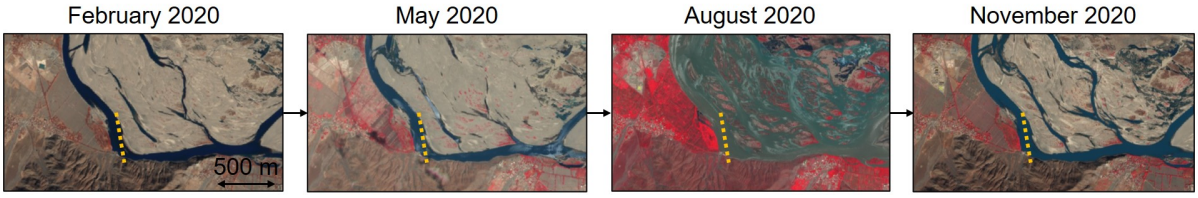

Figure A.10: Cluster location 817. Sentinel-2 images on 04-02-20, 04-05-20, 07-08-20 and 05-11-20 (ESA, NDb).

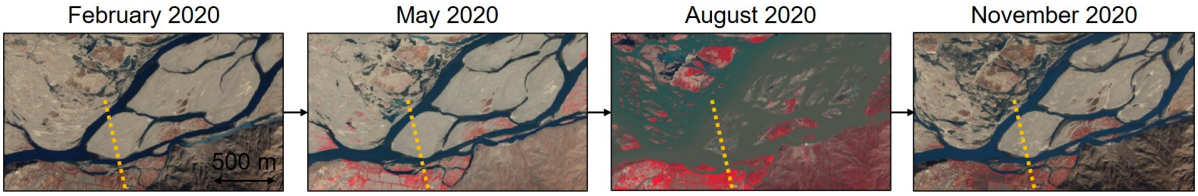

Figure A.11: Cluster location 820. Sentinel-2 images on 14-02-20, 06-05-20, 19-08-20 and 21-11-20 (ESA, NDb).

B

Appendix: Timeseries of the river surface heights

The timeseries of the eleven locations in the river with at least four ICESat-2 passings.

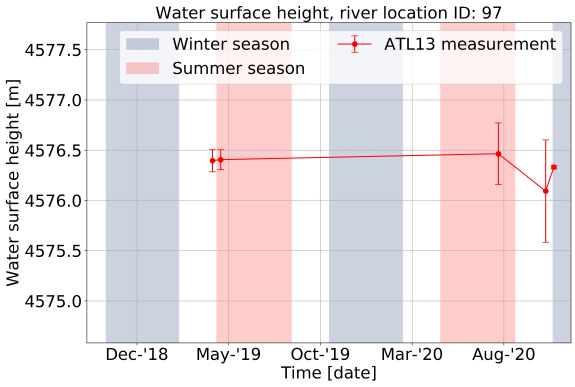

(a)

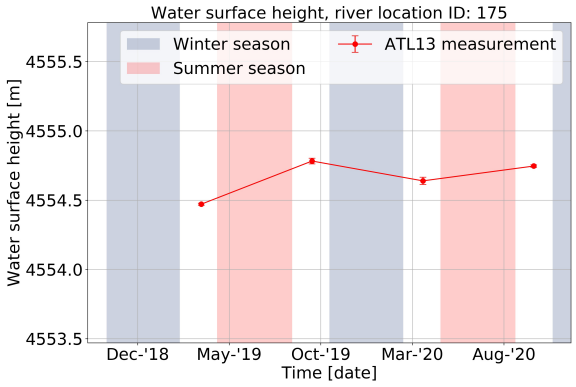

(b)

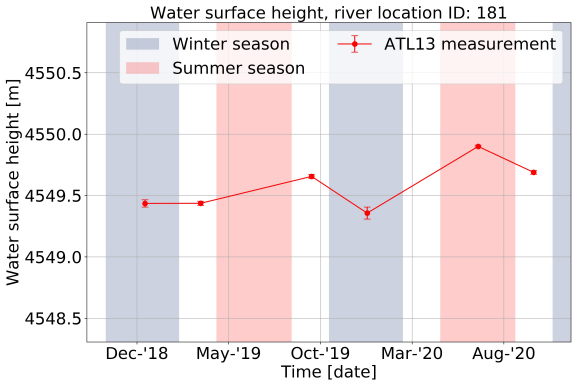

(c)

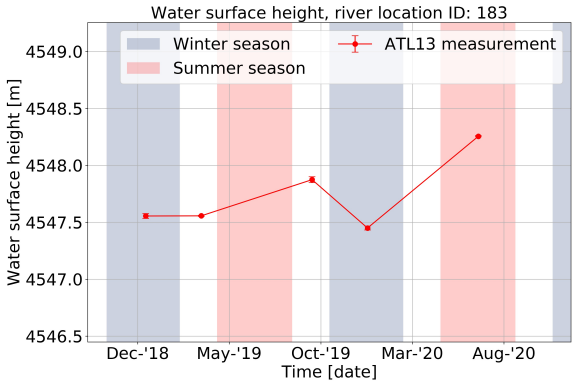

(d)

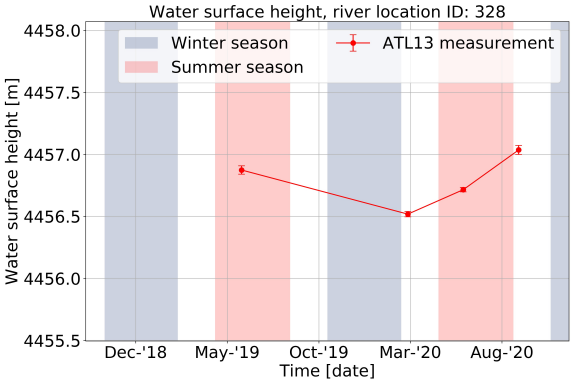

(e)

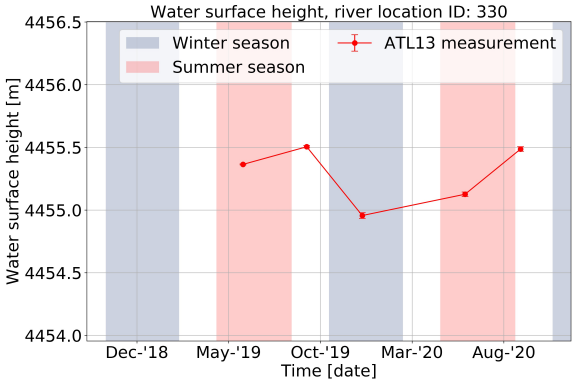

(f)

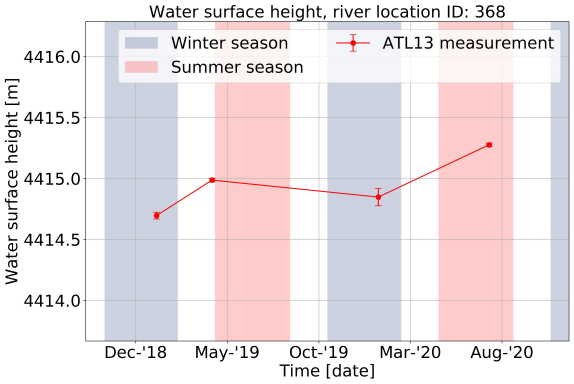

(g)

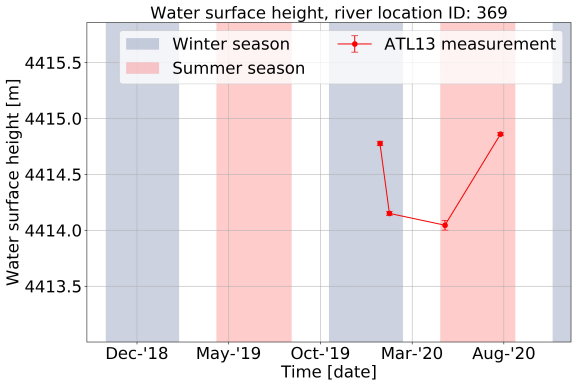

(h)

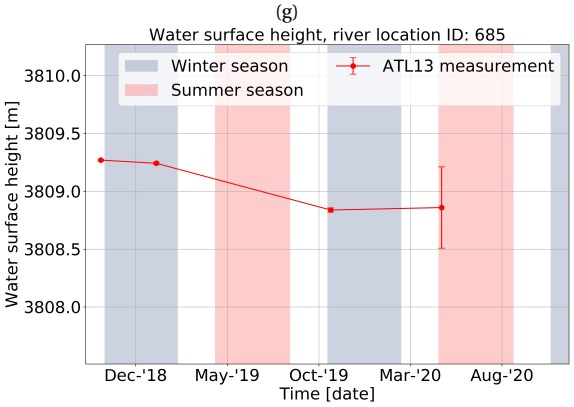

(i)

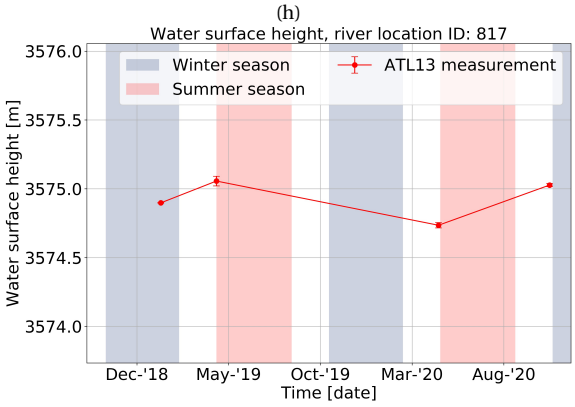

(j)

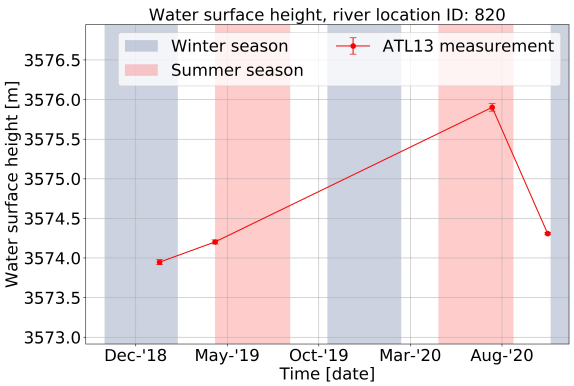

(k)

Figure B.1 Timeseries of the eleven locations in the river with at least four ICESat-2 passings.